Volumetric postmortem MRI of the medial temporal lobe in Alzheimer's disease and related disorders: methodological advances and implications for *in vivo* biomarker development

Yasmine Salman[a], Amanda E Denning[b], Jolien M Schaeverbeke[c,d], Sandra O Tomé[c], Nicolas Joudiou[e], Pulkit Khandelwal[f,g] Paul A Yushkevich[f], Rik Vandenberghe[d,h], Bernard Gallez[i] Laura EM Wisse[j]*, Bernard J Hanseeuw[a,g,k]*.

*These authors equally supervised this work

Authors affiliations :

a. Institute of Neuroscience, Avenue E. Mounier 52, Université Catholique de Louvain, 1200 Brussels, Belgium
b. Department of Neuroscience, University of Pennsylvania, 415 Curie Blvd, Philadelphia, PA, 19104
c. Laboratory of Neuropathology - Department of Imaging and Pathology and Leuven Brain Institute (LBI), KU Leuven (University of Leuven), O&N IV, Herestraat 49, box 1032, 3000, Leuven, Belgium.
d. Laboratory for Cognitive Neurology, Department of Neurosciences, Leuven Brain Institute (LBI), KU Leuven (University of Leuven), Leuven, Belgium
e. Nuclear and Electron Spin Technologies (NEST) Platform, Louvain Drug Research Institute (LDRI), Avenue E. Mounier 73, Université Catholique de Louvain (UCLouvain), 1200 Brussels, Belgium.
f. Department of Radiology, University of Pennsylvania, Philadelphia, PA, USA.
g. Department of Radiology, Massachusetts General Hospital, Harvard Medical School, B 55 Fruit Street, Boston, MA 02155, USA
h. Department of Neurology, UZ Leuven, Leuven, Belgium, Herestraat 49, 3000 Leuven, Belgium
i. Biomedical Magnetic Resonance Research Group, Louvain Drug Research Institute, Avenue E. Mounier 73, Université Catholique de Louvain, 1200 Brussels, Belgium
j. Department of Clinical Sciences Lund, Lund University, Klinikgatan 13B, 22185, Lund, Sweden
k. Department of Neurology, Department of Neurology, Cliniques Universitaires, 10 Avenue Hippocrate, 1200 Brussels, Belgium

Author's information :

Yasmine Salman (corresponding author): yasmine.salman@uclouvain.be; ORCID: 0000-0002-8564-5136

Amanda E Denning: Amanda.Denning@Pennmedicine.upenn.edu ; ORCID: 0009-0005-2531-9346

Jolien M Schaeverbeke: jolien.schaeverbeke@kuleuven.be ; ORCID: 0000-0003-2257-0568

Sandra O Tomé: sandra.tome@kuleuven.be; ORCID:0000-0001-5253-0730

Nicolas Joudiou: nicolas.joudiou@uclouvain.be ; ORCID: 0000-0002-6760-7400

Pulkit Khandelwal: pkhandelwal1@mgh.harvard.edu ; ORCID: 0000-0003-1397-3496

Paul A Yushkevich: pauly2@pennmedicine.upenn.edu ; ORCID: 0000-0001-8543-4016

Rik Vandenberghe: rik.vandenberghe@uzleuven.be ; ORCID: 0000-0001-6237-2502

Bernard Gallez: Bernard.gallez@uclouvain.be ; ORCID: 0000-0002-5708-1302

Laura EM Wisse: laura.wisse@med.lu.se ; ORCID: 0000-0001-7504-3943

Bernard J Hanseeuw: bernard.hanseeuw@uclouvain.be ; ORCID: 0000-0002-3102-6778

Keywords: Postmortem MRI; medial temporal lobe; neurodegenerative diseases

1. Abstract

Magnetic resonance imaging (MRI) is central to the study and diagnosis of neurodegenerative diseases. Yet, no MRI biomarker is currently specific to a given neurodegenerative disease. This may result from the limited resolution of conventional MRI, which restricts detailed investigation of medial temporal lobe (MTL) subregions, a crucial hub for many neuropathologies. Moreover, *in vivo* MRI cannot be directly compared with neuropathological data, the gold standard for disease definition. Even when antemortem MRI and postmortem analyses are combined, the time gap between imaging and neuropathological examination allows pathogenic processes to progress, reducing the accuracy of these correlations.

Over the past two decades, postmortem MRI has gained increasing interest because it enables long, motion-free acquisitions and the use of specialized coils and preclinical scanners, providing ultra-high spatial resolution. Additionally, it allows direct correspondence between imaging and neuropathological

measures. Consequently, volumetric postmortem MRI, particularly investigations of the MTL, has become an increasingly common approach in Alzheimer's disease and related disorders (ADRD).

This narrative review specifically focuses on volumetric postmortem MRI of the MTL and summarizes the main methodologies for anatomical postmortem MTL imaging in ADRD and recent advances in the characterization of neurodegenerative changes, from brain preparation to MRI acquisition. It also highlights the translational potential of volumetric postmortem MRI for developing *in vivo* biomarkers, optimizing imaging protocols and segmentation methods, and assessing the impact of proteinopathies. Finally, it outlines current limitations, technical challenges, and perspectives for future research.

2. Introduction

Magnetic resonance imaging (MRI) is commonly used to diagnose and study neurodegenerative diseases: in clinical practice, it is routinely used to diagnose and monitor the severity of these diseases, and, more recently, to monitor treatment safety. In clinical research, structural MRI is also used to study quantitative volumetric changes, regional patterns of atrophy, and their evolution over time, suggesting spread in neurodegenerative pathologies. Providing anatomical MRI has proven important for both clinicians and clinical scientists, as neurological symptoms are more closely related to the topography of the affected brain region than to the nature of the underlying pathology (Ossenkoppele et al., 2015). Due to its non-invasiveness and cost-effectiveness, significant efforts have been made to develop MRI biomarkers specific to particular neurodegenerative diseases (Jack et al., 2018). Although atrophy patterns have been observed in different neurodegenerative diseases (Harper et al., 2017), no MRI biomarkers have been clinically validated for an etiological diagnosis of neurodegenerative disorders, due to limited specificity. For instance, hippocampal atrophy is observed in Alzheimer's disease (AD, Scheltens et al., 1992), but also in frontotemporal lobar degeneration (FTLD, Planche et al., 2023), Lewy-Body disease (LBD, Ye et al., 2024), and limbic predominant age-related TDP-43 encephalopathy (LATE, Wolk et al., 2025).

Specific molecular biomarkers for AD have been developed, including amyloid-beta (Aβ) and tau quantification by cerebrospinal fluid (CSF) analyses (Hansson et al., 2006, 2007; Mattsson, 2009; Bayart et al., 2019), positron emission tomography (PET) imaging (Klunk et al., 2004, 2015; Johnson et al., 2016; Schöll et al., 2016; Hanseeuw et al., 2019; Ossenkoppele et al., 2022), and more recently, plasma-based assays (Therriault et al., 2024; Yakoub et al., 2025; Ossenkoppele et al., 2025). Ongoing efforts also aim to extend this approach to α-synuclein (Fairfoul et al., 2016; Singer et al., 2021) and TDP-43 pathologies. (Chatterjee et al., 2024; Irwin et al., 2024; Seddighi et al., 2024). Nevertheless, MRI provides unique spatial insights into neurodegenerative processes that molecular biomarkers alone cannot capture. MRI serves, therefore, as a supportive diagnostic tool in memory clinics, provides valuable prognostic information, and is widely used as an outcome measure in clinical trials (Sims et al., 2023). Additionally, when combined with molecular markers, MRI can enhance our understanding of disease mechanisms. However, to facilitate the development of MRI-based biomarkers for clinical applications, it is crucial to establish more precise associations between specific pathological processes and their corresponding patterns of atrophy.

To date, most volumetric studies have relied on global volumetric measures, such as total hippocampal (Scheltens et al., 1992; Ten Kate et al., 2018; Hanseeuw et al., 2023; Wesseling et al., 2025) or whole brain volume, which lack disease specificity and often fail to capture subtle. Region-specific atrophy patterns may more accurately reflect the underlying neuropathology or detect earlier changes. Over the past fifteen years, interest in volumetric measures of hippocampal subfields as potential biomarkers for AD has grown. However, no consensus has been reached across studies (see De Flores et al., 2015 & Zhang et al., 2023 for review), likely due to the limited resolution of *in vivo* imaging, which hampers reliable visualization of subfields, as well as the lack of standardized subfield segmentation protocols (Yushkevich et al., 2015; Wisse et al., 2017; Giuliano et al., 2017). While other MRI approaches, such as microstructural imaging (Rodriguez-Vieitez et al., 2021; Vogt et al., 2022; Gagliardi et al., 2023; Spotorno et al., 2023; Weston et al., 2023; Brown et al., 2024; Parker et al., 2025), may provide complementary information on early pathological processes, the present work specifically focuses on anatomical volumetric MRI.

Many neuropathologies affect the medial temporal lobe (MTL) early in disease progression, as shown in several neuropathology studies: AD neuropathological changes (ADNC) accumulates early in the (trans)entorhinal cortex (Braak and Braak, 1995, 1991), LATE neuropathological changes (LATE-NC) in the amygdala (Nelson et al., 2023, 2019), some forms of FTLD impact the temporal cortex and the amygdala (Cairns et al., 2007; Brettschneider et al., 2014), and α-synuclein typically affects the amygdala and hippocampus early on when co-occuring with AD (Braak et al., 2002; Gawor et al., 2024) when co-occurring with ADNC (Hamilton, 2000; Jellinger, 2003). Therefore, efforts have been made to disentangle the contributions of these pathologies to MTL atrophy.

To capture the ground truth of pathology-specific neurodegenerative changes, most research has relied on matching antemortem MRI with postmortem neuropathology (Jack et al., 2002; Jagust et al., 2008; Kantarci et al., 2012; Toledo et al., 2013; Josephs et al., 2017; Hanko et al., 2019; Dallaire-Théroux et al., 2019; Bejanin et al., 2019; De Flores et al., 2020b; Wisse et al., 2021a; Heywood et al., 2022; Mohanty et al., 2022; Denning et al., 2024). However, using MRI scans acquired several years before death creates a time gap during which pathogenic processes can develop. As a result, postmortem neuropathology evaluation may not completely match the neurodegeneration observed on antemortem MRI. Moreover, heterogeneity in MRI protocols and image quality across antemortem studies limits the ability to study MTL subregions (Ver Hoef et al., 2021; Wisse et al., 2021).

In contrast, there is no significant temporal gap between imaging and pathology when using postmortem imaging. In addition, it allows for long acquisition times, enabling the acquisition of high-resolution data. If the structure is isolated from the brain and scanned alone, it can even be scanned using preclinical scanner (i.e., 9.4 T or 11.7 T), yielding ultra-high-resolution images. In this framework, postmortem MRI constitutes a critical bridge between microscopic neuropathology and macroscopic *in vivo* imaging. By enabling direct correspondence between MRI data and histological analyses, it allows the validation of MRI-derived measures against underlying tissue alterations. It also facilitates the identification of disease- and proteinopathy-specific patterns of atrophy, thereby improving the interpretation of *in vivo* MRI biomarkers in terms of their underlying pathological substrates.

In this narrative review, we provide a comprehensive overview of postmortem MRI studies in the context of AD and related disorders (ADRD). In this context, postmortem MRI refers to imaging performed after death, either *in situ* (with the brain still in the skull) or *ex vivo* (after brain removal and fixation). We specifically focus on anatomical MRI approaches targeting volumetric and morphometric measures of MTL structures, reviewing methodological considerations from tissue preparation to MRI acquisition. Given the central role of MTL in neurodegenerative diseases, this review synthesizes postmortem MRI evidence on this region to provide a more granular characterization of disease- and proteinopathy-specific patterns of macroscopic neurodegeneration. While this review focuses on anatomical *ex vivo* MRI, we refer the interested reader to recent reviews on *ex vivo* diffusion MRI (Karat et al., 2024; Schilling et al., 2025).

3. What are the main advantages and disadvantages of postmortem MRI?

Compared to *in vivo* imaging, postmortem MRI allows for extended scanning times with no movement artifacts, such as cardiorespiratory or head movements, which are particularly problematic in patients with dementia. Additionally, it enables the use of specialized coils (Edlow et al., 2019; Scholz et al., 2021) with reduced distance from the sample. Altogether, these advantages allow for increasing the signal-to-noise ratio and images resolution. Finally, studies with a specific focus on a single brain region, such as the MTL, can make use of preclinical animal MRI scanners with significantly higher magnetic fields, as smaller excised brain samples fit into the smaller bore of these scanners. Collectively, these advantages have led to improved resolution for examining structures with greater precision as compared to *in vivo* imaging, as illustrated in Figure 1.

Compared to antemortem *in vivo* imaging, postmortem MRI enables a direct comparison between MRI and histology without significant time delay as observed in antemortem studies, during which pathology may further progress (Jack et al., 2002; Jagust et al., 2008; Kantarci et al., 2012; Josephs et al., 2017; Dallaire-Théroux et al., 2019; Hanko et al., 2019; Bejanin et al., 2019; De Flores et al., 2020b; Heywood et al., 2022; Mohanty et al., 2022; Denning et al., 2024).

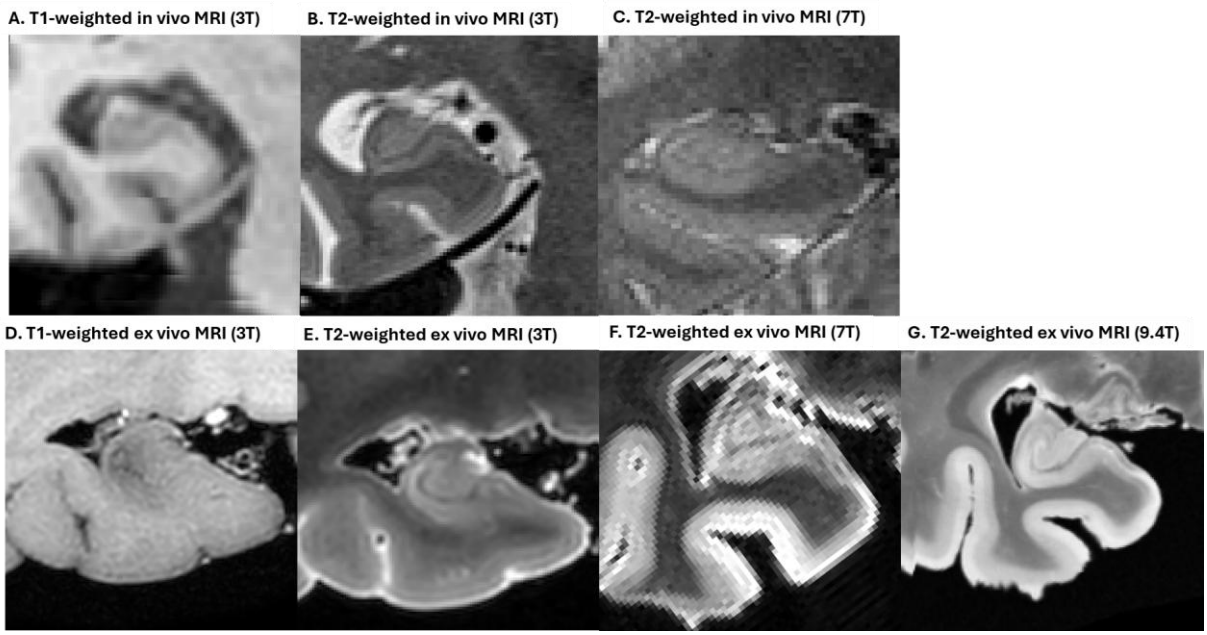

Figure 1. Comparison of medial temporal lobe (MTL) MRI acquired at comparable magnetic field strengths in vivo and ex vivo. *(A) In vivo T1-weighted MRI at 3T (University of Pennsylvania, Philadelphia, USA; 1.0 × 1.0 × 1.0 mm³; 5 min 13 s). (B) In vivo T2-weighted MRI at 3T (University of Pennsylvania, Philadelphia, USA; 0.4 × 0.4 mm² in-plane, 2.6 mm slice thickness; 7 min 12 s). (C) In vivo T2-weighted MRI at 7T (GIGA-CRC, University of Liège, Belgium; 0.42 × 0.42 mm² in-plane, 1.0 mm slice thickness; 7 min 33 s). (D) Ex vivo T1-weighted MRI at 3T (KU Leuven, Leuven, Belgium; 0.2 × 0.2 × 0.2 mm³; 1 h 44 min). (E) Ex vivo T2-weighted MRI at 3T (KU Leuven, Leuven, Belgium; 0.25 × 0.25 × 0.25 mm³; 1 h 56 min). (F) Ex vivo T2-weighted MRI at 7T (University of Pennsylvania, Philadelphia, USA; 0.4 × 0.4 × 0.4 mm³; 19 min). (G) Ex vivo T1-weighted MRI at 9.4T (University of Pennsylvania, Philadelphia, USA; 0.2 × 0.2 × 0.2 mm³; 16 h). Panels (A), (B), (F), and (G) were acquired from the same specimen.*

Compared to histology, postmortem MRI is less affected by distortion or tearing and provides a continuous high-resolution three-dimensional (3D) representation of brain anatomy, which can serve as a valuable reference for histological reconstruction (Adler et al., 2018; Mancini et al., 2020; Yushkevich et al., 2021a; Stouffer et al., 2023; Oltmer et al., 2023; Ravikumar et al., 2024; Casamitjana et al., 2024; DeKraker et al., 2025; Saifullah et al., 2025). In ADRD, diagnostic histopathology typically examines three standard coronal MTL levels (the amygdala, anterior hippocampus, and middle hippocampus) on

which classical staging systems are based. Compared to histology, postmortem MRI thus allows detailed investigation of anterior–posterior MTL involvement beyond these conventional sections.

Despite its many advantages, postmortem MRI, especially *ex vivo* MRI, also presents several limitations. Tissue alterations resulting from preparation procedures, such as brain extraction and fixation, can affect both image quality and tissue integrity. A few studies have compared *ex vivo* and *in vivo* MRI in the same subjects and are suggestive of tissue deformations *ex vivo*, but the exact differences are not well characterized yet (Kotrotsou et al., 2014; Wisse et al., 2016; Boon et al., 2019, also see section 6.1). Therefore, *ex vivo* MRI results should be interpreted with caution, as they may include volume changes or tissue deformations due to preparation methods. Moreover, *ex vivo* MRI generally requires access to specialized imaging facilities and dedicated image-processing pipelines, which can limit its widespread adoption. Another important challenge is the lack of standardized and widely applicable brain preparation protocols across studies.

4. Methodological aspects

This section focuses on how different research groups perform *ex vivo* anatomical MRI to visualize the MTL, either using whole-hemisphere preparations or excised MTL specimens. *Ex vivo* diffusion MRI is beyond the scope of this section; detailed recommendations and dedicated protocols have been reviewed elsewhere (Karat et al., 2024; Schilling et al., 2025). In addition, *in situ* postmortem MRI, which is conceptually closer to *in vivo* imaging, is not discussed in detail here. This approach has been mainly implemented within the Normal Aging Brain Collection Amsterdam (NABCA) cohort. Consequently, there is limited methodological variability in the literature, and comprehensive descriptions of the existing *in situ* protocols are already available (Jonkman et al., 2019).

4.1. Brain preparation

4.1.1. Postmortem delay

The postmortem delay, defined as the time between death and brain fixation, varied from a few hours to seven days in the studies included in this review (Table 1). A longer postmortem delay has been shown

to affect image contrast (Grinberg et al., 2008; Augustinack et al., 2014). Moreover, prolonged delays may influence fixation-induced brain swelling and distortion (Grinberg et al., 2008; Boon et al., 2019), which can, in turn, alter brain anatomy and thus affect volumetric assessment on MRI scans. An optimal postmortem delay has been suggested to be less than 6-10 hours (Grinberg et al., 2008; Augustinack and Van Der Kouwe, 2016). However, most studies reporting this information indicate a postmortem delay of less than 24 hours, as shorter delays are often constrained by logistical challenges. Of note, more than half of the studies reviewed do not report their postmortem delay (Table 1).

4.1.2. Fixation

Most protocols immersed their tissue in 4 or 10% formalin for approximately three or four weeks, which corresponds to a standard protocol. However, alternative fixation approaches have also been reported, including tissue first fixed *in situ* by perfusing 4% paraformaldehyde through both carotid arteries before submerging the tissue in 4% paraformaldehyde (Insausti et al., 2023; Ravikumar et al., 2024).

Ensuring complete fixation is essential for reliable MRI contrast, as uneven fixation can produce artifacts (Augustinack and Van Der Kouwe, 2016; Dadar et al., 2024a). While fixation time can affect MRI contrast, it does not significantly influence cortical thickness measurements (Khandelwal et al., 2024) nor hippocampal length (Tucker et al., 2025).

4.1.3. MTL Excision

In preclinical scanner studies, the MTL was excised from the brain after fixation. However, detailed descriptions of the dissection procedure are only provided in a limited number of studies (Yushkevich et al., 2009; Adler et al., 2014; Shih et al., 2023; Stouffer et al., 2023). The size of the excised specimen varied according to the diameter of the coil or the bore of the preclinical MRI scanner used, but in all cases, it was reported that the whole hippocampus was excised intact (Yushkevich et al., 2009; Adler et al., 2014; Ravikumar et al., 2021; Shih et al., 2023; Stouffer et al., 2023). This delicate step requires meticulous handling to avoid tissue tearing, given the fragility of the fixed brain tissue (Figure 2).

4.2. Scanning protocol

4.2.1.Scanning environment

The majority of protocols included immersing their tissue in perfluoropolyether oils as Fomblin (Solvay; Simons, 1949) or Fluorintert (3M; Caporiccio et al., 1989), before scanning (Table 1). These oils are composed solely of carbon, fluorine, and oxygen atoms and do not contribute to the MRI signal due to the absence of ^{1}H nuclei, thereby acting as a proton quencher. This approach reduces susceptibility artifacts arising from tissue-air interfaces. Of note, it has been demonstrated that prolonged immersion of tissue in these oils does not alter the tissue's anatomical or histological features (Hyare et al., 2008; Iglesias et al., 2018a). There are, however, reported alternatives, in which the specimens were scanned under vacuum (Augustinack et al., 2013), in formaldehyde (Oltmer et al., 2022), or in agar gels (Liou et al., 2024; Table 1).

4.2.2.Scanner and Field Strength

The type of scanner used varies significantly among research groups (Table 1). Approximately half of the groups included in this review use whole-body MRI scanners with field strengths of 3 to 7T (Augustinack et al., 2005; Fischl et al., 2009; Dawe et al., 2011; Kotrotsou et al., 2014, 2015; Makkinejad et al., 2019; Kenkhuis et al., 2019; Dawe et al., 2020; Sadaghiani et al., 2023; Khandelwal et al., 2024; Saifullah et al., 2025) while the other half use preclinical scanners at 7T (Coras et al., 2014), 9.4T (Fatterpekar et al., 2002; Yushkevich et al., 2009, 2021a; Adler et al., 2014, 2018; Wisse et al., 2016; Wisse et al., 2021b; De Flores et al., 2020a; Ravikumar et al., 2021, 2024), 11T (Stouffer et al., 2023), or 16.7T (Shih et al., 2023). Although higher field strengths generally improve resolution and signal-to-noise ratio, they may also accentuate magnetic susceptibility artifacts (Stanisz et al., 2005). University of Pennsylvania's group therefore implemented bias and non-uniformity correction and intensity normalization (Adler et al., 2018; Yushkevich et al., 2021a) using the N4ITK algorithm (Tustison et al., 2010). In addition, when using preclinical scanners, geometric distortions caused by gradient field non-linearity may occur; to correct for this, some teams perform registration between preclinical and clinical MRI postmortem scans (Yushkevich et al., 2021a).

4.2.3.Specimen preparation and air bubble management

The preparation of *ex vivo* brain specimens for MRI is a critical and challenging step, particularly due to the need to avoid air bubbles, which can compromise image quality (Figure 2). Air bubbles have been reported to be more difficult to remove when scanning whole hemispheres than smaller excised blocks (Augustinack et al., 2014). Unfortunately, relatively few studies provide detailed descriptions of their complete preparation protocols. Accordingly, this section primarily draws on the protocols developed by four research groups: Massachusetts General Hospital (Augustinack et al., 2014; Fischl et al., 2021), the University of Pennsylvania (Yushkevich et al., 2021b), Amsterdam UMC (Jonkman et al., 2019) and Zhejiang University (Zhu et al., 2025).

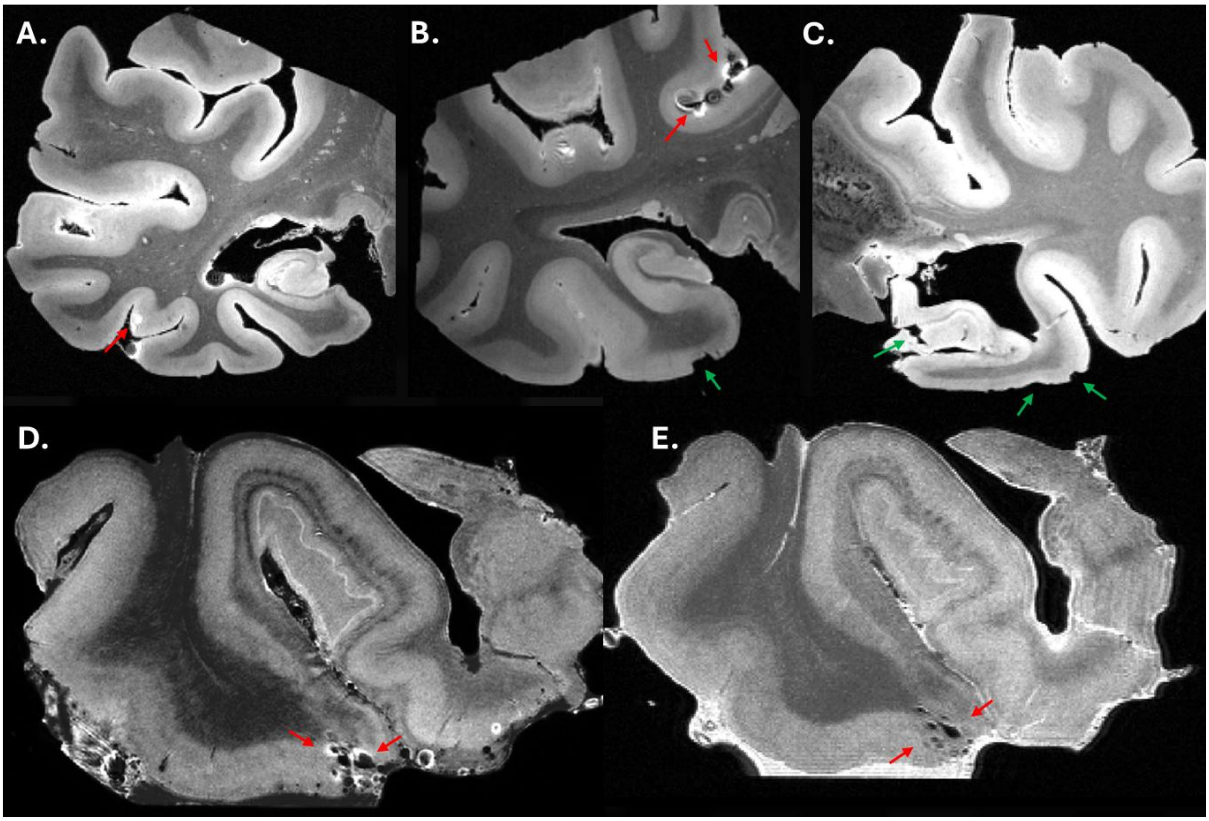

Figure 2. Examples of ex vivo MRI artifacts. *Air bubbles (red arrows, panels A, B, D, E) produce susceptibility-related signal loss and are more conspicuous on the T1-FLASH (Fast Low Angle Shot) image (panel D) than on the T2-RARE (Rapid Acquisition with Refocused Echoes) image (panel E) because gradient-echo sequences are more sensitive to magnetic-field inhomogeneities. Tissue tears (green arrows, panels B, C) result from specimen handling, specifically when extracting the MTL. Panels A–C were acquired on a Varian 9.4 T animal scanner*

(University of Pennsylvania, Philadelphia, USA) using a multi-slice spin-echo sequence (200 × 200 × 200 µm³; typical TR ≈ 9330 ms; TE ≈ 23 ms). Panels D–E were acquired on an 11.7 T Bruker MRI scanner (UCLouvain, Brussels, Belgium) using (D) a T1-weighted FLASH 3D sequence (TE = 4.425 ms, TR = 70 ms, flip angle = 20°, resolution 50 × 150 × 100 µm³) and (E) a T2-weighted RARE 3D sequence (TE = 18.5 ms, TR = 4 000 ms, RARE factor 5, resolution 100 × 100 × 200 µm³).

Across the four protocols reviewed, hemispheres are first fixed whole. Dissection of specific regions is subsequently performed on fixed tissue. In studies using preclinical MRI scanners, specimen selection is constrained by size considerations related to the diameter of the MRI scanner (Yushkevich et al., 2021b). After fixation, some teams rinse specimens in water for 24 hours to partially restore relaxation parameters altered by formalin fixation (Jonkman et al., 2019; Zhu et al., 2025). Additionally, multiple preparation protocols recommend removal of the pia mater, as this membrane can trap air and promote bubble formation (Augustinack et al., 2014; Fischl et al., 2021; Yushkevich et al., 2021b).

Before immersion in the scanning solution, the University of Pennsylvania's group places the specimen in a desiccator to remove residual moisture (Figure 3A-B-C; Yushkevich et al., 2021b), although absorbent paper has also been reported as an alternative method for drying the brain (Zhu et al., 2025). The brain is then immersed in Fomblin (rather than having the liquid poured over it) to reduce further bubble formation (Figure 3D-E-F; Yushkevich et al., 2021b). After immersion, vacuum can then be applied overnight to remove any remaining air (Fischl et al., 2021; Jonkman et al., 2019; Zhu et al., 2025). Gentle agitation of the holder overnight has also been reported to help extract air trapped in the sulci (Yushkevich et al., 2021b). Additional technical solutions reported include the use of degassing ports to remove bubbles from the container (Edlow et al., 2019).

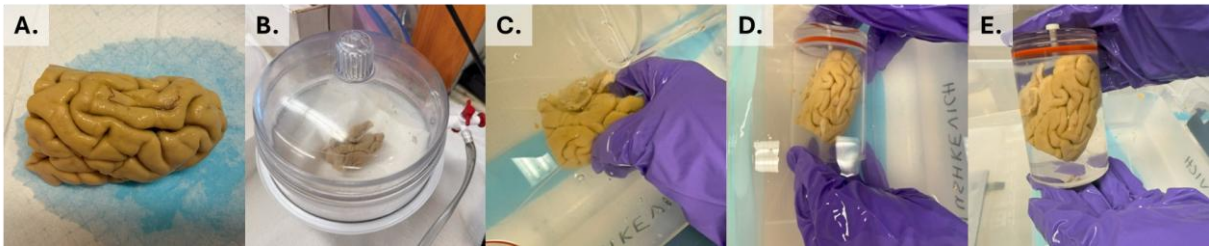

Figure 3. Example of specimen-preparation protocol for ex vivo MRI, as developed and performed at the University of Pennsylvania (Philadelphia, USA). *The medial temporal lobe (MTL) is first isolated (A). The tissue is then placed in a desiccator to dry (B). The tissue is subsequently immersed in Fomblin (rather than simply covered) and agitated to minimize bubble formation and allow any bubbles to escape (C). Some transient bubbles appear but quickly dissipate. The specimen is finally positioned in its container within the Fomblin bath (D-E).*

In general, it is recommended to place the specimen in its scanning container at least the day before imaging to minimize residual bubbles (Augustinack et al., 2014; Fischl et al., 2021). Throughout all steps, careful handling of both the brain and the surrounding liquid is essential to avoid generating new bubbles. In our group at UCLouvain, a 3D-printed bubble trap was designed to capture any remaining air without it adhering to the tissue. Note that even with all these precautions, air bubbles can still occur, particularly in deep sulci, where post-mortem decay gases can occur, as fixation primarily affects the upper cortical layers.

4.2.4.Coils

The coils used vary across research groups (Table 1). Approximately half of the studies reviewed use conventional coils that fit the shape of their tissue, while the other half have designed custom coils that conform more closely to the brain's surface. Custom-designed coils improve the signal-to-noise ratio and spatial resolution (Edlow et al., 2019). Most of the coils used, whether classical or custom-built, were solenoid coils that fully enclose the specimen. Solenoid coils have been shown to improve the signal-to-noise ratio (Augustinack et al., 2014).

Study	University	Postmortem delay	N of specimens	Whole hesmisphere or MTL	Fixative	Fixation duration	Scanner	Sequence	Coil	Scanning environment	Scan duration	Resolution
Fatterpekar et al. (2002)	Mount Sinai School of Medicine	Not specified	N = 2	MTL	Formalin	Not specified	9.4 T preclinical MRI scanner	Not specified	Classical coil	Fomblin	14h17	78 x 78 x 500µm
Augustinack et al. (2005)	Athinoula A. Martinos Center for Biomedical Imaging, Massachusetts General Hospital	< 24h	N = 5	MTL	Formalin (10%)	≥ 14 days	7T whole-body MRI scanner	gradient-echo T1	Custom-built solenoid coil	Heptacosafluoro-tributylamine	0h45	70 to 100µm isotropic
Yushkevich et al. (2009)	University of Pennsylvania	Not specified	N = 5	MTL	Not specified	≥ 21 days	9.4 T preclinical MRI scanner	multi-slice spin echo	Classical coil	Not specified	13h13 to 62h30	200µm isotropic
Fischl et al. (2009)	Athinoula A. Martinos Center for Biomedical Imaging, Massachusetts General Hospital	< 25h	N = 17	MTL	Formalin	Not specified	7T whole-body MRI scanner	multi-echo FLASH	Custom-built solenoid coil	Not specified	Not specified	100µm isotropic

Dawe et al. (2011)	Rush University Medical Center	7.2±4.5 h	N = 100	Whole hemisphere	Formaldehyde (4%)	22–200 days	3T whole-body MRI scanner	Multi-slice spin echo	Classical coil	Formaldehyde (4%)	~ 00h30	600 x 600 x 1500 µm
Kotrotsou et al., (2014)		Not specified	N = 37			Varying (variable of interest)						
Kotrotsou et al. (2015)		8 ± 5h	N = 165			49 ± 21 days						
Dawe et al. (2020)		8.8 ± 5.8h	N = 531			≥ 30 days						
Makkinejad et al. (2019)		8.6 ± 6.5h	N = 198			49.6 ± 24.0 days						
Saifullah et al. (2025)		9.9 ± 8h	N = 842			37.5 ± 18.1 days						
Adler et al. (2014)	University of Pennsylvania	Not specified	N = 1	MTL	Formalin	≥ 21 days	9.4 T preclinical MRI scanner	multi-slice spin echo	Classical coil	Perfluoropolyether	13h33	160µm isotropic
Coras et al. (2014)	University Hospital Erlangen	Not specified	N = 15	MTL	Formalin (4%)	Not specified	7T preclinical MRI scanner	T2	Classical coil	Not specified	14h to 38h	Not specified
Wisse et al. (2016)	University of Pennsylvania	Not specified	N = 15	MTL	Formalin (10%)	38.0 ± 17.7 days	9.4 T preclinical MRI scanner	multi-slice spin echo	custom-built coil	Fomblin	Not specified	200µm isotropic

Adler et al. (2018)	University of Pennsylvania	Not specified	N = 31	MTL	Formalin	≥ 21 days	9.4 T preclinical MRI scanner	multi-slice spin echo	Classical coil (N = 9) & custom built coil (N = 23)[1]	MRI-neutral fluid	7h30 to 16h00	200µm isotropic
De Flores et al. (2020a)			N = 9[2]						Classical coil			
Kenkhuis et al. (2019)	Leiden University Medical Center	Not specified	N = 35	Whole hesmisphere	Formalin (4%)	28 days	7T whole-body MRI scanner	T2*-weighted[3]	Classical coil	Fomblin	Not specified	3000µm isotropic
Yushkevich et al. (2021)	University of Pennsylvania	Not specified	N = 18	MTL	Formalin Or Paraformaldehyde (4%)	≥ 21 days	9.4 T preclinical MRI scanner	multi-slice spin echo	custom-built coil	Fomblin	Not specified	200µm isotropic
Ravikumar et al. (2021)			N = 29									
Ravikumar et al. (2024)			N = 55									

[1] One specimen was further excluded
[2] Same specimens as Adler et al. (2018)
[3] The sequence is referred as a T2-weighted sequence in the article, but acquisition parameters correspond to a T1 FLASH sequence.

Llamas-Rodríguez et al. (2022) Oltmer et al. (2022) Oltmer et al. (2023)	Athinoula A. Martinos Center for Biomedical Imaging, Massachusetts General Hospital	< 24h	N = 10	MTL	Formalin (10%) Or Paraformaldehyde (2 %)	Not specified	7T whole-body MRI scanner	T1-FLASH	custom-built solenoid coil	2% paraformaldehyde or Fomblin	18 to 22h	100µm isotropic
Shih et al. (2023)	University of Southern California, Los Angeles	5.3h - 7 days	N = 10	MTL	Formalin (10%)	15-48 hours [4]	16.4T preclinical MRI scanner	T1 FLASH & T2 RARE	Classical coil	Fomblin	3h50	50µm and 75µm isotropic
Stouffer et al. (2023)	John Hopkins University	Not specified	N = 2	MTL	Formalin (10%)	Not specified	11T preclinical MRI scanner	Not Specified	Not Specified	Not Specified	Not specified	125 µm isotropic
Sadaghiani et al. (2023)	University of Pennsylvania	Not specified	N = 33	Whole hesmisphere	Formalin (10%)	≥ 30 days	7T whole-body MRI scanner	3D T2	Custom build-coil	Fomblin	2h	300µm isotropic
Khandelwal et al. (2024)			N = 135									

[4] The fixation timing reported in this article (in hours) is unusual compared to the standard typically expressed in days. This might be an error, but the information is included as reported for transparency.

Liou et al. (2024)	University of Pittsburgh	Mean = 8.7h	N = 66	Whole hemisphere	Formalin (10%)	≥ three weeks	7T whole-body MRI scanner	T1w, T2w, T2* GRE	Classical coil	1.5% agar & 30% sucrose	0h32 to 0h46	370 to 410 µm isotropic

Table 1. Overview of ex vivo MRI protocols, including postmortem delay and fixation procedures for ex vivo MRI and scanner type, sequence, coil, and scanning environment, scanning duration, and resolution for studies investigating the human MTL. Abbreviations: *FLASH: Fast Low Angle Shot; GRE : Gradient Recall Echo; MRI : Magnetic Resonance Imaging; RARE : Rapid Acquisition with Refocused Echoes; T : tesla.*

4.2.5.Sequences

As this review focuses on anatomical MRI, this section is dedicated to T1- and T2-weighted sequences commonly used in *ex vivo* imaging. Other MRI modalities, such as diffusion, provide complementary microstructural information and have been summarized in recent reviews (Karat et al., 2024; Schilling et al., 2025).

The choice of sequences in *ex vivo* MRI is influenced by the effects of formalin fixation on brain tissue. Formalin fixation, commonly used in *ex vivo* MRI, induces significant biophysical changes that alter image contrast. One of the most consistently reported effects in the literature is the reduction of both T1 and T2 relaxation times, particularly in gray matter (Tovi and Ericsson, 1992; Blamire et al., 1999; Pfefferbaum et al., 2004). The shortening of T1 reduces the differentiation between gray and white matter on T1-weighted images, making them visually resemble proton density–weighted images. Similarly, T2 contrast is diminished, and T2* effects become dominant (Tovi and Ericsson, 1992).

Among the most used sequences in *ex vivo* MRI, T1-weighted Fast Low Angle Shot (FLASH) and T2-weighted Rapid Acquisition with Refocused Echoes (RARE) offer complementary contrast mechanisms (Table 2). T1-weighted FLASH sequences are frequently used for their ability to produce images that combine favorable T2* and proton density contrast (Augustinack et al., 2014). These sequences typically use a relatively short echo time ((TE) ranging from 7.8 to 32 ms) and a low flip angle (5° to 30°; Table 2). Although originally designed to rely on T1 contrast through differences in longitudinal relaxation properties, in the context of *ex vivo* MRI, the contrast is largely influenced by T2* effects and proton density. Additionally, since FLASH is a gradient-echo sequence without refocusing pulses, it is particularly sensitive to magnetic field inhomogeneities and susceptibility artifacts, which may result in signal loss or geometric distortions (Manson et al., 2022).

In contrast, T2-weighted RARE sequences (based on spin-echo principles) use 180° refocusing pulses to compensate for local magnetic field inhomogeneities, thereby reducing susceptibility artifacts. These sequences generate T2-weighted contrast based on transverse relaxation and are more robust in fixed

tissue. Typical *ex vivo* RARE protocols use short TEs (13-383 ms) and long repetition times ((TR) 30000–5000 ms; Table 2).

Despite differences in sequence type and acquisition parameters, the visual appearance of *ex vivo* MRI scans often remains similar across protocols (Figure 4; Augustinack and Van Der Kouwe, 2016; Shih et al., 2023; Dadar et al., 2024a). This is likely due to the convergence of contrast sources after fixation, involving multiple mechanisms, including protein cross-linking (Blamire et al., 1999; Dawe et al., 2009) and immobilization of water molecules, which may lead to a reduction of the T2 relaxation time (Pfefferbaum et al., 2004). Another possible explanation for this is that the decomposition of the myelin phospholipid structure by formalin somewhat counteracts the general reductive effect of the fixation procedure on relaxation times (Tovi and Ericsson, 1992).

353

354

T1 SEQUENCES					
Study	**University**	**Sequence**	**TR**	**TE**	**Flip angle**
Augustinack et al. (2005)	Athinoula A. Martinos Center for Biomedical Imaging, Massachusetts General Hospital	T1 FLASH	20 ms	7.8 ms	5 - 25°
Fischl et al. (2009) Augustinack et al. (2013)	Athinoula A. Martinos Center for Biomedical Imaging, Massachusetts General Hospital	T1 FLASH	40ms	8 – 32 ms	15 - 25°
(Kenkhuis et al., 2019)	Leiden University Medical Center, Leiden, the Netherlands	T1 FLASH[5]	36 ms	20 ms	10°
(Llamas-Rodríguez et al., 2022; Oltmer et al., 2023, 2022)	Athinoula A. Martinos Center for Biomedical Imaging, Massachusetts General Hospital	T1 FLASH	45-60 ms	10.75 – 30 ms	20-25°
Shih et al. (2023)	University of Southern California, Los Angeles	T1 FLASH	40 ms	12ms	30°
T2 SEQUENCES					
Study	**University**	**Sequence**	**TR**	**TE**	
(Yushkevich et al., 2009; Adler et al., 2014; Wisse et al., 2016; Adler et al., 2018; De Flores et al., 2020a; Ravikumar et al., 2021, 2024)	University of Pennsylvania	Multi-slice spin echo	4000 -5000 ms	21-26 ms	
(Dawe et al., 2011, 2020; Makkinejad et al., 2019; Saifullah et al., 2025) 2011	Rush University Medical Center	Multi-slice spin echo	3600 ms	13-52 ms	
(Sadaghiani et al., 2023;	University of Pennsylvania	Multi-spin echo	3000 ms	383 ms	

[5] The sequence is referred as a T2-weighted sequence in the article, but acquisition parameters correspond to a T1 FLASH sequence.

Khandelwal et al., 2024)				

Table 2. Overview of ex vivo MRI detailed sequences for studies investigating human MTL. *Abbreviations: FLASH: Fast Low Angle Shot; GRE: Gradient Recall Echo; MRI: Magnetic Resonance Imaging; RARE: Rapid Acquisition with Refocused Echoes; T: tesla; TE=echo time; TR=repetition time.*

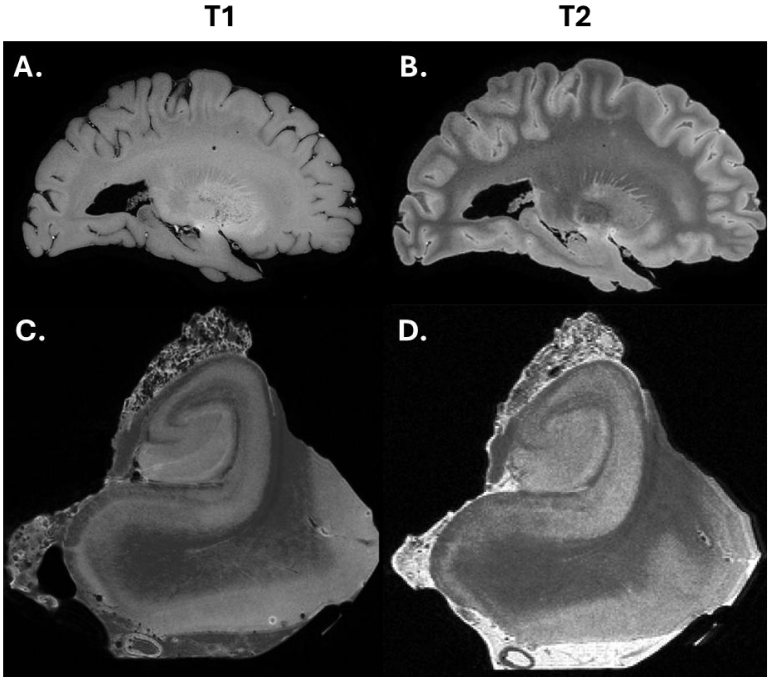

Figure 4. Comparison of ex vivo T1- and T2-weighted sequences *for whole-hemisphere (A–B) and medial temporal lobe (MTL; C–D) scans, illustrating hyperintense gray matter and hypointense white matter in two different datasets. Whole-hemisphere scans were acquired at KU Leuven (Leuven, Belgium) using a T2-weighted sequence (250 x 250 x 250 µm³; TR = 3 000s ms; TE = 200 ms) and a T1-weighted sequence (200 x 200 x 200 µm³; TR = 17.68 ms ; TE = 8.36 ms. MTL scans were acquired at UCLouvain (Brussels, Belgium) on an 11.7 T Bruker MRI using a T2-weighted RARE sequence (100 × 100 × 200 µm³; TR = 4 000 ms; TE = 18.5 ms; RARE factor = 5) and a T1-weighted FLASH sequence (50 × 150 × 100 µm³; TR = 70 ms; TE = 4.425 ms; flip angle = 20°).*

4.3. Matching MRI and histology

Efforts have been made to help with co-registration between MRI scans and histological slices. For instance, some teams report using a mold designed to tightly fit the MTL specimen during scanning, to stabilize the specimen and guide tissue sectioning for neuropathology. This ensures that MRI and histological slides are aligned along the same axis, thereby reducing the complexity of subsequent MRI–histology registration (Yushkevich et al., 2021a; Dadar et al., 2024a). In our centers (UCLouvain/KULeuven), a custom-made cutting apparatus with an integrated mirror was used to

produce 0.5cm slices for histological analysis. This allows orientation of the specimen using a 3D reconstruction model generated during the scan as a guideline for positioning the specimen for cutting, enabling a similar anatomical orientation between the scan and the histological sections.

5. Applications of postmortem MRI

5.1. Improving segmentation protocols

Because postmortem MRI allows for ultra-high-resolution imaging, it contributes to a more precise understanding of the detailed anatomy of the brain. This enables the identification of subtle anatomical structures but also supports the development of more accurate segmentation protocols for *in vivo* applications. These postmortem datasets are particularly valuable when made publicly available either for MTL scans (Adler et al., 2018; Ravikumar et al., 2024; DeKraker et al., 2025) or whole-hemisphere scans (Amunts et al., 2013, 2020; Tendler et al., 2022; Zhu et al., 2025), since they provide the broader scientific community with unique access to high-resolution images, thereby fostering a deeper understanding of e.g. MTL anatomy.

Since hippocampal subfield definitions are grounded in cytoarchitecture, direct comparison between histology and postmortem MRI scans of the same tissue section allows for the identification of MRI-visible features that reflect cytoarchitectonic boundaries or landmarks to approximate cytoarchitectonic boundaries. For instance, comparative analyses of *ex vivo* MRI and histological slices clarified the nature of the so-called “dark band”, a hypointense line in high-resolution T2-weighted images (Figure 5; De Flores et al., 2020a). Contrary to some prior assumptions, this band was shown to correspond solely to the Cornu Ammonis (CA) stratum lacunosum-moleculare (SLM), and not the stratum radiatum of CA nor the molecular layer of the dentate gyrus (Figure 5; De Flores et al., 2020a). Thus, integrating postmortem MRI with histology allows linking image features to their underlying anatomy, providing a more precise framework for interpreting *in vivo* MRI measurements.

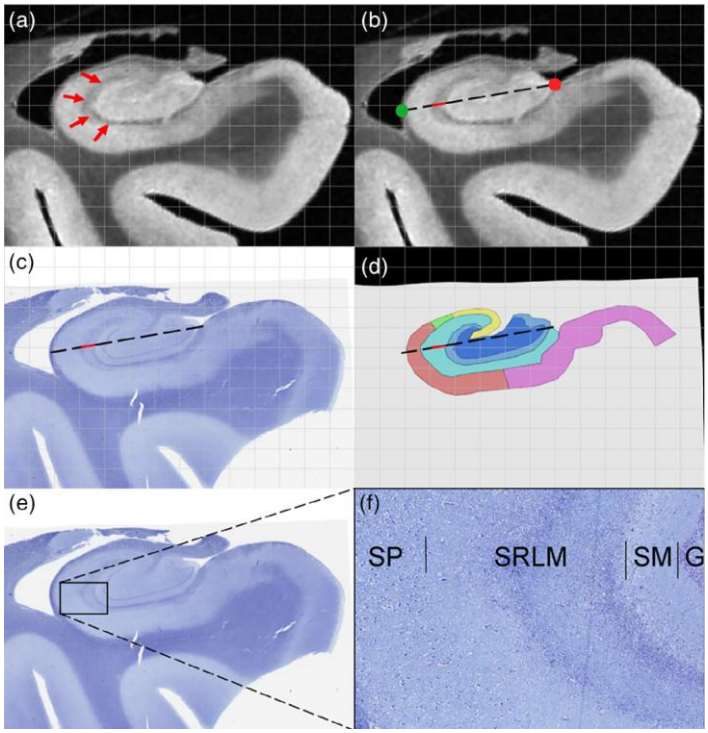

Figure 5. Characterization of the hippocampal dark band. This figure illustrates how direct comparison between ex vivo MRI and histology enables precise anatomical interpretation of MRI-visible features. *Dark band thickness was measured along a dashed line from the medial anchor point (red circle) to the most lateral hippocampal point (green circle). Corresponding histology (c) and segmentation (d) were registered to MRI for the same measurement. Regions labeled: CA1 (red), CA2 (green), CA3 (yellow), DG-SM (light blue), DG-G/H (dark blue), SRLM (cyan), SUB (pink). Figure and caption reproduced with permission from* De Flores et al. (2020a)

Abbreviations: CA=cornu ammonis; DG-SM=dentate gyrus stratum moleculare; DG-SM=dentate gyrus granular cell layer/Hilus; SRLM=stratum radiatum lacunosum moleculare; SUB=subiculum; SP= stratum pyramidale; SM=stratum moleculare; G= granule cell layer

In addition, comparing *ex vivo* MRI and histology also revealed a consistent pattern in the appearance and disappearance of subfields along the anterior-posterior MTL axis; for instance, CA1 has been shown to appear posterior to the subiculum (De Flores et al., 2020a). Additional analyses were performed in Tucker et al. (2025), providing further characterization of hippocampal anatomy in individuals with and without neurodegenerative diseases, including a clear delineation of the subicular complex boundaries, as well as CA3 boundaries and the transition between CA1 and the subiculum. These results offer new insights into the internal hippocampal architecture and provide clear guidelines to improve *in vivo* segmentation in these populations (De Flores et al., 2020a; Tucker et al., 2025)

Beyond the hippocampus, postmortem MRI has also been useful in refining our understanding of extra-hippocampal MTL structures. This technique allowed the prediction of location and the boundaries of BA35 and the perirhinal cortex as a whole (Augustinack et al., 2013) on *in vivo* MRI. It also allowed for segmenting entorhinal cortex (ERC) subfields, initially defined in histology, on postmortem MRI (Figure 6; Llamas-Rodríguez et al., 2022; Oltmer et al., 2023; Ravikumar et al., 2024). These advances were only possible through direct comparison between histological sections and postmortem MRI data acquired in the same subjects. While detailed segmentation of ERC subfields is not yet implemented in *in vivo* settings, this body of work lays a solid foundation for the development of future *in vivo* segmentation protocols using lower-resolution *in vivo* MRI. A similar approach was previously applied tohippocampal subfields (Iglesias et al., 2015) and amygdala nuclei (Saygin et al., 2017), which were first defined on *ex vivo* scans before being implemented in automatic segmentation tools for *in vivo* MRI as FreeSurfer (Fischl, 2012).

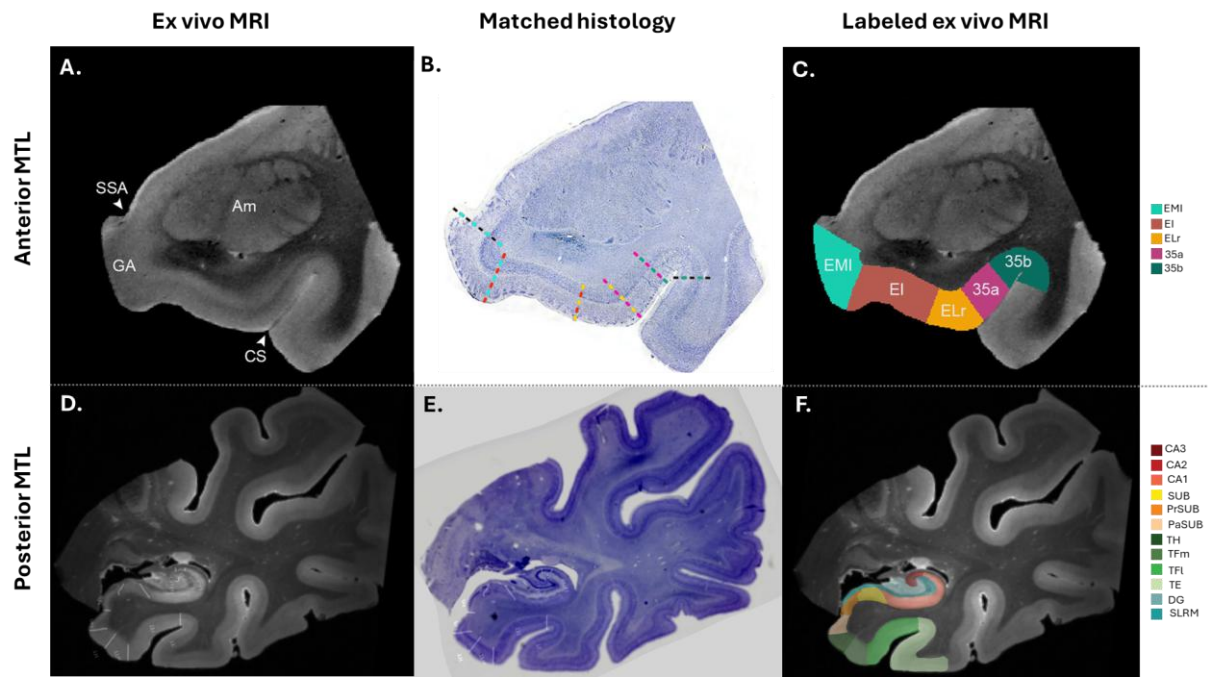

Figure 6. Direct comparison of histological sections and ex vivo MRI used to develop new postmortem atlases. *A–C: anterior MTL and entorhinal cortex atlas* (Oltmer et al., 2023). *D–F: posterior MTL and whole-MTL atlas* (Ravikumar et al., 2024, 2021). *Histology panels (B,E) show subfield boundaries guiding segmentation of ex vivo scans (C,F). Panels A–C reproduced with permission from Oltmer et al. (2023); panels D–F courtesy of the University of Pennsylvania (Philadelphia, USA) .*

Abbreviations (Panels A–C): AM = amygdala; CS = collateral sulcus; EC = entorhinal caudal; EI = entorhinal intermediate; ELr = entorhinal lateral rostral; EMI = entorhinal medial intermediate; GA = gyrus ambiens; SSA

= sulcus semi-annularis; 35a/b = Brodmann area 35; CA1–3 = Cornu Ammonis 1–3; DG = Dentate Gyrus; SUB = Subiculum; PrS = Presubiculum; PaS = Parasubiculum; TH = area TH; TFm = area TF medial; TFl = area TF lateral; TE = inferior temporal cortex

5.2. Studying the impact of proteinopathies on brain structure

Because postmortem MRI can be directly compared with neuropathological assessments from the same brain without a time interval, it provides a unique framework to investigate the impact of specific proteinopathies on MTL morphometry.

The most common approach to achieve this consists of combining imaging-derived morphometric measures, such as regional volumes or cortical thickness, with quantitative or semi-quantitative neuropathological measures (e.g., pathology scores or burden) in the same region, typically through spatially grounded association analyses. This was first performed with global hippocampal volume (Dawe et al., 2011, 2020; Kotrotsou et al., 2015; Yu et al., 2020). Subsequently, this approach was extended to MTL regions that are difficult or impossible to reliably assess *in vivo*, leveraging the higher spatial resolution and anatomical specificity of postmortem MRI. Importantly, these approaches do not aim to infer causality, but rather to establish robust spatial correspondences between imaging and histopathology, thereby providing critical validation and biological interpretation of in vivo MRI markers

Beyond regional morphometry, postmortem MRI also enables the study of MTL structures in 3D, in contrast to histology, which is inherently limited to two-dimensional tissue sections. Several research teams have developed 3D computational atlases of the MTL and its subregions (Adler et al., 2018; Yushkevich et al., 2021a; Stouffer et al., 2023; Ravikumar et al., 2024; Dawe et al., 2011; Yushkevich et al., 2009; Llamas-Rodríguez et al., 2022; Oltmer et al., 2023). These atlases allow for a comprehensive and detailed visualization of MTL structures along all axes, including the anterior–posterior axis. Using this framework combined with serial immunohistochemistry, several studies have identified spatial gradients of tau pathology within the MTL, such as an anterior–posterior tau gradient within the MTL (Yushkevich et al., 2021a; Stouffer et al., 2023; Ravikumar et al., 2024). Moreover, such 3D pathology maps may serve as valuable spatial references for *in vivo* MRI analyses by helping to identify

pathological hotspots that should be prioritized in the search for *in vivo* biomarkers (Yushkevich et al., 2021a), as recently done by Brown et al. (2024).

Together, morphometry–pathology correlations and 3D neuropathology heat maps have enabled detailed analysis of pathology–structure relationships within fine-grained MTL regions, including hippocampal and ERC subfields, as well as cortical layers of the ERC and perirhinal cortices, as detailed in the following sections.

5.2.1. The hippocampus

Within the hippocampus, tau pathology has been shown to predominantly affect CA1 and the subiculum, based on both volumetric and thickness measurements (Table 3; Ravikumar et al., 2021, 2024; Bouwman et al., 2025) and tau heat maps (Table 3; Yushkevich et al., 2021a; Ravikumar et al., 2024). Interestingly, TDP-43 pathology appears to affect the same regions (Wisse et al., 2021b; Ravikumar et al., 2024; Wesseling et al., 2025). In contrast, age-related effects have been more pronounced in the DG, though CA1 was also affected (Adler et al., 2018). Aβ and α-synuclein, however, have not shown significant associations with hippocampal subfield volumes or thickness (Ravikumar et al., 2021; Wisse et al., 2021b).

Beyond subfield-level analyses, high-resolution *ex vivo* MRI has enabled the visualization of hippocampal cortical layers, including the "dark band", corresponding to the SRLM. This layer is difficult to detect with conventional *in vivo* MRI, yet it is among the earliest affected regions by tau pathology in AD (Thal et al., 2000). Postmortem studies have demonstrated early thinning of the SRLM, with this atrophy correlating with tau burden (Wisse et al., 2021b; Ravikumar et al., 2021, 2024). In contrast, TDP-43 appears to primarily affect the pyramidal layer of CA in AD, which is more accessible in *in vivo* imaging (Ravikumar et al., 2024).

In summary, although tau and TDP-43 affect largely overlapping hippocampal subfields, they preferentially involve different cortical layers within these subfields. This suggests that *in vivo* studies aiming to distinguish ADNC from LATE-NC or mixed ADNC+LATE-NC should move beyond

hippocampal subfield volumetry and instead target hippocampal cortical layers. However, as detailed in Section 5.3, reliably visualizing these layers likely requires an in-plane resolution of 0.7 to 0.5 mm, which is achievable at 3T in optimized protocols (Su et al., 2017; Wang et al., 2026) but is more realistically attainable with ultra-high-field 7T MRI (Kerchner et al., 2012; Wisse et al., 2012; Boutet et al., 2014; Parekh et al., 2015; Yushkevich et al., 2015; Berron et al., 2017).

5.2.2.MTL cortices

Outside the hippocampus proper, MTL cortical areas, including the ERC and the transentorhinal cortex (Brodmann area 35 (BA35)), are also of particular interest due to their early involvement in AD. While the ERC is often treated as a homogeneous structure in *in vivo* MRI, it contains several subfields that are currently not distinguishable using standard imaging techniques. Postmortem high-resolution MRI has been used to characterized these ERC subfields (Figure 6) and their vulnerability to tau pathology (Llamas-Rodríguez et al., 2022; Oltmer et al., 2023, 2022). It was shown that tau pathology predominantly affects the lateral ERC (Llamas-Rodríguez et al., 2022; Oltmer et al., 2023, 2022; Ravikumar et al., 2024), highlighting ERC's heterogeneity and potential as a biomarker for early disease detection. Interestingly, TDP-43 has also been associated with lateral ERC pathology in AD (Llamas Rodríguez et al., 2024). From an *in vivo* biomarker perspective, these findings suggest that future high-resolution MRI studies should explicitly target the lateral ERC. In the absence of *in vivo* segmentation guidelines for ERC subfield segmentation, a pragmatic intermediate step for *in vivo* studies would be to subdivide the ERC into lateral and medial portions (Maass et al., 2015; Tran et al., 2022), which may improve sensitivity to both tau- and TDP-43-related neurodegeneration.

In parallel, BA35 is one of the earliest cortical regions to accumulate neurofibrillary tangles (NFTs) in AD (Braak and Braak, 1991). However, BA35 is difficult to evaluate *in vivo* due to inter-individual anatomical variability (Ding and Van Hoesen, 2010). Postmortem MRI studies have confirmed that BA35 undergoes early atrophy and that this atrophy is closely associated with tau pathology (Wisse et al., 2021b; Sadaghiani et al., 2023; Ravikumar et al., 2024).

5.2.3. The amygdala

Finally, the amygdala has been far less studied in the context of neurodegenerative diseases but has garnered increasing interest in recent years (Stouffer et al., 2024). However, the amygdala is affected early in AD (Braak and Braak, 1991; Yushkevich et al., 2021a; Salman et al., 2024) and other neurodegenerative conditions, including LATE-NC (Nelson et al., 2019, 2023), FTLD with TDP-43 inclusions (Brettschneider et al., 2014; Young et al., 2022) and α-synuclein, especially in the context of AD (Braak et al., 2002; Gawor et al., 2024). Yet, only a few studies have investigated the impact of proteinopathies on amygdala atrophy using postmortem imaging. Findings regarding the effect of proteinopathies on amygdala volume are mixed (Table 3). Some studies report an association between tau pathology and medial amygdala volume (Stouffer et al., 2023), while others suggest an impact on the central and basal nuclei (Makkinejad et al., 2019). To our knowledge, only a few studies have specifically examined the effect of TDP-43 pathology on postmortem amygdala volume (Liou et al., 2024), suggesting that TDP-43 has a more widespread effect than tau, involving basolateral and superficial nuclei of the amygdala (Makkinejad et al., 2019; Wesseling et al., 2025). These patterns indicate that differential involvement of amygdala nuclei may represent a promising *in vivo* biomarker to distinguish AD from LATE-NC, in which the amygdala appears to be more globally affected.

Overall, postmortem MRI allows the study of the contribution of different neuropathologies in more detail on MTL subregions that are difficult to measure *in vivo*. This suggests that improving *in vivo* imaging resolution in the future may guide the development of early and specific MRI biomarkers for the different proteinopathies. More broadly, these approaches provide a spatially grounded framework linking imaging and histopathology, which remains essential for biomarker validation and interpretation.

Study	University	Methodology	Postmortem MRI type	Regions most associated with the NFT burden	Anterior-posterior gradient
Wisse et al. (2021b)	University of Pennsylvania	Thickness analyses	*Ex vivo* MTL	BA35, SRLM	Not assessed

Ravikumar et al. (2021)	University of Pennsylvania	Volume analysis	*Ex vivo* MTL	ERC, CA1, SLRM	Not assessed
Llamas-Rodríguez et al. (2022)	Athinoula A. Martinos Center for Biomedical Imaging, Massachusetts General Hospital	Thickness analysis	*Ex vivo* MTL	lateral ERC subfields	NFT-structure association with Posterior-lateral ERC
Sadaghiani et al. (2023)	University of Pennsylvania	Thickness analysis	*Ex vivo* whole hemisphere	BA35, ERC, SUB, PHG	Not assessed
Ravikumar et al. (2024)	University of Pennsylvania	Thickness analysis	*Ex vivo* MTL	BA35, ERC, CA1, SUB, SRLM.	NFT-structure association with the anterior MTL cortex and the global hippocampus
Khandelwal et al. (2024)	University of Pennsylvania	Thickness analysis	*Ex vivo* whole hemisphere	BA35, ERC	Not assessed
Bouwman et al. (2025)	Amsterdam UMC	Thickness analysis	*In situ*	CA1, SUB, ERC	Not assessed

Table 3. Overview of postmortem MRI studies investigating the impact of tau pathology in the MTL. *Abbreviations: CA1, Cornu Ammonis 1; SUB, Subiculum; SLRM, Stratum Radiatum Lacunosum Moleculare; BA35, Brodmann Area 35; ERC, Entorhinal Cortex; PHG, Parahippocampal Gyrus*.

5.3. Improving *in vivo* MRI sequences

Beyond its contributions to the development of segmentation protocols and to a deeper understanding of how proteinopathies drive regional atrophy, postmortem MRI also offers valuable insights for optimizing *in vivo* MRI sequences.

As illustrated in Figure 7, De Flores et al. (2020a) demonstrated that although two distinct appearances of the hippocampal tail can be observed in the coronal plane, re-slicing the tail orthogonally to its curvature, whether it bends medially or superiorly, consistently results in a uniform appearance (De Flores et al., 2020a). This finding suggests that anatomical variability in hippocampal shape and

subfields composition may, at least in part, be attributable to tail angulation (Adler et al., 2018; De Flores et al., 2020a). Since such re-slicing is only feasible with isotropic data, these results highlight the importance of using isotropic rather than anisotropic sequences in *in vivo* imaging.

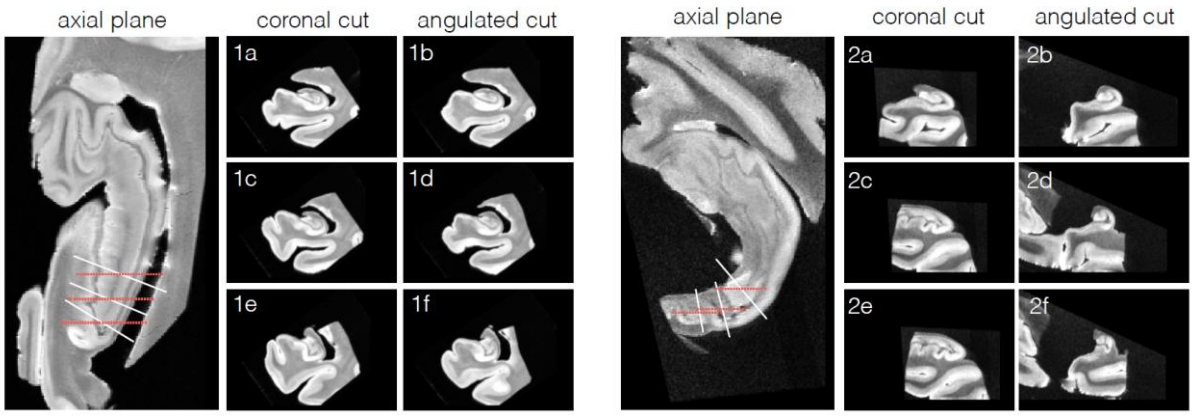

Figure 7: Hippocampal Tail Morphology. *Examples of tail sections of two specimens are shown, resliced perpendicular to the hippocampal long axis at three locations (white lines in the axial plane) as well as sliced in the typical coronal cut at approximately the same location for comparison (red dashed lines in the axial plane). It can be observed that in the two specimens with differing angulations of the tail, the resliced sections have a body-like appearance, in some sections with a slight clockwise rotation (e.g., 1f). The comparison of these angulated cuts with the typical coronal cut shows only small differences in example 1, in which the tail only shows a slight angulation. The differences are more striking, for example, 2, where the angulation of the tail approximates 90 degrees. It was observed that in some specimens, in the most posterior resliced section, there is almost no DG present; an example is presented in 2f. The appearance of the hippocampus in such sections slightly deviates from the body-like appearance. Figure and caption reproduced from Adler et al. (2018) with permission.*

Furthermore, based on group-average analyses, postmortem MRI has shown that a resolution of at least 0.77 mm in cognitively healthy older adults, and at least 0.52 mm in older adults with AD, is required to reliably identify the full SRLM layer (Figure 8A; Adler et al., 2018). Similarly, it was shown that a resolution of at least 100 µm is required to distinguish the microstructural layers of the MTL (Figure 8B; Fischl et al., 2009), including layer II, with the characteristic cell islands, of the ERC (Figure 8C; Augustinack et al., 2005) and the distinct laminae of the dentate gyrus (Figure 8D; Shih et al., 2023). These findings underline the need to refine *in vivo* sequences toward higher resolution and isotropy to better capture the cytoarchitectonic complexity of the MTL.

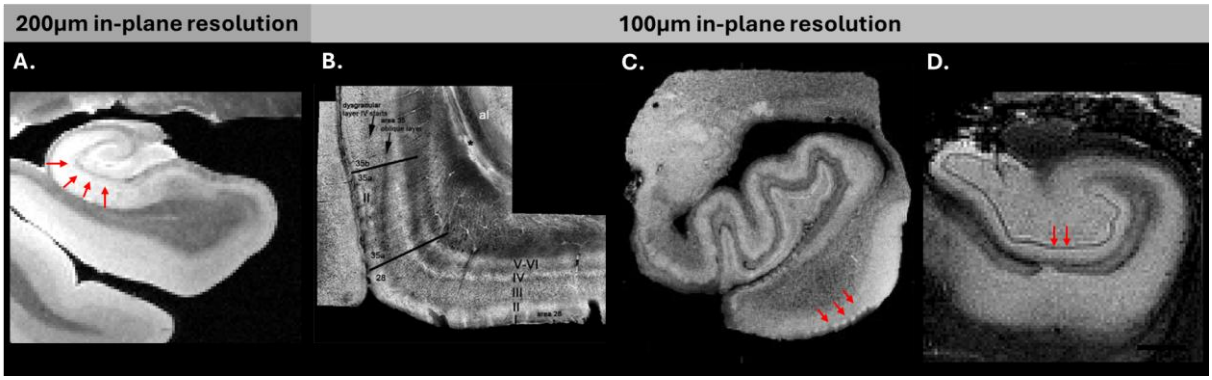

Figure 8. Minimum MRI resolution to visualize key medial temporal lobe (MTL) structures. *(A) Dark band corresponding to the stratum radiatum/lacunosum/moleculare (SRLM; red arrows, courtesy of the University of Pennsylvania, Philadelphia, USA). The example shown was acquired at 200 µm isotropic resolution - well above the minimum needed - but prior work indicates that a resolution of at least 0.77 mm in cognitively healthy older adults and 0.52 mm in older adults with Alzheimer's disease is sufficient to reliably identify the full SRLM* (Adler et al., 2018)*. (B) Cortical microstructural layers of the MTL (Roman numerals), reproduced with permission from Augustinack et al. (2014). (C) Layer II "islands" of the entorhinal cortex (red arrows), reproduced with permission from Augustinack et al. (2005). (D) Granule cell layer of the dentate gyrus (red arrows), reproduced with permission from Shih et al. (2023). At least 100 µm resolution is required to distinguish cortical layers, layer II entorhinal "islands", or the granular cells of the dentate gyrus.*

5.4. Understanding microstructural properties of the MTL

While this review specifically focuses on anatomical postmortem MRI, it is worth noting that other postmortem MRI approaches have been developed to probe microstructural and quantitative properties of brain tissue, providing a potential bridge between microscopic pathology and macroscopic structural changes.

For example, diffusion postmortem MRI has provided the opportunity to examine the hippocampus in detail, including its internal connectivity and mesoscopic organization, such as the visualization of the perforant pathway (Augustinack, 2010). Postmortem diffusion MRI can offer more specific insights into hippocampal microstructure, including laminar-specific characteristics (Scholz et al., 2021; Shih et al., 2023; Zhao et al., 2025), suggesting specific alterations in the strata lacunosum and radiatium (Zhao et al., 2025). A recent review has summarized the methodologies and main findings in this area (Karat et

al., 2024). However, these methods face significant technical challenges in fixed tissue. Formalin fixation reduces the diffusion of water molecules, which diminishes contrast and can limit the interpretability of diffusion metrics compared to *in vivo* acquisitions (Dadar et al., 2024b).

Beyond diffusion, other quantitative MRI approaches have been applied to postmortem brains, although not specifically focused on the MTL. Whole-hemisphere postmortem MRI studies have revealed alterations in the transverse relaxation time T2 (inversely related to R2) in the presence of neuropathological burden. Specifically, decreases in R2, reflecting neuronal or myelin loss and increased free water content, have been reported in AD (Dawe et al., 2014; Yu et al., 2017) and LATE patients (Tazwar et al., 2022). Conversely, R2 increase, reflecting iron deposition, has been associated with AD, microinfarcts, and hippocampal sclerosis (Dawe et al., 2014). Interpretation of these quantitative measures is limited in fixed tissue, as fixation alters relaxation properties and contrast (Augustinack et al., 2014).

Similarly, magnetic susceptibility on T2*-weighted and quantitative susceptibility mapping (QSM) sequences, indicative of iron accumulation (Tisdall et al., 2022), has shown associations with Aβ plaque deposition (Van Rooden et al., 2009; Nabuurs et al., 2013; Zeineh et al., 2015; Yao et al., 2024) and FTLD (Tisdall et al., 2022). Within the MTL, specific alterations were observed in the strata moleculare and lacunosum (Zhao et al., 2021). However, susceptibility contrast can also be affected by air bubbles introduced during tissue preparation, adding another layer of technical complexity.

Although these microstructural and quantitative approaches face technical limitations in fixed tissue, they illustrate the promising potential of postmortem MRI to connect micro- and macroscale measures of neurodegeneration, complementing anatomical imaging and guiding the interpretation of *in vivo* biomarkers in these imaging modalities.

6. Perspectives and limitations

6.1. Characterization of the differences between *in vivo* and postmortem MRI

To our knowledge, few studies have investigated the differences between *in vivo* and postmortem MRI (Kotrotsou et al., 2014; Wisse et al., 2016; Boon et al., 2019). It remains, therefore, unclear to what extent end-of-life physiological changes, brain extraction, and fixation protocols affect MTL anatomy.

By comparing *ex vivo* MRI scans of the MTL with *in vivo* scans from the same individuals, Wisse et al. (2016) demonstrated that the overall hippocampal shape (i.e., outer borders, digitations, and dark band) is similar across modalities. Additionally, several microstructural features, such as the layered organization of the (pre/para)subiculum and perirhinal cortex, were also observed to be comparable. This comparison confirms that certain macrostructural and microstructural features of the hippocampus can indeed be visualized *in vivo*.

However, the study also highlighted notable differences between the two modalities. In particular, the thickness of MTL substructures (especially the CA regions) was found to be greater in the *ex vivo* scans than in the *in vivo* scans. While it may seem counterintuitive that brain volume increases after death and fixation (Dam, 1979), this discrepancy likely reflects physiological changes that occur during or after death. Indeed, a study comparing *in vivo* and *in situ* MRI also reported a postmortem increase in brain volume, with a more pronounced enlargement of white matter than gray matter (Boon et al., 2019). Other possible contributing factors may be brain extraction itself, which may relieve intracranial pressure and thus alter brain volume or the contrast difference between *in* and *ex vivo* MRI that could affect the apparent size of certain structures (Wisse et al., 2016).

Further research is needed to clarify the precise causes of postmortem volumetric changes and to determine whether other differences exist between *in vivo* and postmortem MRI. Studies explicitly comparing *in vivo*, *in situ*, and *ex vivo* imaging together would be especially informative in assessing the role of brain extraction in volume increase. Moreover, it would be valuable to investigate whether the postmortem interval (i.e., the time between death and brain fixation) or brain fixation affects this volumetric gain. Such studies would require access to a large number of individuals who underwent *in vivo* MRI shortly before death and donated their brains for research, a challenging requirement.

6.2. Need for pathology-specific postmortem imaging studies

Another significant limitation lies in the type of pathology included in existing studies. When exploring impact of ADRD neuropathologic changes on the MTL atrophy, most research tends to group a heterogeneous set of tauopathies, including AD, FTLD, corticobasal degeneration (CBD), and progressive supranuclear palsy (PSP), to study the impact of tau on MTL (Wisse et al., 2021b; Ravikumar et al., 2021). While these are all tauopathies, they represent distinct clinical and pathological entities, each characterized by different types of tau lesions (e.g., NFTs *vs.* astrocytic tau). Grouping them into a single category introduces considerable heterogeneity, which not only limits the ability to detect pathology-specific atrophy patterns but also risks overlooking rarer and less-characterized disorders such as CBD or PSP, which become diluted within an AD-dominant spectrum. Furthermore, although TDP-43 has gained growing attention in the field, the few imaging studies that investigated it typically group TDP-43 proteinopathies without accounting for the diversity of associated clinical phenotypes and inclusion types (Wisse et al., 2021b; Ravikumar et al., 2021). This is especially important in the context of FTLD-TDP subtypes and LATE-NC (with or without comorbid ADNC) (Tomé et al., 2025).

In addition, there is a strong need for disease specific studies to identify distinct atrophy patterns and improve the characterization of underexplored pathologies. However, we acknowledge that these studies are inherently challenging, as the inclusion of specific cases depends on the prevalence of the pathology and availability of suitable samples.

Finally, numerous studies have demonstrated interactions between different proteinopathies, such as tau and TDP-43 (Latimer and Liachko, 2021; Tomé et al., 2021), or with α-synuclein (Moussaud et al., 2014; Dhakal et al., 2021). Therefore, enriching postmortem cohorts with non-AD or mixed pathologies as done in more recent cohorts (Li et al., 2023), could be highly informative for evaluating whether the interactions observed at the neuronal level are reflected in specific atrophy patterns observed on structural MRI, and whether they may influence current interpretations of *in vivo* imaging data.

6.3. Extending analyses beyond the medial temporal lobe

Our review focused on the MTL due to its early involvement in neurodegenerative diseases. However, extending postmortem MRI to other brain regions could provide valuable insights. Whole-brain or hemisphere postmortem MRI can help identify areas that warrant more detailed investigation. For example, whole-hemisphere *ex vivo* MRI studies have highlighted the value of examining the nucleus basalis of Meynert (Lin et al., 2022), primary visual cortices, temporal pole, insular and posterior cingulate gyri (Sadaghiani et al., 2023), as well as medial-orbitofrontal, inferior temporal, and parietal lobes (Kotrotsou et al., 2015; Khandelwal et al., 2024, 2025). It would also be valuable to further investigate areas that remain relatively understudied with MRI and may play a role in neurodegenerative processes, such as the locus coeruleus (Hary et al., 2025) or the thalamus (Iglesias et al., 2018b) in AD, the spinal cord and motor cortex (Pallebage-Gamarallage et al., 2018; Neuhaus et al., 2025) in amyotrophic lateral sclerosis (ALS), the brainstem in CBD and PSP (Olchanyi et al., 2024), or the hypothalamus (Rodrigues et al., 2024) in both AD and ALS-FTD spectrum.

6.4. Integrating other neuropathological measurements

We observed that several groups used the hemisphere contralateral to the one scanned with MRI for neuropathological assessments. This represents a significant limitation, as the pathological measures being related to the MRI data do not originate from the same hemisphere, which may impact the reliability of the results. Indeed, some pathologies are known to be lateralized, such as hippocampal sclerosis of aging (Sordo et al., 2023), tau and TDP-43 pathologies (e.g., in the logopenic variant of primary progressive aphasia, semantic and frontotemporal dementia variants, and LATE (Cappa, 2025)), making interhemispheric comparisons not completely reliable. We therefore recommend, whenever possible, using the same hemisphere for all measurements. However, it should be noted that one previous study compared the association of ipsilateral and contralateral tau measures with structural postmortem MRI measures in AD, known to show modest asymmetry, and found roughly similar results (Ravikumar et al., 2021).

Additionally, as most MTL studies currently focus on common pathological markers as tau, TDP-43, Aβ, and α-synuclein, including a wider range of neuropathological measures such as neuronal loss (Lin

et al., 2022), neurodegeneration markers (Frigerio et al., 2023), white matter lesions (Makkinejad et al., 2024), vascular alterations (e.g., small vessel disease, microinfarcts, cerebral amyloid angiopathy, calcifications (Scherlek et al., 2022; Perosa et al., 2022, 2023)), and neuroinflammation (Frigerio et al., 2021) would be highly valuable. Indeed, these neuropathologies are known to contribute to neurodegeneration, specifically in AD and LATE, as well as to cognitive symptoms (Arvanitakis et al., 2011; Corrada et al., 2016; Agrawal et al., 2021; Jäkel et al., 2022; Nelson and Katsumata, 2024).

Finally, it has been shown that quantitative measures of tau (but not TDP-43) lesions allowed a more granular measure of the pathology and showed better association with antemortem *in vivo* MRI volumes and thickness compared to semi-quantitative ratings (Denning et al., 2024). Future work should therefore use quantitative measures of tau instead of semi-quantitative ratings, at least for AD-related tau pathology. Although quantitative ratings can be more fastidious and time-consuming, automated tools to quantify Aβ plaques and NFTs have been developed to overcome these limitations (Yushkevich et al., 2021a; Ingrassia et al., 2024; Scalco et al., 2024; Gonzalez et al., 2025; Gawor et al., 2025), but still need to be tested on different datasets.

6.5. Expanding beyond volumetric *ex vivo* MRI

This work focused specifically on volumetric *ex vivo* MRI of the MTL; however, this represents only one component of the broader methodological potential of *ex vivo* imaging. While volumetric approaches provide robust and anatomically interpretable measures of regional atrophy, they remain limited in their ability to capture underlying microstructural, compositional, and connectivity-related tissue changes, and do not allow direct probing of tissue organization at submillimetric scale. Beyond volumetric measures, *ex vivo* MRI enables the investigation of microstructural organization and tissue properties at submillimetric resolution through ultra-high-resolution diffusion MRI, including diffusion tensor imaging and tractography approaches, which allow the characterization of white matter architecture and connectivity patterns, as well as *ex vivo* white matter changes and alterations in relation to underlying pathology (Back et al., 2011; Arfanakis et al., 2020; Beaujoin et al., 2018; Shih et al., 2023; Zhao et al., 2023; Fracasso et al., 2016a, 2016b). In addition, a wide range of MRI contrasts and

quantitative mapping approaches can be applied, including relaxation-based metrics such as T2 and susceptibility-based techniques such as QSM, which are sensitive to tissue composition changes such as iron deposition and other microstructural alterations (Dawe et al., 2014; Evia et al., 2017; Bulk et al., 2018b, 2018a; De Barros et al., 2019; Gong et al., 2019; Giannini et al., 2023). These approaches further enable the study of MRI-visible changes across white and grey matter in relation to histopathological substrates, including neurodegenerative and vascular-related processes, and allow direct spatial correlation between imaging-derived measures and cellular or molecular markers of disease (Baltes et al., 2011; Van Veluw et al., 2016; Zhao et al., 2021; Perosa et al., 2023; Makkinejad et al., 2024; Barsoum et al., 2025). Taken together, these complementary methods considerably extend the interpretative and mechanistic value of *ex vivo* MRI beyond volumetric assessment alone. In this context, a multimodal approach integrating volumetric, diffusion-based, and quantitative MRI techniques may provide a more comprehensive characterization of *ex vivo* tissue alterations, combining macroscopic structural changes with microstructural and biophysical information within a unified framework.

6.6. Developing automated segmentation tools for *ex vivo* MRI

A long-standing limitation in postmortem MRI data analysis has long been the lack of automated segmentation tools, comparable to those widely used in *in vivo* imaging, such as FreeSurfer (Fischl, 2012) or ASHS (Yushkevich et al., 2010). Classical *in vivo* pipelines have been shown to fail on postmortem MRI data (Kotrotsou et al., 2014), as excised brain specimens or whole hemispheres in postmortem scan preparations are not compatible with their assumptions about intact anatomy and typical intensity distributions. As a result, volumetric *ex vivo* MRI studies have historically relied on manual delineation of regions of interest, a time-consuming process requiring substantial anatomical expertise.

Over the past decade, methodological developments have progressively addressed this limitation through a series of complementary advances. Early efforts focused on structure-specific segmentation, particularly within the MTL, where semi-automated pipelines enabled segmentation of hippocampal and adjacent structures, reducing reliance on fully manual approaches (Ravikumar et al., 2019). In parallel,

substantial progress in spatial normalization and nonlinear registration helped address tissue deformation, shrinkage, and contrast changes induced by fixation, enabling in vivo–ex vivo alignment and normalization to common spaces (Avants et al., 2008, 2011). More recent approaches have further improved registration robustness by using image synthesis models to reduce contrast differences between in vivo and ex vivo MRI prior to alignment (Khandelwal et al., 2026).

Subsequently, the field expanded toward histology-informed and probabilistic atlases derived from cytoarchitectonic data. These rely on 3D reconstructions of histological sections, using ex vivo MRI and intermediate modalities such as blockface imaging to preserve anatomical consistency (Mancini et al., 2020). Examples include probabilistic whole-brain atlases such as NextBrain (Casamitjana et al., 2024), which act as anatomical priors to improve parcellation and multimodal registration. Building on these resources, automated whole-hemisphere segmentation pipelines have been developed using Bayesian frameworks (Casamitjana et al., 2024; Puonti et al., 2025) as well as hybrid deep learning and surface-based approaches (Khandelwal et al., 2025, 2024, see Figure 9), enabling more anatomically coherent parcellation of high-resolution postmortem MRI. In parallel, domain-robust deep learning methods have been introduced to improve generalization across imaging contrasts and acquisition protocols (Billot et al., 2023a, 2023b).

Despite these advances, generalization across acquisition settings (e.g., 3T vs 7T), fixation protocols, and tissue properties remains a challenge. This is particularly relevant for smaller and more variable structures such as the MTL. Unlike whole-hemisphere datasets, MTL samples are often acquired as isolated tissue blocks with variability in orientation, extent, and preservation. Differences in resolution and partial coverage further limit the reproducibility of anatomical landmarks. Consequently, while full automation has progressed substantially at the whole-brain level, MTL segmentation still relies mainly on semi-automated approaches combining manual delineation and computational tools, which remain the most robust solution for high-resolution *ex vivo* studies (Ravikumar et al., 2019; Wisse et al., 2021b).

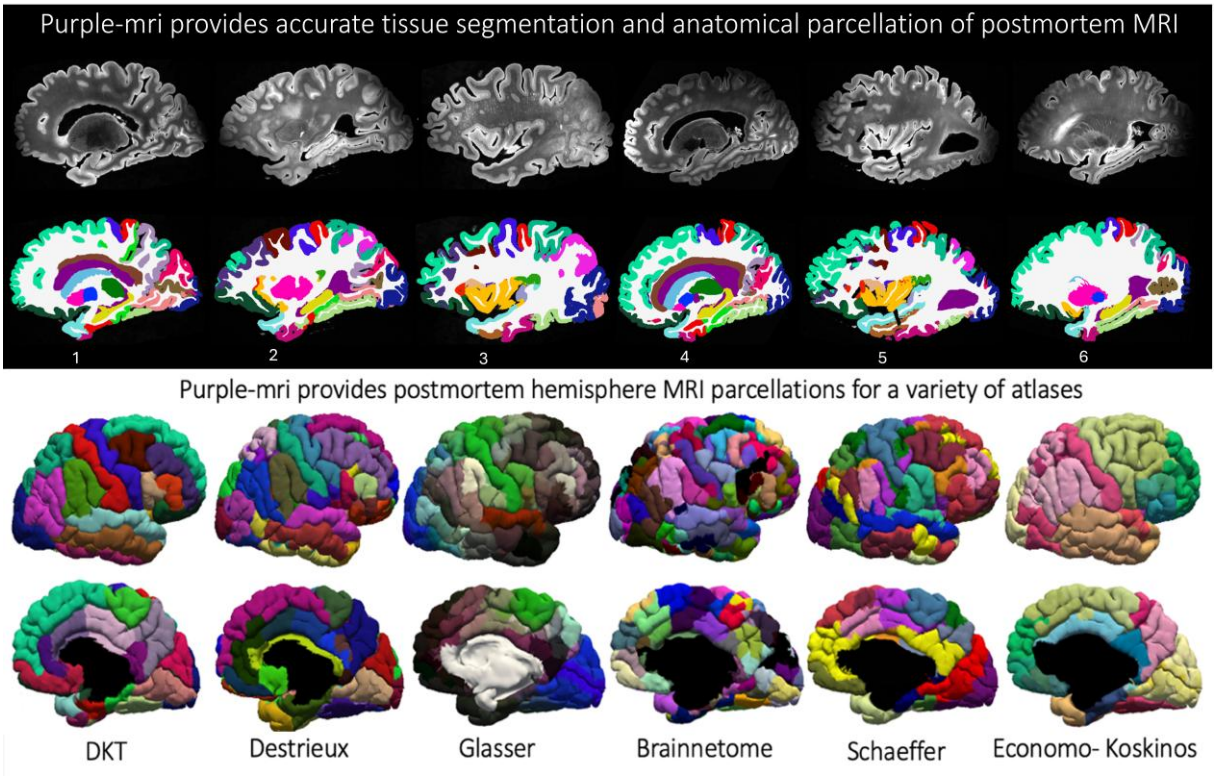

Figure 9. Segmentation of whole-hemisphere ex vivo MRI. *Purple-mri provides tissue segmentation and anatomical parcellation of whole-hemisphere 7 tesla postmortem MRI. The top panel shows sagittal slices and the corresponding segmentations for the surface-based using a DKT atlas of 6 specimens. The method handles a variety of heterogeneous images involving a spectrum of imaging and brain tissue features: anterior/posterior signal dropout, imaging inhomogeneity, large ventricles, severely atrophied brain, damaged tissue, and missing tissue chunk due to subsequent histopathological sampling. The bottom panel shows the lateral and medial view of the surface-based pial anatomical parcellation of specimen 1 using six commonly used atlases: Desikan-Killiany-Tourville (DKT) [Desikan et al., 2006], Destrieux [Destrieux et al., 2010], Brainnetome [Fan et al., 2016], Schaeffer [Schaefer et al., 2018], Economo-Koskinas [Scholtens et al., 2018], Glasser [Glasser et al., 2016]. Figure adapted Khandelwal (2025)*

6.7. Translating postmortem MRI findings to *in vivo* MRI

Translating observations from postmortem MRI back to *in vivo* imaging is critical as these findings are to ultimately benefit living patients and contribute to the development of clinically relevant biomarkers. However, this translation remains challenging due to the substantial resolution gap between *in vivo* MRI

and high-resolution *ex vivo* MTL imaging. In this context, leveraging whole-hemisphere *ex vivo* MRI as well as *in situ* MRI could be particularly valuable, as they provide intermediate imaging scales that help bridge this gap. Whole-hemisphere imaging facilitates direct comparisons between postmortem and antemortem scans (Khandelwal et al., 2026), while *in situ* MRI provides an imaging appearance closely resembling *in vivo* acquisitions (Jonkman et al., 2019; Boon et al., 2019), thereby facilitating the integration of findings across scales.

Ex vivo MRI can support *in vivo* applications in several complementary ways (see Section 5). It can highlight regions strongly associated with pathology that warrant further investigation *in vivo* (see Section 5.2), provide detailed anatomical knowledge to guide the refinement of segmentation protocols (see Section 5.1), and inform the optimization of MRI sequences to better visualize targeted structures (see Section 5.3). By providing this anatomical and pathological framework, *ex vivo* imaging facilitates the development of new *in vivo* segmentation approaches. Such protocols must, however, be designed and validated on *in vivo* data, focusing on landmarks that remain detectable at clinical resolution. Similar to the approach of the Hippocampal Subfields Group, which integrates histological knowledge to identify features observable on high-resolution *in vivo* T2-weighted images (0.4 mm in-plane) (Wisse et al., 2017; Olsen et al., 2019; Daugherty et al., 2025; De Flores et al., 2025), *ex vivo* MRI could be used in a similar way to guide the development of harmonized segmentation protocols based on landmarks that are actually visible *in vivo.*

Another approach for transferring *ex vivo* findings to *in vivo* imaging relies on computational modeling. Bayesian and atlas-based methods trained on ultra–high-resolution *ex vivo* segmentations have been adapted to perform automated parcellation at lower *in vivo* resolutions. This strategy underlies widely used tools such as FreeSurfer, enabling the measurement of hippocampal subfields (Iglesias et al., 2015), amygdalar nuclei (Saygin et al., 2017), and thalamic nuclei (Iglesias et al., 2018b) *in vivo*.

7. Conclusion

Postmortem MRI of the MTL has emerged as a powerful tool to bridge the gap between *in vivo* neuroimaging and neuropathology in neurodegenerative diseases. By enabling high-resolution, three-

dimensional imaging without the constraints of patient motion or limited scan duration, this technique offers unique advantages over both *in vivo* imaging and traditional histology. It has significantly advanced both fundamental and clinical understanding of neurodegenerative diseases. On a fundamental level, postmortem MRI has deepened our knowledge of MTL anatomy and clarified how proteinopathies (particularly tau) affect its subregions. Clinically, these insights are useful for guiding future *in vivo* research, including the development of MRI-based biomarkers, the refinement of segmentation protocols, and the design of *in vivo* imaging sequences optimized for early and region-specific detection of pathology, especially when combined with robust neuropathological data. Future research should aim to investigate the differences between *in vivo* and postmortem MRI, include more diverse data from multiple cohorts, and quantify neuropathological measures. The question is whether we have yet reached the limit of postmortem imaging, or if additional anatomical features can be uncovered for the study of neurodegenerative diseases in the next generation of postmortem MRI scans.

8. Acknowledgements

The authors are deeply grateful to the patients, donors, and their families for their generous brain donations, which make postmortem research possible. The authors also thank GIGA-CRC, University of Liège, Belgium, and particularly Prof. Christine Bastin and Prof. Gilles Vandewalle for their support in the acquisition of the *in vivo* 7T MRI data presented in Figure 1.

9. Author's contributions

YS: Conceptualization, Data Curation, Funding Acquisition, Investigation, Visualization, Writing – Original Draft Preparation, Writing – Review & Editing. **AED:** Visualization, Writing – Review & Editing. JMS: Data Curation, Writing – Review & Editing. **SOT:** Writing – Review & Editing. NJ: Data Curation, Writing – Review & Editing. **PK:** Validation, Visualization, Writing – Review & Editing. **PAY:** Data Curation, Validation, Writing – Review & Editing. **RV:** Data Curation, Writing – Review & Editing. **BG:** Data Curation, Resources, Writing – Review & Editing. **LEMW:** Conceptualization, Supervision, Writing – Original Draft Preparation, Writing – Review & Editing. **BH:** Conceptualization, Funding Acquisition, Supervision, Writing – Original Draft Preparation, Writing – Review & Editing

10. Funding

YS was funded by the Belgian Fund for Scientific Research (FNRS; FRIA40014635) and received mobility grants from European Graduate School of Neuroscience (EURON), Erasmus+, and Wallonia-Brussels International (WBI.World) for this collaborative work. **JMS** obtained funding through FWO (12Y1623N) and Stichting Alzheimer onderzoek #SAO-FRA 2021/0022. **SOT** was funded by Fonds Wetenschappelijk Onderzoek (FWO; 1225725N) and Alzheimer's Association (AARF-24-1300693). **PAY** was funded by National Institute on Aging (P30 AG072979) and National Institute of Health (RF1 AG056014). **LEMW** was supported by MultiPark, a strategic research area at Lund University, and project grants from the Swedish Alzheimer Foundation (AF-980872) and the Bente Rexed Gerstedt Foundation. **BH** was funded by the FNRS (CCL40010417), the FRFS-WELBIO (40010035), and Fondation Recherche Alzheimer/Stichting Alzheimer Onderzoek (SAO20240044).

11. Declaration of competing interests

SOT received consultancy honoraria from Mura Therapeutics (Belgium). **RV**'s institution has clinical trial agreements (RV as PI) with Alector, AviadoBio, Biogen, Denali, J&J, Eli Lilly, and UCB. **RV**'s institution has consultancy agreements (RV as member of DSMB) with AC Immune. **BH**'s institution has clinical trial agreements (BH as PI) with Biogen, J&J, BMS, and MSD. **BH**'s institution has consultancy agreements with Eisai and Eli Lilly.

12. References

Adler, D.H., Pluta, J., Kadivar, S., Craige, C., Gee, J.C., Avants, B.B., Yushkevich, P.A., 2014. Histology-derived volumetric annotation of the human hippocampal subfields in postmortem MRI. NeuroImage 84, 505–523. https://doi.org/10.1016/j.neuroimage.2013.08.067

Adler, D.H., Wisse, L.E.M., Ittyerah, R., Pluta, J.B., Ding, S.-L., Xie, L., Wang, J., Kadivar, S., Robinson, J.L., Schuck, T., Trojanowski, J.Q., Grossman, M., Detre, J.A., Elliott, M.A., Toledo, J.B., Liu, W., Pickup, S., Miller, M.I., Das, S.R., Wolk, D.A., Yushkevich, P.A., 2018. Characterizing the human hippocampus in aging and Alzheimer's disease using a computational atlas derived from ex vivo MRI and histology. Proc. Natl. Acad. Sci. 115, 4252–4257. https://doi.org/10.1073/pnas.1801093115

Agrawal, S., Yu, L., Kapasi, A., James, B.D., Arfanakis, K., Barnes, L.L., Bennett, D.A., Nag, S., Schneider, J.A., 2021. Limbic-predominant age-related TDP-43 encephalopathy neuropathologic change and microvascular pathologies in community-dwelling older persons. Brain Pathol. 31, e12939. https://doi.org/10.1111/bpa.12939

Amunts, K., Lepage, C., Borgeat, L., Mohlberg, H., Dickscheid, T., Rousseau, M.-É., Bludau, S., Bazin, P.-L., Lewis, L.B., Oros-Peusquens, A.-M., Shah, N.J., Lippert, T., Zilles, K., Evans, A.C., 2013. BigBrain: An Ultrahigh-Resolution 3D Human Brain Model. Science 340, 1472–1475. https://doi.org/10.1126/science.1235381

Amunts, K., Mohlberg, H., Bludau, S., Zilles, K., 2020. Julich-Brain: A 3D probabilistic atlas of the human brain's cytoarchitecture. Science 369, 988–992. https://doi.org/10.1126/science.abb4588

Arfanakis, K., Evia, A.M., Leurgans, S.E., Cardoso, L.F.C., Kulkarni, A., Alqam, N., Lopes, L.F., Vieira, D., Bennett, D.A., Schneider, J.A., 2020. Neuropathologic Correlates of White Matter Hyperintensities in a Community-Based Cohort of Older Adults. J. Alzheimer's Dis. 73, 333–345. https://doi.org/10.3233/JAD-190687

Arvanitakis, Z., Leurgans, S.E., Barnes, L.L., Bennett, D.A., Schneider, J.A., 2011. Microinfarct Pathology, Dementia, and Cognitive Systems. Stroke 42, 722–727. https://doi.org/10.1161/STROKEAHA.110.595082

Augustinack, J., 2010. Direct visualization of the perforant pathway in the human brain with ex vivo diffusion tensor imaging. Front. Hum. Neurosci. https://doi.org/10.3389/fnhum.2010.00042

Augustinack, J.C., Huber, K.E., Stevens, A.A., Roy, M., Frosch, M.P., Van Der Kouwe, A.J.W., Wald, L.L., Van Leemput, K., McKee, A.C., Fischl, B., 2013. Predicting the location of human perirhinal cortex, Brodmann's area 35, from MRI. NeuroImage 64, 32–42. https://doi.org/10.1016/j.neuroimage.2012.08.071

Augustinack, J.C., Magnain, C., Reuter, M., Van Der Kouwe, A.J.W., Boas, D., Fischl, B., 2014. MRI parcellation of ex vivo medial temporal lobe. NeuroImage 93, 252–259. https://doi.org/10.1016/j.neuroimage.2013.05.053

Augustinack, J.C., Van Der Kouwe, A.J.W., 2016. Postmortem imaging and neuropathologic correlations, in: Handbook of Clinical Neurology. Elsevier, pp. 1321–1339. https://doi.org/10.1016/B978-0-444-53486-6.00069-7

Augustinack, J.C., Van Der Kouwe, A.J.W., Blackwell, M.L., Salat, D.H., Wiggins, C.J., Frosch, M.P., Wiggins, G.C., Potthast, A., Wald, L.L., Fischl, B.R., 2005. Detection of entorhinal layer II using Tesla magnetic resonance imaging. Ann. Neurol. 57, 489–494. https://doi.org/10.1002/ana.20426

Avants, B., Epstein, C., Grossman, M., Gee, J., 2008. Symmetric diffeomorphic image registration with cross-correlation: Evaluating automated labeling of elderly and neurodegenerative brain. Med. Image Anal. 12, 26–41. https://doi.org/10.1016/j.media.2007.06.004

Avants, B.B., Tustison, N.J., Song, G., Cook, P.A., Klein, A., Gee, J.C., 2011. A reproducible evaluation of ANTs similarity metric performance in brain image registration. NeuroImage 54, 2033–2044. https://doi.org/10.1016/j.neuroimage.2010.09.025

Back, S.A., Kroenke, C.D., Sherman, L.S., Lawrence, G., Gong, X., Taber, E.N., Sonnen, J.A., Larson, E.B., Montine, T.J., 2011. White matter lesions defined by diffusion tensor imaging in older adults. Ann. Neurol. 70, 465–476. https://doi.org/10.1002/ana.22484

Baltes, C., Princz-Kranz, F., Rudin, M., Mueggler, T., 2011. Detecting Amyloid-β Plaques in Alzheimer's Disease, in: Modo, M., Bulte, J.W.M. (Eds.), Magnetic Resonance Neuroimaging, Methods in Molecular Biology. Humana Press, Totowa, NJ, pp. 511–533. https://doi.org/10.1007/978-1-61737-992-5_26

Barsoum, S., Latimer, C.S., Nolan, A.L., Barrett, A., Chang, K., Troncoso, J.C., Keene, C.D., Benjamini, D., 2025. Multidimensional MRI reveals cortical astrogliosis linked to dementia in Alzheimer's disease. Brain Commun. 7, fcaf245. https://doi.org/10.1093/braincomms/fcaf245

Bayart, J.-L., Hanseeuw, B., Ivanoiu, A., Van Pesch, V., 2019. Analytical and clinical performances of the automated Lumipulse cerebrospinal fluid Aβ42 and T-Tau assays for Alzheimer's disease diagnosis. J. Neurol. 266, 2304–2311. https://doi.org/10.1007/s00415-019-09418-6

Beaujoin, J., Palomero-Gallagher, N., Boumezbeur, F., Axer, M., Bernard, J., Poupon, F., Schmitz, D., Mangin, J.-F., Poupon, C., 2018. Post-mortem inference of the human hippocampal connectivity and microstructure using ultra-high field diffusion MRI at 11.7 T. Brain Struct. Funct. 223, 2157–2179. https://doi.org/10.1007/s00429-018-1617-1

Bejanin, A., Murray, M.E., Martin, P., Botha, H., Tosakulwong, N., Schwarz, C.G., Senjem, M.L., Chételat, G., Kantarci, K., Jack, C.R., Boeve, B.F., Knopman, D.S., Petersen, R.C., Giannini, C., Parisi, J.E., Dickson, D.W., Whitwell, J.L., Josephs, K.A., 2019. Antemortem volume loss mirrors TDP-43 staging in older adults with non-frontotemporal lobar degeneration. Brain 142, 3621–3635. https://doi.org/10.1093/brain/awz277

Berron, D., Vieweg, P., Hochkeppler, A., Pluta, J.B., Ding, S.-L., Maass, A., Luther, A., Xie, L., Das, S.R., Wolk, D.A., Wolbers, T., Yushkevich, P.A., Düzel, E., Wisse, L.E.M., 2017. A protocol for manual segmentation of medial temporal lobe subregions in 7 Tesla MRI. NeuroImage Clin. 15, 466–482. https://doi.org/10.1016/j.nicl.2017.05.022

Billot, B., Greve, D.N., Puonti, O., Thielscher, A., Van Leemput, K., Fischl, B., Dalca, A.V., Iglesias, J.E., 2023a. SynthSeg: Segmentation of brain MRI scans of any contrast and resolution without retraining. Med. Image Anal. 86, 102789. https://doi.org/10.1016/j.media.2023.102789

Billot, B., Magdamo, C., Cheng, Y., Arnold, S.E., Das, S., Iglesias, J.E., 2023b. Robust machine learning segmentation for large-scale analysis of heterogeneous clinical brain MRI datasets. Proc. Natl. Acad. Sci. 120, e2216399120. https://doi.org/10.1073/pnas.2216399120

Blamire, A.M., Rowe, J.G., Styles, P., McDonald, B., 1999. Optimising Imaging Parameters for *Post Mortem* MR Imaging of the Human Brain. Acta Radiol. 40, 593–597. https://doi.org/10.3109/02841859909175593

Boon, B.D.C., Pouwels, P.J.W., Jonkman, L.E., Keijzer, M.J., Preziosa, P., Van De Berg, W.D.J., Geurts, J.J.G., Scheltens, P., Barkhof, F., Rozemuller, A.J.M., Bouwman, F.H., Steenwijk, M.D., 2019. Can post-mortem MRI be used as a proxy for in vivo? A case study. Brain Commun. 1, fcz030. https://doi.org/10.1093/braincomms/fcz030

Boutet, C., Chupin, M., Lehéricy, S., Marrakchi-Kacem, L., Epelbaum, S., Poupon, C., Wiggins, C., Vignaud, A., Hasboun, D., Defontaines, B., Hanon, O., Dubois, B., Sarazin, M., Hertz-Pannier, L., Colliot, O., 2014. Detection of volume loss in hippocampal layers in Alzheimer's disease using 7 T MRI: A feasibility study. NeuroImage Clin. 5, 341–348. https://doi.org/10.1016/j.nicl.2014.07.011

Bouwman, M.M.A., Frigerio, I., Lin, C.-P., Reijner, N., Van De Berg, W.D.J., Jonkman, L.E., 2025. Hippocampal subfields: volume, neuropathological vulnerability and cognitive decline in Alzheimer's and Parkinson's disease. Alzheimers Res. Ther. 17, 121. https://doi.org/10.1186/s13195-025-01768-w

Braak, H., Braak, E., 1995. Staging of alzheimer's disease-related neurofibrillary changes. Neurobiol. Aging 16, 271–278. https://doi.org/10.1016/0197-4580(95)00021-6

Braak, H., Braak, E., 1991. Neuropathological stageing of Alzheimer-related changes. Acta Neuropathol. (Berl.) 82, 239–259. https://doi.org/10.1007/BF00308809

Braak, H., Del Tredici, K., Bratzke, H., Hamm-Clement, J., Sandmann-Keil, D., Rüb, U., 2002. Staging of the intracerebral inclusion body pathology associated with idiopathic Parkinson's disease (preclinical and clinical stages). J. Neurol. 249, 1–1. https://doi.org/10.1007/s00415-002-1301-4

Brettschneider, J., Del Tredici, K., Irwin, D.J., Grossman, M., Robinson, J.L., Toledo, J.B., Fang, L., Van Deerlin, V.M., Ludolph, A.C., Lee, V.M.-Y., Braak, H., Trojanowski, J.Q., 2014. Sequential distribution of pTDP-43 pathology in behavioral variant frontotemporal dementia (bvFTD). Acta Neuropathol. (Berl.) 127, 423–439. https://doi.org/10.1007/s00401-013-1238-y

Brown, C., Das, S., Xie, L., Nasrallah, I., Detre, J., Chen-Plotkin, A., Shaw, L., McMillan, C., Yushkevich, P., Wolk, D., 2024. Medial temporal lobe gray matter microstructure in preclinical Alzheimer's disease. Alzheimers Dement. 20, 4147–4158. https://doi.org/10.1002/alz.13832

Bulk, M., Abdelmoula, W.M., Nabuurs, R.J.A., Van Der Graaf, L.M., Mulders, C.W.H., Mulder, A.A., Jost, C.R., Koster, A.J., Van Buchem, M.A., Natté, R., Dijkstra, J., Van Der Weerd, L.,

2018a. Postmortem MRI and histology demonstrate differential iron accumulation and cortical myelin organization in early- and late-onset Alzheimer's disease. Neurobiol. Aging 62, 231–242. https://doi.org/10.1016/j.neurobiolaging.2017.10.017

Bulk, M., Kenkhuis, B., Van Der Graaf, L.M., Goeman, J.J., Natté, R., Van Der Weerd, L., 2018b. Postmortem T_2^* - Weighted MRI Imaging of Cortical Iron Reflects Severity of Alzheimer's Disease. J. Alzheimer's Dis. 65, 1125–1137. https://doi.org/10.3233/JAD-180317

Cairns, N.J., Bigio, E.H., Mackenzie, I.R.A., Neumann, M., Lee, V.M.-Y., Hatanpaa, K.J., White, C.L., Schneider, J.A., Grinberg, L.T., Halliday, G., Duyckaerts, C., Lowe, J.S., Holm, I.E., Tolnay, M., Okamoto, K., Yokoo, H., Murayama, S., Woulfe, J., Munoz, D.G., Dickson, D.W., Ince, P.G., Trojanowski, J.Q., Mann, D.M.A., 2007. Neuropathologic diagnostic and nosologic criteria for frontotemporal lobar degeneration: consensus of the Consortium for Frontotemporal Lobar Degeneration. Acta Neuropathol. (Berl.) 114, 5–22. https://doi.org/10.1007/s00401-007-0237-2

Caporiccio, G., Flabbi, L., Marchionni, G., Viola, G.T., 1989. The properties and applications of Perfluoropolyether lubricants. J. Synth. Lubr. 6, 133–149. https://doi.org/10.1002/jsl.3000060205

Casamitjana, A., Mancini, M., Robinson, E., Peter, L., Annunziata, R., Althonayan, J., Crampsie, S., Blackburn, E., Billot, B., Atzeni, A., Puonti, O., Balbastre, Y., Schmidt, P., Hughes, J., Augustinack, J.C., Edlow, B.L., Zöllei, L., Thomas, D.L., Kliemann, D., Bocchetta, M., Strand, C., Holton, J.L., Jaunmuktane, Z., Iglesias, J.E., 2024. A next-generation, histological atlas of the human brain and its application to automated brain MRI segmentation. https://doi.org/10.1101/2024.02.05.579016

Chatterjee, M., Özdemir, S., Fritz, C., Möbius, W., Kleineidam, L., Mandelkow, E., Biernat, J., Doğdu, C., Peters, O., Cosma, N.C., Wang, X., Schneider, L.-S., Priller, J., Spruth, E., Kühn, A.A., Krause, P., Klockgether, T., Vogt, I.R., Kimmich, O., Spottke, A., Hoffmann, D.C., Fliessbach, K., Miklitz, C., McCormick, C., Weydt, P., Falkenburger, B., Brandt, M., Guenther, R., Dinter, E., Wiltfang, J., Hansen, N., Bähr, M., Zerr, I., Flöel, A., Nestor, P.J., Düzel, E., Glanz, W., Incesoy, E., Bürger, K., Janowitz, D., Perneczky, R., Rauchmann, B.S., Hopfner, F., Wagemann, O., Levin, J., Teipel, S., Kilimann, I., Goerss, D., Prudlo, J., Gasser, T., Brockmann, K., Mengel, D., Zimmermann, M., Synofzik, M., Wilke, C., Selma-González, J., Turon-Sans, J., Santos-Santos, M.A., Alcolea, D., Rubio-Guerra, S., Fortea, J., Carbayo, Á., Lleó, A., Rojas-García, R., Illán-Gala, I., Wagner, M., Frommann, I., Roeske, S., Bertram, L., Heneka, M.T., Brosseron, F., Ramirez, A., Schmid, M., Beschorner, R., Halle, A., Herms, J., Neumann, M., Barthélemy, N.R., Bateman, R.J., Rizzu, P., Heutink, P., Dols-Icardo, O., Höglinger, G., Hermann, A., Schneider, A., 2024. Plasma extracellular vesicle tau and TDP-43 as diagnostic biomarkers in FTD and ALS. Nat. Med. 30, 1771–1783. https://doi.org/10.1038/s41591-024-02937-4

Coras, R., Milesi, G., Zucca, I., Mastropietro, A., Scotti, A., Figini, M., Mühlebner, A., Hess, A., Graf, W., Tringali, G., Blümcke, I., Villani, F., Didato, G., Frassoni, C., Spreafico, R., Garbelli, R., 2014. 7 T MRI features in control human hippocampus and hippocampal sclerosis: An ex vivo study with histologic correlations. Epilepsia 55, 2003–2016. https://doi.org/10.1111/epi.12828

Corrada, M.M., Sonnen, J.A., Kim, R.C., Kawas, C.H., 2016. Microinfarcts are common and strongly related to dementia in the oldest-old: The 90+ study. Alzheimers Dement. 12, 900–908. https://doi.org/10.1016/j.jalz.2016.04.006

Dadar, M., Sanches, L., Fouquet, J.P., Moqadam, R., Alasmar, Z., Ruth Leppert, I., Mirault, D., Maranzano, J., Mechawar, N., Chakravarty, M., Zeighami, Y., 2024a. The Douglas-Bell Canada Brain Bank Post-mortem Brain Imaging Protocol. Aperture Neuro 4. https://doi.org/10.52294/001c.123347

Dadar, M., Sanches, L., Fouquet, J.P., Moqadam, R., Alasmar, Z., Ruth Leppert, I., Mirault, D., Maranzano, J., Mechawar, N., Chakravarty, M., Zeighami, Y., 2024b. The Douglas-Bell

Canada Brain Bank Post-mortem Brain Imaging Protocol. Aperture Neuro 4. https://doi.org/10.52294/001c.123347

Dallaire-Théroux, C., Beheshti, I., Potvin, O., Dieumegarde, L., Saikali, S., Duchesne, S., National Alzheimer's Coordinating Center, Alzheimer's Disease Neuroimaging Initiative, 2019. Braak neurofibrillary tangle staging prediction from in vivo MRI metrics. Alzheimers Dement. Diagn. Assess. Dis. Monit. 11, 599–609. https://doi.org/10.1016/j.dadm.2019.07.001

Dam, A.M., 1979. Shrinkage of the brain during histological procedures with fixation in formaldehyde solutions of different concentrations. J. Hirnforsch. 20, 115–119.

Daugherty, A.M., Carr, V., Canada, K.L., Rådman, G., Brown, T., Augustinack, J., Amunts, K., Bakker, A., Berron, D., Burggren, A., Chetelat, G., Flores, R.D., Ding, S.-L., Huang, Y., Insausti, R., Johnson, E., Kanel, P., Keresztes, A., Kedo, O., Kennedy, K.M., Lee, J., Malykhin, N., Martinez, A., Mueller, S., Mulligan, E., Ofen, N., Palombo, D., Pasquini, L., Pluta, J., Raz, N., Riggins, T., Rodrigue, K.M., Saifullah, S., Schlichting, M.L., Stark, C., Wang, L., Yushkevich, P., La Joie, R., Wisse, L., Olsen, R., the Alzheimer's Disease Neuroimaging Initiative, 2025. Harmonized Protocol for Subfield Segmentation in the Hippocampal Body on High-Resolution *in vivo* MRI from the Hippocampal Subfields Group (HSG). https://doi.org/10.1101/2025.04.29.651039

Dawe, R.J., Bennett, D.A., Schneider, J.A., Arfanakis, K., 2011. Neuropathologic Correlates of Hippocampal Atrophy in the Elderly: A Clinical, Pathologic, Postmortem MRI Study. PLoS ONE 6, e26286. https://doi.org/10.1371/journal.pone.0026286

Dawe, R.J., Bennett, D.A., Schneider, J.A., Leurgans, S.E., Kotrotsou, A., Boyle, P.A., Arfanakis, K., 2014. Ex vivo T2 relaxation: associations with age-related neuropathology and cognition. Neurobiol. Aging 35, 1549–1561. https://doi.org/10.1016/j.neurobiolaging.2014.01.144

Dawe, R.J., Bennett, D.A., Schneider, J.A., Vasireddi, S.K., Arfanakis, K., 2009. Postmortem MRI of human brain hemispheres: T_2 relaxation times during formaldehyde fixation. Magn. Reson. Med. 61, 810–818. https://doi.org/10.1002/mrm.21909

Dawe, R.J., Yu, L., Arfanakis, K., Schneider, J.A., Bennett, D.A., Boyle, P.A., 2020. Late-life cognitive decline is associated with hippocampal volume, above and beyond its associations with traditional neuropathologic indices. Alzheimers Dement. 16, 209–218. https://doi.org/10.1002/alz.12009

De Barros, A., Arribarat, G., Combis, J., Chaynes, P., Péran, P., 2019. Matching ex vivo MRI With Iron Histology: Pearls and Pitfalls. Front. Neuroanat. 13, 68. https://doi.org/10.3389/fnana.2019.00068

De Flores, R., Berron, D., Ding, S., Ittyerah, R., Pluta, J.B., Xie, L., Adler, D.H., Robinson, J.L., Schuck, T., Trojanowski, J.Q., Grossman, M., Liu, W., Pickup, S., Das, S.R., Wolk, D.A., Yushkevich, P.A., Wisse, L.E.M., 2020a. Characterization of hippocampal subfields using ex vivo MRI and histology data: Lessons for in vivo segmentation. Hippocampus 30, 545–564. https://doi.org/10.1002/hipo.23172

De Flores, R., Canada, K.L., Brown, T., Gervais, N.J., Maass, A., Rådman, G., Shine, J., Tucker, H.L., Molloy, E.N., Adams, J.N., Reinke, M.B., Bakker, A., Berron, D., Dalton, M.A., Kennedy, K.M., LaJoie, R., Mueller, S.G., Ofen, N., Olsen, R.K., Raz, N., Riggins, T., Rodrigue, K.M., Stark, C., Wang, L., Wisse, L.E.M., Yushkevich, P.A., Carr, V.A., Daugherty, A.M., the Alzheimer's Disease Neuroimaging Initiative, 2025. Harmonized Protocol for Segmentation of the Hippocampal Tail on High-Resolution *in vivo* MRI from the Hippocampal Subfields Group (HSG). https://doi.org/10.1101/2025.11.20.689476

De Flores, R., La Joie, R., Chételat, G., 2015. Structural imaging of hippocampal subfields in healthy aging and Alzheimer's disease. Neuroscience 309, 29–50. https://doi.org/10.1016/j.neuroscience.2015.08.033

De Flores, R., Wisse, L.E.M., Das, S.R., Xie, L., McMillan, C.T., Trojanowski, J.Q., Robinson, J.L., Grossman, M., Lee, E., Irwin, D.J., Yushkevich, P.A., Wolk, D.A., 2020b. Contribution of

mixed pathology to medial temporal lobe atrophy in Alzheimer's disease. Alzheimers Dement. 16, 843–852. https://doi.org/10.1002/alz.12079
DeKraker, J., Cabalo, D.G., Royer, J., Ngo, A., Khan, A.R., Karat, B.G., Benkarim, O., Rodriguez-Cruces, R., Frauscher, B., Pana, R., Hansen, J.Y., Misic, B., Valk, S.L., Lau, J.C., Kirschner, M., Bernasconi, A., Bernasconi, N., Muenzing, S.E.A., Axer, M., Amunts, K., Evans, A.C., Bernhardt, B.C., 2025. HippoMaps: multiscale cartography of human hippocampal organization. Nat. Methods. https://doi.org/10.1038/s41592-025-02783-3
Denning, A.E., Ittyerah, R., Levorse, L.M., Sadeghpour, N., Athalye, C., Chung, E., Ravikumar, S., Dong, M., Duong, M.T., Li, Y., Ilesanmi, A., Sreepada, L.P., Sabatini, P., Lowe, M., Bahena, A., Zablah, J., Spencer, B.E., Watanabe, R., Kim, B., Sørensen, M.H., Khandelwal, P., Brown, C., Hrybouski, S., Xie, S.X., De Flores, R., Robinson, J.L., Schuck, T., Ohm, D.T., Arezoumandan, S., Porta, S., Detre, J.A., Insausti, R., Wisse, L.E.M., Das, S.R., Irwin, D.J., Lee, E.B., Wolk, D.A., Yushkevich, P.A., 2024. Association of quantitative histopathology measurements with antemortem medial temporal lobe cortical thickness in the Alzheimer's disease continuum. Acta Neuropathol. (Berl.) 148, 37. https://doi.org/10.1007/s00401-024-02789-9
Dhakal, S., Wyant, C.E., George, H.E., Morgan, S.E., Rangachari, V., 2021. Prion-like C-Terminal Domain of TDP-43 and α-Synuclein Interact Synergistically to Generate Neurotoxic Hybrid Fibrils. J. Mol. Biol. 433, 166953. https://doi.org/10.1016/j.jmb.2021.166953
Ding, S., Van Hoesen, G.W., 2010. Borders, extent, and topography of human perirhinal cortex as revealed using multiple modern neuroanatomical and pathological markers. Hum. Brain Mapp. 31, 1359–1379. https://doi.org/10.1002/hbm.20940
Edlow, B.L., Mareyam, A., Horn, A., Polimeni, J.R., Witzel, T., Tisdall, M.D., Augustinack, J.C., Stockmann, J.P., Diamond, B.R., Stevens, A., Tirrell, L.S., Folkerth, R.D., Wald, L.L., Fischl, B., Van Der Kouwe, A., 2019. 7 Tesla MRI of the ex vivo human brain at 100 micron resolution. Sci. Data 6, 244. https://doi.org/10.1038/s41597-019-0254-8
Evia, A.M., Kotrotsou, A., Tamhane, A.A., Dawe, R.J., Kapasi, A., Leurgans, S.E., Schneider, J.A., Bennett, D.A., Arfanakis, K., 2017. Ex-vivo quantitative susceptibility mapping of human brain hemispheres. PLOS ONE 12, e0188395. https://doi.org/10.1371/journal.pone.0188395
Fairfoul, G., McGuire, L.I., Pal, S., Ironside, J.W., Neumann, J., Christie, S., Joachim, C., Esiri, M., Evetts, S.G., Rolinski, M., Baig, F., Ruffmann, C., Wade-Martins, R., Hu, M.T.M., Parkkinen, L., Green, A.J.E., 2016. Alpha-synuclein RT -Qu IC in the CSF of patients with alpha-synucleinopathies. Ann. Clin. Transl. Neurol. 3, 812–818. https://doi.org/10.1002/acn3.338
Fatterpekar, G.M., Naidich, T.P., Delman, B.N., Aguinaldo, J.G., Gultekin, S.H., Sherwood, C.C., Hof, P.R., Drayer, B.P., Fayad, Z.A., 2002. Cytoarchitecture of the human cerebral cortex: MR microscopy of excised specimens at 9.4 Tesla. AJNR Am. J. Neuroradiol. 23, 1313–1321.
Fischl, B., 2012. FreeSurfer. NeuroImage 62, 774–781. https://doi.org/10.1016/j.neuroimage.2012.01.021
Fischl, B., Stevens, A.A., Rajendran, N., Yeo, B.T.T., Greve, D.N., Van Leemput, K., Polimeni, J.R., Kakunoori, S., Buckner, R.L., Pacheco, J., Salat, D.H., Melcher, J., Frosch, M.P., Hyman, B.T., Grant, P.E., Rosen, B.R., Van Der Kouwe, A.J.W., Wiggins, G.C., Wald, L.L., Augustinack, J.C., 2009. Predicting the location of entorhinal cortex from MRI. NeuroImage 47, 8–17. https://doi.org/10.1016/j.neuroimage.2009.04.033
Fischl, B., Van Der Kouwe, A., Varadarajan, D., Tisdall, M.D., Morgan, L., Robert, Stevens, A., 2021. High Resolution Ex Vivo Structural MRI Imaging & Analysis Protocol. protocols.io.
Fracasso, A., Van Veluw, S.J., Visser, F., Luijten, P.R., Spliet, W., Zwanenburg, J.J.M., Dumoulin, S.O., Petridou, N., 2016a. Myelin contrast across lamina at 7T, ex-vivo and in-vivo dataset. Data Brief 8, 990–1003. https://doi.org/10.1016/j.dib.2016.06.058

Fracasso, A., Van Veluw, S.J., Visser, F., Luijten, P.R., Spliet, W., Zwanenburg, J.J.M., Dumoulin, S.O., Petridou, N., 2016b. Lines of Baillarger in vivo and ex vivo: Myelin contrast across lamina at 7 T MRI and histology. NeuroImage 133, 163–175. https://doi.org/10.1016/j.neuroimage.2016.02.072

Frigerio, I., Boon, B.D.C., Lin, C.-P., Galis-de Graaf, Y., Bol, J., Preziosa, P., Twisk, J., Barkhof, F., Hoozemans, J.J.M., Bouwman, F.H., Rozemuller, A.J.M., Van De Berg, W.D.J., Jonkman, L.E., 2021. Amyloid-β, p-tau and reactive microglia are pathological correlates of MRI cortical atrophy in Alzheimer's disease. Brain Commun. 3, fcab281. https://doi.org/10.1093/braincomms/fcab281

Frigerio, I., Laansma, M.A., Lin, C.-P., Hermans, E.J.M., Bouwman, M.M.A., Bol, J.G.J.M., Galis-de Graaf, Y., Hepp, D.H., Rozemuller, A.J.M., Barkhof, F., Van De Berg, W.D.J., Jonkman, L.E., 2023. Neurofilament light chain is increased in the parahippocampal cortex and associates with pathological hallmarks in Parkinson's disease dementia. Transl. Neurodegener. 12, 3. https://doi.org/10.1186/s40035-022-00328-8

Gagliardi, G., Rodriguez-Vieitez, E., Montal, V., Sepulcre, J., Diez, I., Lois, C., Hanseeuw, B., Schultz, A.P., Properzi, M.J., Papp, K.V., Marshall, G.A., Fortea, J., Johnson, K.A., Sperling, R.A., Vannini, P., 2023. Cortical microstructural changes predict tau accumulation and episodic memory decline in older adults harboring amyloid. Commun. Med. 3, 106. https://doi.org/10.1038/s43856-023-00324-7

Gawor, K., Tomé, S.O., Vandenberghe, R., Van Damme, P., Vandenbulcke, M., Otto, M., Von Arnim, C.A.F., Ghebremedhin, E., Ronisz, A., Ospitalieri, S., Blaschko, M., Thal, D.R., 2024. Amygdala-predominant α-synuclein pathology is associated with exacerbated hippocampal neuron loss in Alzheimer's disease. Brain Commun. 6, fcae442. https://doi.org/10.1093/braincomms/fcae442

Gawor, K., Verrept, S., Arekatla, G., Wouters, D., Ronisz, A., Hecht, M., Laureyssen, C., Donck, H.V., Lahaije, B., Ospitalieri, S., Vandenbulcke, M., Otto, M., Von Arnim, C.A.F., Ghebremedhin, E., Hanseeuw, B., Vandenberghe, R., Blaschko, M., Sifrim, A., Sleegers, K., Thal, D.R., Tomé, S.O., 2025. Alzheimer's disease and its co-pathologies: Implications for hippocampal degeneration, cognitive decline, and the role of *APOE* ε4. Alzheimers Dement. 21, e70483. https://doi.org/10.1002/alz.70483

Giannini, L.A.A., Bulk, M., Kenkhuis, B., Rajicic, A., Melhem, S., Hegeman-Kleinn, I., Bossoni, L., Suidgeest, E., Dopper, E.G.P., Van Swieten, J.C., Van Der Weerd, L., Seelaar, H., 2023. Cortical iron accumulation in *MAPT* - and *C9orf 72* -associated frontotemporal lobar degeneration. Brain Pathol. 33, e13158. https://doi.org/10.1111/bpa.13158

Giuliano, A., Donatelli, G., Cosottini, M., Tosetti, M., Retico, A., Fantacci, M.E., 2017. H ippocampal subfields at ultra high field MRI: A n overview of segmentation and measurement methods. Hippocampus 27, 481–494. https://doi.org/10.1002/hipo.22717

Gong, N.-J., Dibb, R., Bulk, M., Van Der Weerd, L., Liu, C., 2019. Imaging beta amyloid aggregation and iron accumulation in Alzheimer's disease using quantitative susceptibility mapping MRI. NeuroImage 191, 176–185. https://doi.org/10.1016/j.neuroimage.2019.02.019

Gonzalez, A.D., Wadop, Y.N., Danner, B., Clarke, K.M., Dopler, M.B., Ghaseminejad-Bandpey, A., Babu, S., Parker-Garza, J., Corbett, C., Alhneif, M., Keating, M., Bieniek, K.F., Maestre, G.E., Seshadri, S., Etemadmoghadam, S., Fongang, B., Flanagan, M.E., 2025. Digital pathology in tau research: A comparison of QuPath and HALO. J. Neuropathol. Exp. Neurol. 84, 692–706. https://doi.org/10.1093/jnen/nlaf026

Grinberg, L.T., Amaro, E., Teipel, S., Dos Santos, D.D., Pasqualucci, C.A., Leite, R.E.P., Camargo, C.R., Gonçalves, J.A., Sanches, A.G., Santana, M., Ferretti, R.E.L., Jacob-Filho, W., Nitrini, R., Heinsen, H., 2008. Assessment of factors that confound MRI and neuropathological correlation of human postmortem brain tissue. Cell Tissue Bank. 9, 195. https://doi.org/10.1007/s10561-008-9080-5

Hamilton, R.L., 2000. Lewy Bodies in Alzheimer's Disease: A Neuropathological Review of 145 Cases Using α-Synuclein Immunohistochemistry. Brain Pathol. 10, 378–384. https://doi.org/10.1111/j.1750-3639.2000.tb00269.x

Hanko, V., Apple, A.C., Alpert, K.I., Warren, K.N., Schneider, J.A., Arfanakis, K., Bennett, D.A., Wang, L., 2019. In vivo hippocampal subfield shape related to TDP-43, amyloid beta, and tau pathologies. Neurobiol. Aging 74, 171–181. https://doi.org/10.1016/j.neurobiolaging.2018.10.013

Hanseeuw, B.J., Betensky, R.A., Jacobs, H.I.L., Schultz, A.P., Sepulcre, J., Becker, J.A., Cosio, D.M.O., Farrell, M., Quiroz, Y.T., Mormino, E.C., Buckley, R.F., Papp, K.V., Amariglio, R.A., Dewachter, I., Ivanoiu, A., Huijbers, W., Hedden, T., Marshall, G.A., Chhatwal, J.P., Rentz, D.M., Sperling, R.A., Johnson, K., 2019. Association of Amyloid and Tau With Cognition in Preclinical Alzheimer Disease: A Longitudinal Study. JAMA Neurol. 76, 915. https://doi.org/10.1001/jamaneurol.2019.1424

Hanseeuw, B.J., Jacobs, H.I.L., Schultz, A.P., Buckley, R.F., Farrell, M.E., Guehl, N.J., Becker, J.A., Properzi, M., Sanchez, J.S., Quiroz, Y.T., Vannini, P., Sepulcre, J., Yang, H.-S., Chhatwal, J.P., Gatchel, J., Marshall, G.A., Amariglio, R., Papp, K., Rentz, D.M., Normandin, M., Price, J.C., Healy, B.C., El Fakhri, G., Sperling, R.A., Johnson, K.A., 2023. Association of Pathologic and Volumetric Biomarker Changes With Cognitive Decline in Clinically Normal Adults: Harvard Aging Brain Study. Neurology 101. https://doi.org/10.1212/WNL.0000000000207962

Hansson, O., Zetterberg, H., Buchhave, P., Andreasson, U., Londos, E., Minthon, L., Blennow, K., 2007. Prediction of Alzheimer's Disease Using the CSF Aβ42/Aβ40 Ratio in Patients with Mild Cognitive Impairment. Dement. Geriatr. Cogn. Disord. 23, 316–320. https://doi.org/10.1159/000100926

Hansson, O., Zetterberg, H., Buchhave, P., Londos, E., Blennow, K., Minthon, L., 2006. Association between CSF biomarkers and incipient Alzheimer's disease in patients with mild cognitive impairment: a follow-up study. Lancet Neurol. 5, 228–234. https://doi.org/10.1016/S1474-4422(06)70355-6

Harper, L., Bouwman, F., Burton, E.J., Barkhof, F., Scheltens, P., O'Brien, J.T., Fox, N.C., Ridgway, G.R., Schott, J.M., 2017. Patterns of atrophy in pathologically confirmed dementias: a voxelwise analysis. J. Neurol. Neurosurg. Psychiatry 88, 908–916. https://doi.org/10.1136/jnnp-2016-314978

Hary, A.T., Chadha, S., Mercaldo, N., Smith, E.-M.C., Van Der Kouwe, A.J.W., Fischl, B., Mount, C., Kozanno, L., Frosch, M.P., Augustinack, J.C., 2025. Locus coeruleus tau validates and informs high-resolution MRI in aging and at earliest Alzheimer's pathology stages. Acta Neuropathol. Commun. 13, 44. https://doi.org/10.1186/s40478-025-01957-6

Heywood, A., Stocks, J., Schneider, J.A., Arfanakis, K., Bennett, D.A., Beg, M.F., Wang, L., 2022. The unique effect of TDP-43 on hippocampal subfield morphometry and cognition. NeuroImage Clin. 35, 103125. https://doi.org/10.1016/j.nicl.2022.103125

Hyare, H., Powell, C., Thornton, J., Parkes, H., Mancini, L., Yousry, T., others, 2008. Perfluoropolyethers in magnetic resonance microscopy: Effect on quantitative magnetic resonance imaging measures and histological properties of formalin-fixed brain tissue, in: Proceedings of the International Society for Magnetic Resonance in Medicine. p. 1719.

Iglesias, J.E., Augustinack, J.C., Nguyen, K., Player, C.M., Player, A., Wright, M., Roy, N., Frosch, M.P., McKee, A.C., Wald, L.L., Fischl, B., Van Leemput, K., 2015. A computational atlas of the hippocampal formation using ex vivo, ultra-high resolution MRI: Application to adaptive segmentation of in vivo MRI. NeuroImage 115, 117–137. https://doi.org/10.1016/j.neuroimage.2015.04.042

Iglesias, J.E., Crampsie, S., Strand, C., Tachrount, M., Thomas, D.L., Holton, J.L., 2018a. Effect of Fluorinert on the Histological Properties of Formalin-Fixed Human Brain Tissue. J. Neuropathol. Exp. Neurol. 77, 1085–1090. https://doi.org/10.1093/jnen/nly098

Iglesias, J.E., Insausti, R., Lerma-Usabiaga, G., Bocchetta, M., Van Leemput, K., Greve, D.N., Van Der Kouwe, A., Fischl, B., Caballero-Gaudes, C., Paz-Alonso, P.M., 2018b. A probabilistic atlas of the human thalamic nuclei combining ex vivo MRI and histology. NeuroImage 183, 314–326. https://doi.org/10.1016/j.neuroimage.2018.08.012

Ingrassia, L., Boluda, S., Potier, M.-C., Haïk, S., Jimenez, G., Kar, A., Racoceanu, D., Delatour, B., Stimmer, L., 2024. Automated deep learning segmentation of neuritic plaques and neurofibrillary tangles in Alzheimer disease brain sections using a proprietary software. J. Neuropathol. Exp. Neurol. 83, 752–762. https://doi.org/10.1093/jnen/nlae048

Insausti, R., Insausti, A.M., Muñoz López, M., Medina Lorenzo, I., Arroyo-Jiménez, M.D.M., Marcos Rabal, M.P., De La Rosa-Prieto, C., Delgado-González, J.C., Montón Etxeberria, J., Cebada-Sánchez, S., Raspeño-García, J.F., Iñiguez De Onzoño, M.M., Molina Romero, F.J., Benavides-Piccione, R., Tapia-González, S., Wisse, L.E.M., Ravikumar, S., Wolk, D.A., DeFelipe, J., Yushkevich, P., Artacho-Pérula, E., 2023. Ex vivo, in situ perfusion protocol for human brain fixation compatible with microscopy, MRI techniques, and anatomical studies. Front. Neuroanat. 17, 1149674. https://doi.org/10.3389/fnana.2023.1149674

Irwin, K.E., Jasin, P., Braunstein, K.E., Sinha, I.R., Garret, M.A., Bowden, K.D., Chang, K., Troncoso, J.C., Moghekar, A., Oh, E.S., Raitcheva, D., Bartlett, D., Miller, T., Berry, J.D., Traynor, B.J., Ling, J.P., Wong, P.C., 2024. A fluid biomarker reveals loss of TDP-43 splicing repression in presymptomatic ALS–FTD. Nat. Med. 30, 382–393. https://doi.org/10.1038/s41591-023-02788-5

Jack, C.R., Bennett, D.A., Blennow, K., Carrillo, M.C., Dunn, B., Haeberlein, S.B., Holtzman, D.M., Jagust, W., Jessen, F., Karlawish, J., Liu, E., Molinuevo, J.L., Montine, T., Phelps, C., Rankin, K.P., Rowe, C.C., Scheltens, P., Siemers, E., Snyder, H.M., Sperling, R., Contributors, Elliott, C., Masliah, E., Ryan, L., Silverberg, N., 2018. NIA-AA Research Framework: Toward a biological definition of Alzheimer's disease. Alzheimers Dement. 14, 535–562. https://doi.org/10.1016/j.jalz.2018.02.018

Jack, C.R., Dickson, D.W., Parisi, J.E., Xu, Y.C., Cha, R.H., O'Brien, P.C., Edland, S.D., Smith, G.E., Boeve, B.F., Tangalos, E.G., Kokmen, E., Petersen, R.C., 2002. Antemortem MRI findings correlate with hippocampal neuropathology in typical aging and dementia. Neurology 58, 750–757. https://doi.org/10.1212/wnl.58.5.750

Jagust, W.J., Zheng, L., Harvey, D.J., Mack, W.J., Vinters, H.V., Weiner, M.W., Ellis, W.G., Zarow, C., Mungas, D., Reed, B.R., Kramer, J.H., Schuff, N., DeCarli, C., Chui, H.C., 2008. Neuropathological basis of magnetic resonance images in aging and dementia. Ann. Neurol. 63, 72–80. https://doi.org/10.1002/ana.21296

Jäkel, L., De Kort, A.M., Klijn, C.J.M., Schreuder, F.H.B.M., Verbeek, M.M., 2022. Prevalence of cerebral amyloid angiopathy: A systematic review and meta-analysis. Alzheimers Dement. 18, 10–28. https://doi.org/10.1002/alz.12366

Jellinger, K.A., 2003. α-Synuclein pathology in Parkinson's and Alzheimer's disease brain: incidence and topographic distribution—a pilot study. Acta Neuropathol. (Berl.) 106, 191–202. https://doi.org/10.1007/s00401-003-0725-y

Johnson, K.A., Schultz, A., Betensky, R.A., Becker, J.A., Sepulcre, J., Rentz, D., Mormino, E., Chhatwal, J., Amariglio, R., Papp, K., Marshall, G., Albers, M., Mauro, S., Pepin, L., Alverio, J., Judge, K., Philiossaint, M., Shoup, T., Yokell, D., Dickerson, B., Gomez-Isla, T., Hyman, B., Vasdev, N., Sperling, R., 2016. Tau positron emission tomographic imaging in aging and early Alzheimer disease. Ann. Neurol. 79, 110–119. https://doi.org/10.1002/ana.24546

Jonkman, L.E., Graaf, Y.G., Bulk, M., Kaaij, E., Pouwels, P.J.W., Barkhof, F., Rozemuller, A.J.M., Van Der Weerd, L., Geurts, J.J.G., Van De Berg, W.D.J., 2019. Normal Aging Brain Collection Amsterdam (NABCA): A comprehensive collection of postmortem high-field imaging, neuropathological and morphometric datasets of non-neurological controls. NeuroImage Clin. 22, 101698. https://doi.org/10.1016/j.nicl.2019.101698

Josephs, K.A., Dickson, D.W., Tosakulwong, N., Weigand, S.D., Murray, M.E., Petrucelli, L., Liesinger, A.M., Senjem, M.L., Spychalla, A.J., Knopman, D.S., Parisi, J.E., Petersen, R.C., Jack, C.R., Whitwell, J.L., 2017. Rates of hippocampal atrophy and presence of post-mortem TDP-43 in patients with Alzheimer's disease: a longitudinal retrospective study. Lancet Neurol. 16, 917–924. https://doi.org/10.1016/S1474-4422(17)30284-3

Kantarci, K., Ferman, T.J., Boeve, B.F., Weigand, S.D., Przybelski, S., Vemuri, P., Murray, M.M., Senjem, M.L., Smith, G.E., Knopman, D.S., Petersen, R.C., Jack, C.R., Parisi, J.E., Dickson, D.W., 2012. Focal atrophy on MRI and neuropathologic classification of dementia with Lewy bodies. Neurology 79, 553–560. https://doi.org/10.1212/wnl.0b013e31826357a5

Karat, B.G., Khler, S., Khan, A.R., 2024. Diffusion MRI of the Hippocampus. J. Neurosci. 44, e1705232024. https://doi.org/10.1523/JNEUROSCI.1705-23.2024

Kenkhuis, B., Jonkman, L.E., Bulk, M., Buijs, M., Boon, B.D.C., Bouwman, F.H., Geurts, J.J.G., Van De Berg, W.D.J., Van Der Weerd, L., 2019. 7T MRI allows detection of disturbed cortical lamination of the medial temporal lobe in patients with Alzheimer's disease. NeuroImage Clin. 21, 101665. https://doi.org/10.1016/j.nicl.2019.101665

Kerchner, G.A., Deutsch, G.K., Zeineh, M., Dougherty, R.F., Saranathan, M., Rutt, B.K., 2012. Hippocampal CA1 apical neuropil atrophy and memory performance in Alzheimer's disease. NeuroImage 63, 194–202. https://doi.org/10.1016/j.neuroimage.2012.06.048

Khandelwal, P., 2025. Postmortem Image Analysis of the Human Brain to Characterize Alzheimer's Disease and Related Dementias (Doctoral dissertation). University of Pennsylvania.

Khandelwal, P., Duong, M.T., Levorse, L., Fuentes, C., Denning, A.E., Trotman, W., Ittyerah, R., Bahena, A., Schuck, T., Gabrielyan, M., Prabhakaran, K., Ohm, D.T., Mizsei, G., Robinson, J., Muñoz, M., Detre, J.A., Lee, E.B., Irwin, D.J., McMillan, C., Tisdall, M.D., Das, S.R., Wolk, D.A., Yushkevich, P.A., 2025. Surface-Based Parcellation and Vertex-wise Analysis of Ultra High-resolution ex vivo 7 tesla MRI in Alzheimer's disease and related dementias, in: Bathula, D.R., Benet Nirmala, A., Dvornek, N.C., Govindarajan, S.T., Habes, M., Kumar, V., Nebli, A., Wolfers, T., Xiao, Y. (Eds.), Machine Learning in Clinical Neuroimaging, Lecture Notes in Computer Science. Springer Nature Switzerland, Cham, pp. 134–144. https://doi.org/10.1007/978-3-031-78761-4_13

Khandelwal, P., Duong, M.T., Levorse, L.M., A. Lim, S., Gauthier, N., Shenoy, V., Chung, E., Denning, A.E., Bahena, A., Trotman, W., Olm, C.A., Radhakrishnan, H., Ittyerah, R., Prabhakaran, K., Mizsei, G., Schuck, T., Robinson, J., Ohm, D.T., Phillips, J.S., Detre, J.A., Lee, E.B., Irwin, D.J., McMillan, C.T., Tisdall, M.D., Das, S.R., Wolk, D.A., Yushkevich, P.A., 2026. VIOLET: Volumetric Image registration via Optimization and Learning for Efficient image Translation, in: Fernandez, V., Wiesner, D., Zuo, L., Casamitjana, A., Remedios, S.W. (Eds.), Simulation and Synthesis in Medical Imaging. Springer Nature Switzerland, Cham, pp. 84–96.

Khandelwal, P., Duong, M.T., Sadaghiani, S., Lim, S., Denning, A.E., Chung, E., Ravikumar, S., Arezoumandan, S., Peterson, C., Bedard, M., Capp, N., Ittyerah, R., Migdal, E., Choi, G., Kopp, E., Loja, B., Hasan, E., Li, J., Bahena, A., Prabhakaran, K., Mizsei, G., Gabrielyan, M., Schuck, T., Trotman, W., Robinson, J., Ohm, D.T., Lee, E.B., Trojanowski, J.Q., McMillan, C., Grossman, M., Irwin, D.J., Detre, J.A., Tisdall, M.D., Das, S.R., Wisse, L.E.M., Wolk, D.A., Yushkevich, P.A., 2024. Automated deep learning segmentation of high-resolution 7 Tesla postmortem MRI for quantitative analysis of structure-pathology correlations in neurodegenerative diseases. Imaging Neurosci. 2, 1–30. https://doi.org/10.1162/imag_a_00171

Klunk, W.E., Engler, H., Nordberg, A., Wang, Y., Blomqvist, G., Holt, D.P., Bergström, M., Savitcheva, I., Huang, G., Estrada, S., Ausén, B., Debnath, M.L., Barletta, J., Price, J.C., Sandell, J., Lopresti, B.J., Wall, A., Koivisto, P., Antoni, G., Mathis, C.A., Långström, B.,

2004. Imaging brain amyloid in Alzheimer's disease with Pittsburgh Compound-B. Ann. Neurol. 55, 306–319. https://doi.org/10.1002/ana.20009
Klunk, W.E., Koeppe, R.A., Price, J.C., Benzinger, T.L., Devous, M.D., Jagust, W.J., Johnson, K.A., Mathis, C.A., Minhas, D., Pontecorvo, M.J., Rowe, C.C., Skovronsky, D.M., Mintun, M.A., 2015. The Centiloid Project: Standardizing quantitative amyloid plaque estimation by PET. Alzheimers Dement. 11, 1. https://doi.org/10.1016/j.jalz.2014.07.003
Kotrotsou, A., Bennett, D.A., Schneider, J.A., Dawe, R.J., Golak, T., Leurgans, S.E., Yu, L., Arfanakis, K., 2014. Ex vivo MR volumetry of human brain hemispheres. Magn. Reson. Med. 71, 364–374. https://doi.org/10.1002/mrm.24661
Kotrotsou, A., Schneider, J.A., Bennett, D.A., Leurgans, S.E., Dawe, R.J., Boyle, P.A., Golak, T., Arfanakis, K., 2015. Neuropathologic correlates of regional brain volumes in a community cohort of older adults. Neurobiol. Aging 36, 2798–2805. https://doi.org/10.1016/j.neurobiolaging.2015.06.025
Latimer, C.S., Liachko, N.F., 2021. Tau and TDP-43 synergy: a novel therapeutic target for sporadic late-onset Alzheimer's disease. GeroScience 43, 1627–1634. https://doi.org/10.1007/s11357-021-00407-0
Li, K., Rashid, T., Li, J., Honnorat, N., Nirmala, A.B., Fadaee, E., Wang, D., Charisis, S., Liu, H., Franklin, C., Maybrier, M., Katragadda, H., Abazid, L., Ganapathy, V., Valaparla, V.L., Badugu, P., Vasquez, E., Solano, L., Clarke, G., Maestre, G., Richardson, T., Walker, J., Fox, P.T., Bieniek, K., Seshadri, S., Habes, M., 2023. Postmortem Brain Imaging in Alzheimer's Disease and Related Dementias: The South Texas Alzheimer's Disease Research Center Repository. J. Alzheimer's Dis. 96, 1267–1283. https://doi.org/10.3233/JAD-230389
Lin, C.P., Frigerio, I., Boon, B.D.C., Zhou, Z., Rozemuller, A.J.M., Bouwman, F.H., Schoonheim, M.M., Van De Berg, W.D.J., Jonkman, L.E., 2022. Structural (dys)connectivity associates with cholinergic cell density in Alzheimer's disease. Brain 145, 2869–2881. https://doi.org/10.1093/brain/awac093
Liou, J.-J., Li, J., Berardinelli, J., Jin, H., Santini, T., Noh, J., Farhat, N., Wu, M., Aizenstein, H., Mettenburg, J.M., Yong, W., Head, E., Ikonomovic, M., Ibrahim, T., Kofler, J., the Alzheimer's Biomarker Consortium on Down syndrome study, 2024. Correlating hippocampal and amygdala volumes with neuropathological burden in neurodegenerative diseases using 7T postmortem MRI. https://doi.org/10.1101/2024.05.15.24307354
Llamas Rodríguez, J., Van Der Kouwe, A.J.W., Oltmer, J., Rosenblum, E., Mercaldo, N., Fischl, B., Marshall, M., Frosch, M.P., Augustinack, J.C., 2024. Entorhinal vessel density correlates with phosphorylated tau and TDP-43 pathology. Alzheimers Dement. 20, 4649–4662. https://doi.org/10.1002/alz.13896
Llamas-Rodríguez, J., Oltmer, J., Greve, D.N., Williams, E., Slepneva, N., Wang, R., Champion, S., Lang-Orsini, M., Fischl, B., Frosch, M.P., Van Der Kouwe, A.J.W., Augustinack, J.C., 2022. Entorhinal Subfield Vulnerability to Neurofibrillary Tangles in Aging and the Preclinical Stage of Alzheimer's Disease. J. Alzheimers Dis. 87, 1379–1399. https://doi.org/10.3233/JAD-215567
Maass, A., Berron, D., Libby, L.A., Ranganath, C., Düzel, E., 2015. Functional subregions of the human entorhinal cortex. eLife 4, e06426. https://doi.org/10.7554/eLife.06426
Makkinejad, N., Schneider, J.A., Yu, J., Leurgans, S.E., Kotrotsou, A., Evia, A.M., Bennett, D.A., Arfanakis, K., 2019. Associations of amygdala volume and shape with transactive response DNA-binding protein 43 (TDP-43) pathology in a community cohort of older adults. Neurobiol. Aging 77, 104–111. https://doi.org/10.1016/j.neurobiolaging.2019.01.022
Makkinejad, N., Zanon Zotin, M.C., Van Den Brink, H., Auger, C.A., Vom Eigen, K.A., Iglesias, J.E., Greenberg, S.M., Perosa, V., Van Veluw, S.J., 2024. Neuropathological Correlates of

White Matter Hyperintensities in Cerebral Amyloid Angiopathy. J. Am. Heart Assoc. 13, e035744. https://doi.org/10.1161/JAHA.124.035744
Mancini, M., Casamitjana, A., Peter, L., Robinson, E., Crampsie, S., Thomas, D.L., Holton, J.L., Jaunmuktane, Z., Iglesias, J.E., 2020. A multimodal computational pipeline for 3D histology of the human brain. Sci. Rep. 10. https://doi.org/10.1038/s41598-020-69163-z
Manson, E.N., Inkoom, S., Mumuni, A.N., 2022. Impact of Magnetic Field Inhomogeneity on the Quality of Magnetic Resonance Images and Compensation Techniques: A Review. Rep. Med. Imaging Volume 15, 43–56. https://doi.org/10.2147/RMI.S369491
Mattsson, N., 2009. CSF Biomarkers and Incipient Alzheimer Disease in Patients With Mild Cognitive Impairment. JAMA 302, 385. https://doi.org/10.1001/jama.2009.1064
Mohanty, R., Ferreira, D., Frerich, S., Muehlboeck, J.-S., Grothe, M.J., Westman, E., on behalf of the Alzheimer's Disease Neuroimaging Initiative, 2022. Neuropathologic Features of Antemortem Atrophy-Based Subtypes of Alzheimer Disease. Neurology 99. https://doi.org/10.1212/WNL.0000000000200573
Moussaud, S., Jones, D.R., Moussaud-Lamodière, E.L., Delenclos, M., Ross, O.A., McLean, P.J., 2014. Alpha-synuclein and tau: teammates in neurodegeneration? Mol. Neurodegener. 9, 43. https://doi.org/10.1186/1750-1326-9-43
Nabuurs, R.J.A., Natté, R., De Ronde, F.M., Hegeman-Kleinn, I., Dijkstra, J., Van Duinen, S.G., Webb, A.G., Rozemuller, A.J., Van Buchem, M.A., Van Der Weerd, L., 2013. MR Microscopy of Human Amyloid-β Deposits: Characterization of Parenchymal Amyloid, Diffuse Plaques, and Vascular Amyloid. J. Alzheimer's Dis. 34, 1037–1049. https://doi.org/10.3233/JAD-122215
Nelson, P.T., Dickson, D.W., Trojanowski, J.Q., Jack, C.R., Boyle, P.A., Arfanakis, K., Rademakers, R., Alafuzoff, I., Attems, J., Brayne, C., Coyle-Gilchrist, I.T.S., Chui, H.C., Fardo, D.W., Flanagan, M.E., Halliday, G., Hokkanen, S.R.K., Hunter, S., Jicha, G.A., Katsumata, Y., Kawas, C.H., Keene, C.D., Kovacs, G.G., Kukull, W.A., Levey, A.I., Makkinejad, N., Montine, T.J., Murayama, S., Murray, M.E., Nag, S., Rissman, R.A., Seeley, W.W., Sperling, R.A., White Iii, C.L., Yu, L., Schneider, J.A., 2019. Limbic-predominant age-related TDP-43 encephalopathy (LATE): consensus working group report. Brain 142, 1503–1527. https://doi.org/10.1093/brain/awz099
Nelson, P.T., Katsumata, Y., 2024. Arteriolosclerosis and LATE-NC: two common and inter-related contributors to Alzheimer's-type dementia. Alzheimers Dement. 20, e085805. https://doi.org/10.1002/alz.085805
Nelson, P.T., Lee, E.B., Cykowski, M.D., Alafuzoff, I., Arfanakis, K., Attems, J., Brayne, C., Corrada, M.M., Dugger, B.N., Flanagan, M.E., Ghetti, B., Grinberg, L.T., Grossman, M., Grothe, M.J., Halliday, G.M., Hasegawa, M., Hokkanen, S.R.K., Hunter, S., Jellinger, K., Kawas, C.H., Keene, C.D., Kouri, N., Kovacs, G.G., Leverenz, J.B., Latimer, C.S., Mackenzie, I.R., Mao, Q., McAleese, K.E., Merrick, R., Montine, T.J., Murray, M.E., Myllykangas, L., Nag, S., Neltner, J.H., Newell, K.L., Rissman, R.A., Saito, Y., Sajjadi, S.A., Schwetye, K.E., Teich, A.F., Thal, D.R., Tomé, S.O., Troncoso, J.C., Wang, S.-H.J., White, C.L., Wisniewski, T., Yang, H.-S., Schneider, J.A., Dickson, D.W., Neumann, M., 2023. LATE-NC staging in routine neuropathologic diagnosis: an update. Acta Neuropathol. (Berl.) 145, 159–173. https://doi.org/10.1007/s00401-022-02524-2
Neuhaus, D., Wendebourg, M.J., Deigendesch, N., Berger, C., Bauer, M., Haas, T., Scheurer, E., Schlaeger, R., Lenz, C., 2025. Exploring Potential Biomarkers for Amyotrophic Lateral Sclerosis Using Postmortem In Situ Magnetic Resonance Imaging. NMR Biomed. 38, e70059. https://doi.org/10.1002/nbm.70059
Olchanyi, M., Augustinack, J., Haynes, R.L., Lewis, L.D., Cicero, N., Li, J., Destrieux, C., Folkerth, R.D., Kinney, H.C., Fischl, B., Brown, E.N., Iglesias, J.E., Edlow, B.L., 2024. Histology-guided MRI segmentation of brainstem nuclei critical to consciousness. https://doi.org/10.1101/2024.09.26.24314117

Olsen, R.K., Carr, V.A., Daugherty, A.M., La Joie, R., Amaral, R.S.C., Amunts, K., Augustinack, J.C., Bakker, A., Bender, A.R., Berron, D., Boccardi, M., Bocchetta, M., Burggren, A.C., Chakravarty, M.M., Chételat, G., De Flores, R., DeKraker, J., Ding, S., Geerlings, M.I., Huang, Y., Insausti, R., Johnson, E.G., Kanel, P., Kedo, O., Kennedy, K.M., Keresztes, A., Lee, J.K., Lindenberger, U., Mueller, S.G., Mulligan, E.M., Ofen, N., Palombo, D.J., Pasquini, L., Pluta, J., Raz, N., Rodrigue, K.M., Schlichting, M.L., Lee Shing, Y., Stark, C.E.L., Steve, T.A., Suthana, N.A., Wang, L., Werkle-Bergner, M., Yushkevich, P.A., Yu, Q., Wisse, L.E.M., Hippocampal Subfields Group, 2019. Progress update from the hippocampal subfields group. Alzheimers Dement. Diagn. Assess. Dis. Monit. 11, 439–449. https://doi.org/10.1016/j.dadm.2019.04.001

Oltmer, J., Greve, D.N., Cerri, S., Slepneva, N., Llamas-Rodríguez, J., Iglesias, J.E., Van Leemput, K., Champion, S.N., Frosch, M.P., Augustinack, J.C., 2023. Assessing individual variability of the entorhinal subfields in health and disease. J. Comp. Neurol. 531, 2062–2079. https://doi.org/10.1002/cne.25538

Oltmer, J., Slepneva, N., Llamas Rodriguez, J., Greve, D.N., Williams, E.M., Wang, R., Champion, S.N., Lang-Orsini, M., Nestor, K., Fernandez-Ros, N., Fischl, B., Frosch, M.P., Magnain, C., Van Der Kouwe, A.J.W., Augustinack, J.C., 2022. Quantitative and histologically validated measures of the entorhinal subfields in *ex vivo* MRI. Brain Commun. 4, fcac074. https://doi.org/10.1093/braincomms/fcac074

Ossenkoppele, R., Cohn-Sheehy, B.I., La Joie, R., Vogel, J.W., Möller, C., Lehmann, M., Van Berckel, B.N.M., Seeley, W.W., Pijnenburg, Y.A., Gorno-Tempini, M.L., Kramer, J.H., Barkhof, F., Rosen, H.J., Van Der Flier, W.M., Jagust, W.J., Miller, B.L., Scheltens, P., Rabinovici, G.D., 2015. Atrophy patterns in early clinical stages across distinct phenotypes of Alzheimer's disease. Hum. Brain Mapp. 36, 4421–4437. https://doi.org/10.1002/hbm.22927

Ossenkoppele, R., Salvadó, G., Janelidze, S., Pichet Binette, A., Bali, D., Karlsson, L., Palmqvist, S., Mattsson-Carlgren, N., Stomrud, E., Therriault, J., Rahmouni, N., Rosa-Neto, P., Coomans, E.M., Van De Giessen, E., Van Der Flier, W.M., Teunissen, C.E., Jonaitis, E.M., Johnson, S.C., Villeneuve, S., PREVENT-AD Research Group, Benzinger, T.L.S., Schindler, S.E., Bateman, R.J., Doecke, J.D., Doré, V., Feizpour, A., Masters, C.L., Rowe, C., Wiste, H.J., Petersen, R.C., Jack, C.R., Hansson, O., 2025. Plasma p-tau217 and tau-PET predict future cognitive decline among cognitively unimpaired individuals: implications for clinical trials. Nat. Aging 5, 883–896. https://doi.org/10.1038/s43587-025-00835-z

Ossenkoppele, R., Van Der Kant, R., Hansson, O., 2022. Tau biomarkers in Alzheimer's disease: towards implementation in clinical practice and trials. Lancet Neurol. 21, 726–734. https://doi.org/10.1016/S1474-4422(22)00168-5

Pallebage-Gamarallage, M., Foxley, S., Menke, R.A.L., Huszar, I.N., Jenkinson, M., Tendler, B.C., Wang, C., Jbabdi, S., Turner, M.R., Miller, K.L., Ansorge, O., 2018. Dissecting the pathobiology of altered MRI signal in amyotrophic lateral sclerosis: A post mortem whole brain sampling strategy for the integration of ultra-high-field MRI and quantitative neuropathology. BMC Neurosci. 19. https://doi.org/10.1186/s12868-018-0416-1

Parekh, M.B., Rutt, B.K., Purcell, R., Chen, Y., Zeineh, M.M., 2015. Ultra-high resolution in-vivo 7.0 T structural imaging of the human hippocampus reveals the endfolial pathway. NeuroImage 112, 1–6. https://doi.org/10.1016/j.neuroimage.2015.02.029

Parker, D.M., Adams, J.N., Kim, S., McMillan, L., Yassa, M.A., 2025. NODDI-derived measures of microstructural integrity in medial temporal lobe white matter pathways are associated with Alzheimer's disease pathology and cognition. Imaging Neurosci. 3, IMAG.a.950. https://doi.org/10.1162/IMAG.a.950

Perosa, V., Auger, C.A., Zanon Zotin, M.C., Oltmer, J., Frosch, M.P., Viswanathan, A., Greenberg, S.M., Van Veluw, S.J., 2023. Histopathological Correlates of Lobar Microbleeds in False-Positive Cerebral Amyloid Angiopathy Cases. Ann. Neurol. 94, 856–870. https://doi.org/10.1002/ana.26761

Perosa, V., Oltmer, J., Munting, L.P., Freeze, W.M., Auger, C.A., Scherlek, A.A., Van Der Kouwe, A.J., Iglesias, J.E., Atzeni, A., Bacskai, B.J., Viswanathan, A., Frosch, M.P., Greenberg, S.M., Van Veluw, S.J., 2022. Perivascular space dilation is associated with vascular amyloid-β accumulation in the overlying cortex. Acta Neuropathol. (Berl.) 143, 331–348. https://doi.org/10.1007/s00401-021-02393-1

Pfefferbaum, A., Sullivan, E.V., Adalsteinsson, E., Garrick, T., Harper, C., 2004. Postmortem MR imaging of formalin-fixed human brain. NeuroImage 21, 1585–1595. https://doi.org/10.1016/j.neuroimage.2003.11.024

Planche, V., Mansencal, B., Manjon, J.V., Tourdias, T., Catheline, G., Coupé, P., For the Frontotemporal Lobar Degeneration Neuroimaging Initiative and the National Alzheimer's Coordinating Center cohort, 2023. Anatomical MRI staging of frontotemporal dementia variants. Alzheimers Dement. 19, 3283–3294. https://doi.org/10.1002/alz.12975

Puonti, O., Nolan, J., Dicamillo, R., Balbastre, Y., Casamitjana, A., Mancini, M., Robinson, E., Peter, L., Annunziata, R., Althonayan, J., Crampsie, S., Blackburn, E., Billot, B., Atzeni, A., Schmidt, P., Hughes, J., Augustinack, J., Edlow, B., Zöllei, L., Thomas, D.L., Kliemann, D., Bocchetta, M., Strand, C., Holton, J., Jaunmuktane, Z., Iglesias, J.E., 2025. Fast segmentation with the NextBrain histological atlas. https://doi.org/10.1101/2025.09.22.673638

Ravikumar, S., Denning, A.E., Lim, S., Chung, E., Sadeghpour, N., Ittyerah, R., Wisse, L.E.M., Das, S.R., Xie, L., Robinson, J.L., Schuck, T., Lee, E.B., Detre, J.A., Tisdall, M.D., Prabhakaran, K., Mizsei, G., De Onzono Martin, M.M.I., Arroyo Jiménez, M.D.M., Mũnoz, M., Marcos Rabal, M.D.P., Cebada Sánchez, S., Delgado González, J.C., De La Rosa Prieto, C., Irwin, D.J., Wolk, D.A., Insausti, R., Yushkevich, P.A., 2024. Postmortem imaging reveals patterns of medial temporal lobe vulnerability to tau pathology in Alzheimer's disease. Nat. Commun. 15, 4803. https://doi.org/10.1038/s41467-024-49205-0

Ravikumar, S., Wisse, L., Gao, Y., Gerig, G., Yushkevich, P., 2019. Facilitating Manual Segmentation of 3D Datasets Using Contour And Intensity Guided Interpolation, in: 2019 IEEE 16th International Symposium on Biomedical Imaging (ISBI 2019). pp. 714–718. https://doi.org/10.1109/ISBI.2019.8759500

Ravikumar, S., Wisse, L.E.M., Lim, S., Ittyerah, R., Xie, L., Bedard, M.L., Das, S.R., Lee, E.B., Tisdall, M.D., Prabhakaran, K., Lane, J., Detre, J.A., Mizsei, G., Trojanowski, J.Q., Robinson, J.L., Schuck, T., Grossman, M., Artacho-Pérula, E., De Onzoño Martin, M.M.I., Del Mar Arroyo Jiménez, M., Muñoz, M., Romero, F.J.M., Del Pilar Marcos Rabal, M., Sánchez, S.C., González, J.C.D., De La Rosa Prieto, C., Parada, M.C., Irwin, D.J., Wolk, D.A., Insausti, R., Yushkevich, P.A., 2021. Ex vivo MRI atlas of the human medial temporal lobe: characterizing neurodegeneration due to tau pathology. Acta Neuropathol. Commun. 9, 173. https://doi.org/10.1186/s40478-021-01275-7

Rodrigues, L., Bocchetta, M., Puonti, O., Greve, D., Londe, A.C., França, M., Appenzeller, S., Rittner, L., Iglesias, J.E., 2024. High-resolution segmentations of the hypothalamus and its subregions for training of segmentation models. Sci. Data 11, 940. https://doi.org/10.1038/s41597-024-03775-2

Rodriguez-Vieitez, E., Montal, V., Sepulcre, J., Lois, C., Hanseeuw, B., Vilaplana, E., Schultz, A.P., Properzi, M.J., Scott, M.R., Amariglio, R., Papp, K.V., Marshall, G.A., Fortea, J., Johnson, K.A., Sperling, R.A., Vannini, P., 2021. Association of cortical microstructure with amyloid-β and tau: impact on cognitive decline, neurodegeneration, and clinical progression in older adults. Mol. Psychiatry 26, 7813–7822. https://doi.org/10.1038/s41380-021-01290-z

Sadaghiani, S., Trotman, W., Lim, S.A., Chung, E., Ittyerah, R., Ravikumar, S., Khandelwal, P., Prabhakaran, K., Lavery, M.L., Ohm, D.T., Gabrielyan, M., Das, S.R., Schuck, T., Capp, N., Peterson, C.S., Migdal, E., Artacho-Pérula, E., Jiménez, M.D.M.A., Rabal, M.D.P.M., Sánchez, S.C., Prieto, C.D.L.R., Parada, M.C., Insausti, R., Robinson, J.L., McMillan, C.,

Grossman, M., Lee, E.B., Detre, J.A., Xie, S.X., Trojanowski, J.Q., Tisdall, M.D., Wisse, L.E.M., Irwin, D.J., Wolk, D.A., Yushkevich, P.A., 2023. Associations of phosphorylated tau pathology with whole-hemisphere ex vivo morphometry in 7 tesla MRI. Alzheimers Dement. 19, 2355–2364. https://doi.org/10.1002/alz.12884

Saifullah, K., Makkinejad, N., Yasar, M.T., Evia, A.M., Leurgans, S.E., Bennett, D.A., Schneider, J.A., Arfanakis, K., 2025. Neuropathological Correlates of Volume and Shape of Deep Gray Matter Structures in Community-Based Older Adults. Hum. Brain Mapp. 46, e70273. https://doi.org/10.1002/hbm.70273

Salman, Y., Gérard, T., Huyghe, L., Colmant, L., Quenon, L., Malotaux, V., Ivanoiu, A., Lhommel, R., Dricot, L., Hanseeuw, B.J., for the Alzheimer's Disease Neuroimaging Initiative, 2024. Amygdala atrophies in specific subnuclei in preclinical Alzheimer's disease. Alzheimers Dement. alz.14235. https://doi.org/10.1002/alz.14235

Saygin, Z.M., Kliemann, D., Iglesias, J.E., Van Der Kouwe, A.J.W., Boyd, E., Reuter, M., Stevens, A., Van Leemput, K., McKee, A., Frosch, M.P., Fischl, B., Augustinack, J.C., 2017. High-resolution magnetic resonance imaging reveals nuclei of the human amygdala: manual segmentation to automatic atlas. NeuroImage 155, 370–382. https://doi.org/10.1016/j.neuroimage.2017.04.046

Scalco, R., Oliveira, L.C., Lai, Z., Harvey, D.J., Abujamil, L., DeCarli, C., Jin, L.-W., Chuah, C.-N., Dugger, B.N., 2024. Machine learning quantification of Amyloid-β deposits in the temporal lobe of 131 brain bank cases. Acta Neuropathol. Commun. 12, 134. https://doi.org/10.1186/s40478-024-01827-7

Scheltens, P., Leys, D., Barkhof, F., Huglo, D., Weinstein, H.C., Vermersch, P., Kuiper, M., Steinling, M., Wolters, E.C., Valk, J., 1992. Atrophy of medial temporal lobes on MRI in "probable" Alzheimer's disease and normal ageing: diagnostic value and neuropsychological correlates. J. Neurol. Neurosurg. Psychiatry 55, 967–972. https://doi.org/10.1136/jnnp.55.10.967

Scherlek, A.A., Kozberg, M.G., Nicoll, J.A.R., Perosa, V., Freeze, W.M., Van Der Weerd, L., Bacskai, B.J., Greenberg, S.M., Frosch, M.P., Boche, D., Van Veluw, S.J., 2022. Histopathological correlates of haemorrhagic lesions on *ex vivo* magnetic resonance imaging in immunized Alzheimer's disease cases. Brain Commun. 4, fcac021. https://doi.org/10.1093/braincomms/fcac021

Schilling, K.G., Grussu, F., Ianus, A., Hansen, B., Howard, A.F.D., Barrett, R.L.C., Aggarwal, M., Michielse, S., Nasrallah, F., Syeda, W., Wang, N., Veraart, J., Roebroeck, A., Bagdasarian, A.F., Eichner, C., Sepehrband, F., Zimmermann, J., Soustelle, L., Bowman, C., Tendler, B.C., Hertanu, A., Jeurissen, B., Verhoye, M., Frydman, L., Van De Looij, Y., Hike, D., Dunn, J.F., Miller, K., Landman, B.A., Shemesh, N., Anderson, A., McKinnon, E., Farquharson, S., Dell'Acqua, F., Pierpaoli, C., Drobnjak, I., Leemans, A., Harkins, K.D., Descoteaux, M., Xu, D., Huang, H., Santin, M.D., Grant, S.C., Obenaus, A., Kim, G.S., Wu, D., Le Bihan, D., Blackband, S.J., Ciobanu, L., Fieremans, E., Bai, R., Leergaard, T.B., Zhang, J., Dyrby, T.B., Johnson, G.A., Cohen-Adad, J., Budde, M.D., Jelescu, I.O., 2025. Considerations and recommendations from the ISMRM diffusion study group for preclinical diffusion MRI : Part 2—Ex vivo imaging: Added value and acquisition. Magn. Reson. Med. 93, 2535–2560. https://doi.org/10.1002/mrm.30435

Schöll, M., Lockhart, S.N., Schonhaut, D.R., O'Neil, J.P., Janabi, M., Ossenkoppele, R., Baker, S.L., Vogel, J.W., Faria, J., Schwimmer, H.D., Rabinovici, G.D., Jagust, W.J., 2016. PET Imaging of Tau Deposition in the Aging Human Brain. Neuron 89, 971–982. https://doi.org/10.1016/j.neuron.2016.01.028

Scholz, A., Etzel, R., May, M.W., Mahmutovic, M., Tian, Q., Ramos-Llordén, G., Maffei, C., Bilgiç, B., Witzel, T., Stockmann, J.P., Mekkaoui, C., Wald, L.L., Huang, S.Y., Yendiki, A., Keil, B., 2021. A 48-channel receive array coil for mesoscopic diffusion-weighted MRI of ex vivo human brain on the 3 T connectome scanner. NeuroImage 238, 118256. https://doi.org/10.1016/j.neuroimage.2021.118256

Seddighi, S., Qi, Y.A., Brown, A.-L., Wilkins, O.G., Bereda, C., Belair, C., Zhang, Y.-J., Prudencio, M., Keuss, M.J., Khandeshi, A., Pickles, S., Kargbo-Hill, S.E., Hawrot, J., Ramos, D.M., Yuan, H., Roberts, J., Sacramento, E.K., Shah, S.I., Nalls, M.A., Colón-Mercado, J.M., Reyes, J.F., Ryan, V.H., Nelson, M.P., Cook, C.N., Li, Z., Screven, L., Kwan, J.Y., Mehta, P.R., Zanovello, M., Hallegger, M., Shantaraman, A., Ping, L., Koike, Y., Oskarsson, B., Staff, N.P., Duong, D.M., Ahmed, A., Secrier, M., Ule, J., Jacobson, S., Reich, D.S., Rohrer, J.D., Malaspina, A., Dickson, D.W., Glass, J.D., Ori, A., Seyfried, N.T., Maragkakis, M., Petrucelli, L., Fratta, P., Ward, M.E., 2024. Mis-spliced transcripts generate de novo proteins in TDP-43–related ALS/FTD. Sci. Transl. Med. 16. https://doi.org/10.1126/scitranslmed.adg7162

Shih, N.-C., Kurniawan, N.D., Cabeen, R.P., Korobkova, L., Wong, E., Chui, H.C., Clark, K.A., Miller, C.A., Hawes, D., Jones, K.T., Sepehrband, F., 2023. Microstructural mapping of dentate gyrus pathology in Alzheimer's disease: A 16.4 Tesla MRI study. NeuroImage Clin. 37, 103318. https://doi.org/10.1016/j.nicl.2023.103318

Simons, J.H., 1949. Production of Fluorocarbons. J. Electrochem. Soc. 95, 47. https://doi.org/10.1149/1.2776733

Sims, J.R., Zimmer, J.A., Evans, C.D., Lu, M., Ardayfio, P., Sparks, J., Wessels, A.M., Shcherbinin, S., Wang, H., Monkul Nery, E.S., Collins, E.C., Solomon, P., Salloway, S., Apostolova, L.G., Hansson, O., Ritchie, C., Brooks, D.A., Mintun, M., Skovronsky, D.M., TRAILBLAZER-ALZ 2 Investigators, Abreu, R., Agarwal, P., Aggarwal, P., Agronin, M., Allen, A., Altamirano, D., Alva, G., Andersen, J., Anderson, A., Anderson, D., Arnold, J., Asada, T., Aso, Y., Atit, V., Ayala, R., Badruddoja, M., Badzio-jagiello, H., Bajacek, M., Barton, D., Bear, D., Benjamin, S., Bergeron, R., Bhatia, P., Black, S., Block, A., Bolouri, M., Bond, W., Bouthillier, J., Brangman, S., Brew, B., Brisbin, S., Brisken, T., Brodtmann, A., Brody, M., Brosch, J., Brown, C., Brownstone, P., Bukowczan, S., Burns, J., Cabrera, A., Capote, H., Carrasco, A., Cevallos Yepez, J., Chavez, E., Chertkow, H., Chyrchel-paszkiewicz, U., Ciabarra, A., Clemmons, E., Cohen, D., Cohen, R., Cohen, I., Concha, M., Costell, B., Crimmins, D., Cruz-pagan, Y., Cueli, A., Cupelo, R., Czarnecki, M., Darby, D., Dautzenberg, P. l. j., De Deyn, P., De La Gandara, J., Deck, K., Dibenedetto, D., Dibuono, M., Dinnerstein, E., Dirican, A., Dixit, S., Dobryniewski, J., Drake, R., Drysdale, P., Duara, R., Duffy, J., Ellenbogen, A., Faradji, V., Feinberg, M., Feldman, R., Fishman, S., Flitman, S., Forchetti, C., Fraga, I., Frank, A., Frishberg, B., Fujigasaki, H., Fukase, H., Fumero, I., Furihata, K., Galloway, C., Gandhi, R., George, K., Germain, M., Gitelman, D., Goetsch, N., Goldfarb, D., Goldstein, M., Goldstick, L., Gonzalez Rojas, Y., Goodman, I., Greeley, D., Griffin, C., Grigsby, E., Grosz, D., Hafner, K., Hart, D., Henein, S., Herskowitz, B., Higashi, S., Higashi, Y., Ho, G., Hodgson, J., Hohenberg, M., Hollenbeck, L., Holub, R., Hori, T., Hort, J., Ilkowski, J., Ingram, K.J., Isaac, M., Ishikawa, M., Janu, L., Johnston, M., Julio, W., Justiz, W., Kaga, T., Kakigi, T., Kalafer, M., Kamijo, M., Kaplan, J., Karathanos, M., Katayama, S., Kaul, S., Keegan, A., Kerwin, D., Khan, U., Khan, A., Kimura, N., Kirk, G., Klodowska, G., Kowa, H., Kutz, C., Kwentus, J., Lai, R., Lall, A., Lawrence, M., Lee, E., Leon, R., Linker, G., Lisewski, P., Liss, J., Liu, C., Losk, S., Lukaszyk, E., Lynch, J., Macfarlane, S., Macsweeney, J., Mannering, N., Markovic, O., Marks, D., Masdeu, J., Matsui, Y., Matsuishi, K., Mcallister, P., Mcconnehey, B., Mcelveen, A., Mcgill, L., Mecca, A., Mega, M., Mensah, J., Mickielewicz, A., Minaeian, A., Mocherla, B., Murphy, C., Murphy, P., Nagashima, H., Nair, A., Nair, M., Nardandrea, J., Nash, M., Nasreddine, Z., Nishida, Y., Norton, J., Nunez, L., Ochiai, J., Ohkubo, T., Okamura, Y., Okorie, E., Olivera, E., O'mahony, J., Omidvar, O., Ortiz-Cruz, D., Osowa, A., Papka, M., Parker, A., Patel, P., Patel, A., Patel, M., Patry, C., Peckham, E., Pfeffer, M., Pietras, A., Plopper, M., Porsteinsson, A., Poulin Robitaille, R., Prins, N., Puente, O., Ratajczak, M., Rhee, M., Ritter, A., Rodriguez, R., Rodriguez Ables, L., Rojas, J., Ross, J., Royer, P., Rubin, J., Russell, D., Rutgers, S.M., Rutrick, S., Sadowski, M., Safirstein, B., Sagisaka, T., Scharre, D., Schneider, L., Schreiber, C., Schrift, M., Schulz, P., Schwartz, H., Schwartzbard, J.,

Scott, J., Selem, L., Sethi, P., Sha, S., Sharlin, K., Sharma, S., Shiovitz, T., Shiwach, R., Sladek, M., Sloan, B., Smith, A., Solomon, P., Sorial, E., Sosa, E., Stedman, M., Steen, S., Stein, L., Stolyar, A., Stoukides, J., Sudoh, S., Sutton, J., Syed, J., Szigeti, K., Tachibana, H., Takahashi, Y., Tateno, A., Taylor, J.D., Taylor, K., Tcheremissine, O., Thebaud, A., Thein, S., Thurman, L., Toenjes, S., Toji, H., Toma, M., Tran, D., Trueba, P., Tsujimoto, M., Turner, R., Uchiyama, A., Ussorowska, D., Vaishnavi, S., Valor, E., Vandersluis, J., Vasquez, A., Velez, J., Verghese, C., Vodickova-borzova, K., Watson, D., Weidman, D., Weisman, D., White, A., Willingham, K., Winkel, I., Winner, P., Winston, J., Wolff, A., Yagi, H., Yamamoto, H., Yathiraj, S., Yoshiyama, Y., Zboch, M., 2023. Donanemab in Early Symptomatic Alzheimer Disease: The TRAILBLAZER-ALZ 2 Randomized Clinical Trial. JAMA 330, 512. https://doi.org/10.1001/jama.2023.13239

Singer, W., Schmeichel, A.M., Shahnawaz, M., Schmelzer, J.D., Sletten, D.M., Gehrking, T.L., Gehrking, J.A., Olson, A.D., Suarez, M.D., Misra, P.P., Soto, C., Low, P.A., 2021. Alpha-Synuclein Oligomers and Neurofilament Light Chain Predict Phenoconversion of Pure Autonomic Failure. Ann. Neurol. 89, 1212–1220. https://doi.org/10.1002/ana.26089

Sordo, L., Qian, T., Bukhari, S.A., Nguyen, K.M., Woodworth, D.C., Head, E., Kawas, C.H., Corrada, M.M., Montine, T.J., Sajjadi, S.A., 2023. Characterization of hippocampal sclerosis of aging and its association with other neuropathologic changes and cognitive deficits in the oldest-old. Acta Neuropathol. (Berl.) 146, 415–432. https://doi.org/10.1007/s00401-023-02606-9

Spotorno, N., Strandberg, O., Vis, G., Stomrud, E., Nilsson, M., Hansson, O., 2023. Measures of cortical microstructure are linked to amyloid pathology in Alzheimer's disease. Brain 146, 1602–1614. https://doi.org/10.1093/brain/awac343

Stanisz, G.J., Odrobina, E.E., Pun, J., Escaravage, M., Graham, S.J., Bronskill, M.J., Henkelman, R.M., 2005. T_1 , T_2 relaxation and magnetization transfer in tissue at 3T. Magn. Reson. Med. 54, 507–512. https://doi.org/10.1002/mrm.20605

Stouffer, K.M., Chen, C., Kulason, S., Xu, E., Witter, M.P., Ceritoglu, C., Albert, M.S., Mori, S., Troncoso, J., Tward, D.J., Miller, M.I., 2023. Early amygdala and ERC atrophy linked to 3D reconstruction of rostral neurofibrillary tau tangle pathology in Alzheimer's disease. NeuroImage Clin. 38, 103374. https://doi.org/10.1016/j.nicl.2023.103374

Stouffer, K.M., Grande, X., Düzel, E., Johansson, M., Creese, B., Witter, M.P., Miller, M.I., Wisse, L.E.M., Berron, D., 2024. Amidst an amygdala renaissance in Alzheimer's disease. Brain 147, 816–829. https://doi.org/10.1093/brain/awad411

Su, L., Hayes, L., Soteriades, S., Williams, G., Brain, S.A.E., Firbank, M.J., Longoni, G., Arnold, R.J., Rowe, J.B., O'Brien, J.T., 2017. Hippocampal Stratum Radiatum, Lacunosum, and Moleculare Sparing in Mild Cognitive Impairment. J. Alzheimers Dis. 61, 415–424. https://doi.org/10.3233/JAD-170344

Tazwar, M., Evia, A.M., Tamhane, A.A., Ridwan, A.R., Leurgans, S.E., Bennett, D.A., Schneider, J.A., Arfanakis, K., 2022. Limbic-predominant age-related TDP-43 encephalopathy neuropathological change (LATE-NC) is associated with lower R2 relaxation rate: an ex-vivo MRI and pathology investigation. Neurobiol. Aging 117, 128–138. https://doi.org/10.1016/j.neurobiolaging.2022.05.009

Ten Kate, M., Redolfi, A., Peira, E., Bos, I., Vos, S.J., Vandenberghe, R., Gabel, S., Schaeverbeke, J., Scheltens, P., Blin, O., Richardson, J.C., Bordet, R., Wallin, A., Eckerstrom, C., Molinuevo, J.L., Engelborghs, S., Van Broeckhoven, C., Martinez-Lage, P., Popp, J., Tsolaki, M., Verhey, F.R.J., Baird, A.L., Legido-Quigley, C., Bertram, L., Dobricic, V., Zetterberg, H., Lovestone, S., Streffer, J., Bianchetti, S., Novak, G.P., Revillard, J., Gordon, M.F., Xie, Z., Wottschel, V., Frisoni, G., Visser, P.J., Barkhof, F., 2018. MRI predictors of amyloid pathology: results from the EMIF-AD Multimodal Biomarker Discovery study. Alzheimers Res. Ther. 10, 100. https://doi.org/10.1186/s13195-018-0428-1

Tendler, B.C., Hanayik, T., Ansorge, O., Bangerter-Christensen, S., Berns, G.S., Bertelsen, M.F., Bryant, K.L., Foxley, S., Van Den Heuvel, M.P., Howard, A.F., Huszar, I.N., Khrapitchev,

A.A., Leonte, A., Manger, P.R., Menke, R.A., Mollink, J., Mortimer, D., Pallebage-Gamarallage, M., Roumazeilles, L., Sallet, J., Scholtens, L.H., Scott, C., Smart, A., Turner, M.R., Wang, C., Jbabdi, S., Mars, R.B., Miller, K.L., 2022. The Digital Brain Bank, an open access platform for post-mortem imaging datasets. eLife 11, e73153. https://doi.org/10.7554/eLife.73153

Thal, D.R., Holzer, M., Rüb, U., Waldmann, G., Günzel, S., Zedlick, D., Schober, R., 2000. Alzheimer-Related τ-Pathology in the Perforant Path Target Zone and in the Hippocampal Stratum Oriens and Radiatum Correlates with Onset and Degree of Dementia. Exp. Neurol. 163, 98–110. https://doi.org/10.1006/exnr.2000.7380

Therriault, J., Janelidze, S., Benedet, A.L., Ashton, N.J., Arranz Martínez, J., Gonzalez-Escalante, A., Bellaver, B., Alcolea, D., Vrillon, A., Karim, H., Mielke, M.M., Hyung Hong, C., Roh, H.W., Contador, J., Puig Pijoan, A., Algeciras-Schimnich, A., Vemuri, P., Graff-Radford, J., Lowe, V.J., Karikari, T.K., Jonaitis, E., Brum, W., Tissot, C., Servaes, S., Rahmouni, N., Macedo, A.C., Stevenson, J., Fernandez-Arias, J., Wang, Y.-T., Woo, M.S., Friese, M.A., Jia, W.L., Dumurgier, J., Hourregue, C., Cognat, E., Ferreira, P.L., Vitali, P., Johnson, S., Pascoal, T.A., Gauthier, S., Lleó, A., Paquet, C., Petersen, R.C., Salmon, D., Mattsson-Carlgren, N., Palmqvist, S., Stomrud, E., Galasko, D., Son, S.J., Zetterberg, H., Fortea, J., Suárez-Calvet, M., Jack, C.R., Blennow, K., Hansson, O., Rosa-Neto, P., 2024. Diagnosis of Alzheimer's disease using plasma biomarkers adjusted to clinical probability. Nat. Aging 4, 1529–1537. https://doi.org/10.1038/s43587-024-00731-y

Tisdall, M.D., Ohm, D.T., Lobrovich, R., Das, S.R., Mizsei, G., Prabhakaran, K., Ittyerah, R., Lim, S., McMillan, C.T., Wolk, D.A., Gee, J., Trojanowski, J.Q., Lee, E.B., Detre, J.A., Yushkevich, P., Grossman, M., Irwin, D.J., 2022. Ex vivo MRI and histopathology detect novel iron-rich cortical inflammation in frontotemporal lobar degeneration with tau versus TDP-43 pathology. NeuroImage Clin. 33, 102913. https://doi.org/10.1016/j.nicl.2021.102913

Toledo, J.B., Cairns, N.J., Da, X., Chen, K., Carter, D., Fleisher, A., Householder, E., Ayutyanont, N., Roontiva, A., Bauer, R.J., Eisen, P., Shaw, L.M., Davatzikos, C., Weiner, M.W., Reiman, E.M., Morris, J.C., Trojanowski, J.Q., the Alzheimer's Disease Neuroimaging Initiative, 2013. Clinical and multimodal biomarker correlates of ADNI neuropathological findings. Acta Neuropathol. Commun. 1. https://doi.org/10.1186/2051-5960-1-65

Tomé, S.O., Gawor, K., Ospitalieri, S., Ronisz, A., Otto, M., Von Arnim, C.A.F., Ghebremedhin, E., Laureyssen, C., Sleegers, K., Vandenberghe, R., Nelson, P.T., Thal, D.R., 2025. Differences and overlaps in TDP-43 pathology of 'pure' LATE-NC compared to LATE-NC coexisting with Alzheimer's disease. Acta Neuropathol. (Berl.) 150, 28. https://doi.org/10.1007/s00401-025-02929-9

Tomé, S.O., Gomes, L.A., Li, X., Vandenberghe, R., Tousseyn, T., Thal, D.R., 2021. TDP-43 interacts with pathological τ protein in Alzheimer's disease. Acta Neuropathol. (Berl.) 141, 795–799. https://doi.org/10.1007/s00401-021-02295-2

Tovi, M., Ericsson, A., 1992. Measurements of T1 and T2 over time in formalin-fixed human whole-brain specimens. Acta Radiol. 33, 400–404.

Tran, T.T., Speck, C.L., Gallagher, M., Bakker, A., 2022. Lateral entorhinal cortex dysfunction in amnestic mild cognitive impairment. Neurobiol. Aging 112, 151–160. https://doi.org/10.1016/j.neurobiolaging.2021.12.008

Tucker, H., Karat, B., De Ruiter, A., Parker, D., Lim, S., Denning, A., Ittyerah, R., Levorse, L., Trotman, W., Bahena, A., Chung, E., Prabhakaran, K., Bedard, M., Ohm, D., Xie, L., Das, S., Pluta, J., Schuck, T., Liu, W., Pickup, S., Artacho-Pérula, E., Martin, M.I.D.O., Muñoz, M., Romero, F., González, J.D., Jiménez, M.A., Rabal, M.M., Serrano, A.I., González, N.V., Sánchez, S.C., De La Rosa Prieto, C., Lee, E., Detre, J., Tisdall, M., Irwin, D., Wolk, D., Adler, D., De Flores, R., Berron, D., Ding, S., Yushkevich, P., Hodgetts, C., Wisse, L., 2025. Characterization of hippocampal subfields using histology-based annotated postmortem MRI: Lessons for in vivo segmentation II. https://doi.org/10.1101/2025.11.21.689744

Tustison, N.J., Avants, B.B., Cook, P.A., Yuanjie Zheng, Egan, A., Yushkevich, P.A., Gee, J.C., 2010. N4ITK: Improved N3 Bias Correction. IEEE Trans. Med. Imaging 29, 1310–1320. https://doi.org/10.1109/tmi.2010.2046908

Van Rooden, S., Maat-Schieman, M.L.C., Nabuurs, R.J.A., Van Der Weerd, L., Van Duijn, S., Van Duinen, S.G., Natté, R., Van Buchem, M.A., Van Der Grond, J., 2009. Cerebral Amyloidosis: Postmortem Detection with Human 7.0-T MR Imaging System. Radiology 253, 788–796. https://doi.org/10.1148/radiol.2533090490

Van Veluw, S.J., Charidimou, A., Van Der Kouwe, A.J., Lauer, A., Reijmer, Y.D., Costantino, I., Gurol, M.E., Biessels, G.J., Frosch, M.P., Viswanathan, A., Greenberg, S.M., 2016. Microbleed and microinfarct detection in amyloid angiopathy: a high-resolution MRI-histopathology study. Brain 139, 3151–3162. https://doi.org/10.1093/brain/aww229

Ver Hoef, L., Deshpande, H., Cure, J., Selladurai, G., Beattie, J., Kennedy, R.E., Knowlton, R.C., Szaflarski, J.P., 2021. Clear and Consistent Imaging of Hippocampal Internal Architecture With High Resolution Multiple Image Co-registration and Averaging (HR-MICRA). Front. Neurosci. 15. https://doi.org/10.3389/fnins.2021.546312

Vogt, N.M., Hunt, J.F.V., Adluru, N., Ma, Y., Van Hulle, C.A., Iii, D.C.D., Kecskemeti, S.R., Chin, N.A., Carlsson, C.M., Asthana, S., Johnson, S.C., Kollmorgen, G., Batrla, R., Wild, N., Buck, K., Zetterberg, H., Alexander, A.L., Blennow, K., Bendlin, B.B., 2022. Interaction of amyloid and tau on cortical microstructure in cognitively unimpaired adults. Alzheimers Dement. 18, 65–76. https://doi.org/10.1002/alz.12364

Wang, K., Shao, B., Zeng, Q., Liu, X., Li, K., Luo, X., 2026. Trajectory of stratum radiatum, lacunosum and moleculare integrity in Alzheimer's disease continuum. Sci. Rep. https://doi.org/10.1038/s41598-026-35610-6

Wesseling, A., Calandri, I.L., Bouwman, M.M.A., Reijner, N., Deshayes, N.A.C., Barkhof, F., Ossenkoppele, R., Van De Berg, W.D.J., Rozemuller, A.E., Pijnenburg, Y.A.L., Hoozemans, J.J.M., Jonkman, L.E., 2025. Amygdalar and hippocampal volume loss in limbic-predominant age-related TDP-43 encephalopathy. Brain. https://doi.org/10.1093/brain/awaf201

Weston, P.S.J., Coath, W., Harris, M.J., Malone, I.B., Dickson, J., Aigbirhio, F.I., Cash, D.M., Zhang, H., Schott, J.M., 2023. Cortical tau is associated with microstructural imaging biomarkers of neurite density and dendritic complexity in Alzheimer's disease. Alzheimers Dement. 19, 2750–2754. https://doi.org/10.1002/alz.13011

Wisse, L.E.M., Adler, D.H., Ittyerah, R., Pluta, J.B., Robinson, J.L., Schuck, T., Trojanowski, J.Q., Grossman, M., Detre, J.A., Elliott, M.A., Toledo, J.B., Liu, W., Pickup, S., Das, S.R., Wolk, D.A., Yushkevich, P.A., 2016. Comparison of In Vivo and Ex Vivo MRI of the Human Hippocampal Formation in the Same Subjects. Cereb. Cortex cercor;bhw299v1. https://doi.org/10.1093/cercor/bhw299

Wisse, Laura E. M., Chételat, G., Daugherty, A.M., De Flores, R., La Joie, R., Mueller, S.G., Stark, C.E.L., Wang, L., Yushkevich, P.A., Berron, D., Raz, N., Bakker, A., Olsen, R.K., Carr, V.A., 2021. Hippocampal subfield volumetry from structural isotropic 1 mm^3MRI scans: A note of caution. Hum. Brain Mapp. 42, 539–550. https://doi.org/10.1002/hbm.25234

Wisse, L.E.M., Daugherty, A.M., Olsen, R.K., Berron, D., Carr, V.A., Stark, C.E.L., Amaral, R.S.C., Amunts, K., Augustinack, J.C., Bender, A.R., Bernstein, J.D., Boccardi, M., Bocchetta, M., Burggren, A., Chakravarty, M.M., Chupin, M., Ekstrom, A., De Flores, R., Insausti, R., Kanel, P., Kedo, O., Kennedy, K.M., Kerchner, G.A., LaRocque, K.F., Liu, X., Maass, A., Malykhin, N., Mueller, S.G., Ofen, N., Palombo, D.J., Parekh, M.B., Pluta, J.B., Pruessner, J.C., Raz, N., Rodrigue, K.M., Schoemaker, D., Shafer, A.T., Steve, T.A., Suthana, N., Wang, L., Winterburn, J.L., Yassa, M.A., Yushkevich, P.A., La Joie, R., for the Hippocampal Subfields Group, 2017. A harmonized segmentation protocol for hippocampal and parahippocampal subregions: Why do we need one and what are the key goals?: A HARMONIZED HIPPOCAMPAL SUBFIELD PROTOCOL: KEY GOALS AND IMPACT. Hippocampus 27, 3–11. https://doi.org/10.1002/hipo.22671

Wisse, L. E. M., De Flores, R., Xie, L., Das, S.R., McMillan, C.T., Trojanowski, J.Q., Grossman, M., Lee, E.B., Irwin, D., Yushkevich, P.A., Wolk, D.A., on behalf of the Alzheimer's Disease NeuroImaging Initiative, 2021a. Pathological drivers of neurodegeneration in suspected non-Alzheimer's disease pathophysiology. Alzheimers Res. Ther. 13, 100. https://doi.org/10.1186/s13195-021-00835-2

Wisse, L.E.M., Gerritsen, L., Zwanenburg, J.J.M., Kuijf, H.J., Luijten, P.R., Biessels, G.J., Geerlings, M.I., 2012. Subfields of the hippocampal formation at 7 T MRI: In vivo volumetric assessment. NeuroImage 61, 1043–1049. https://doi.org/10.1016/j.neuroimage.2012.03.023

Wisse, L. E. M., Ravikumar, S., Ittyerah, R., Lim, S., Lane, J., Bedard, M.L., Xie, L., Das, S.R., Schuck, T., Grossman, M., Lee, E.B., Tisdall, M.D., Prabhakaran, K., Detre, J.A., Mizsei, G., Trojanowski, J.Q., Artacho-Pérula, E., De Iñiguez De Onzono Martin, M.M., M. Arroyo-Jiménez, M., Muñoz Lopez, M., Molina Romero, F.J., P. Marcos Rabal, M., Cebada Sánchez, S., Delgado González, J.C., De La Rosa Prieto, C., Córcoles Parada, M., Wolk, D.A., Irwin, D.J., Insausti, R., Yushkevich, P.A., 2021b. Downstream effects of polypathology on neurodegeneration of medial temporal lobe subregions. Acta Neuropathol. Commun. 9, 128. https://doi.org/10.1186/s40478-021-01225-3

Wolk, D.A., Nelson, P.T., Apostolova, L., Arfanakis, K., Boyle, P.A., Carlsson, C.M., Corriveau-Lecavalier, N., Dacks, P., Dickerson, B.C., Domoto-Reilly, K., Dugger, B.N., Edelmayer, R., Fardo, D.W., Grothe, M.J., Hohman, T.J., Irwin, D.J., Jicha, G.A., Jones, D.T., Kawas, C.H., Lee, E.B., Lincoln, K., Maestre, G.E., Mormino, E.C., Onyike, C.U., Petersen, R.C., Rabinovici, G.D., Rademakers, R., Raman, R., Rascovsky, K., Rissman, R.A., Rogalski, E., Scheltens, P., Sperling, R.A., Yang, H., Yu, L., Zetterberg, H., Schneider, J.A., 2025. Clinical criteria for limbic-predominant age-related TDP-43 encephalopathy. Alzheimers Dement. 21. https://doi.org/10.1002/alz.14202

Yakoub, Y., Gonzalez-Ortiz, F., Ashton, N.J., Déry, C., Strikwerda-Brown, C., St-Onge, F., Ourry, V., Schöll, M., Geddes, M.R., Ducharme, S., Montembeault, M., Rosa-Neto, P., Soucy, J., Breitner, J.C.S., Zetterberg, H., Blennow, K., Poirier, J., Villeneuve, S., PREVENT–AD Research Group, 2025. Plasma p-tau217 identifies cognitively normal older adults who will develop cognitive impairment in a 10-year window. Alzheimers Dement. 21. https://doi.org/10.1002/alz.14537

Yao, J., Li, Z., Zhou, Z., Bao, A., Wang, Z., Wei, H., He, H., 2024. Distinct regional vulnerability to Aβ and iron accumulation in *post mortem* AD brains. Alzheimers Dement. 20, 6984–6997. https://doi.org/10.1002/alz.14188

Ye, R., Goodheart, A.E., Locascio, J.J., Peterec, E., Properzi, M., Thibault, E.G., Chuba, E., Johnson, K.A., Brickhouse, M.J., Touroutoglou, A., Growdon, J.H., Dickerson, B.C., Gomperts, S.N., 2024. Differential Vulnerability of Hippocampal Subfields to Amyloid and Tau Deposition in the Lewy Body Diseases. Neurology 102, e209460. https://doi.org/10.1212/WNL.0000000000209460

Young, A.L., Vogel, J.W., Robinson, J., McMillan, C.T., Ossenkoppele, R., Wolk, D.A., Irwin, D.J., Elman, L., Grossman, M., Lee, V.M., Lee, E.B., Trojanowski, J.Q., Hansson, O., 2022. Empirical pathological staging and subtyping of TDP-43 proteinopathies. Alzheimers Dement. 18, e063390. https://doi.org/10.1002/alz.063390

Yu, L., Boyle, P.A., Dawe, R.J., Bennett, D.A., Arfanakis, K., Schneider, J.A., 2020. Contribution of TDP and hippocampal sclerosis to hippocampal volume loss in older-old persons. Neurology 94. https://doi.org/10.1212/wnl.0000000000008679

Yu, L., Dawe, R.J., Buchman, A.S., Boyle, P.A., Schneider, J.A., Arfanakis, K., Bennett, D.A., 2017. Ex vivo MRI transverse relaxation in community based older persons with and without Alzheimer's dementia. Behav. Brain Res. 322, 233–240. https://doi.org/10.1016/j.bbr.2016.09.001

Yushkevich, P., Avants, B., Pluta, J., Das, S., Minkoff, D., Mechanichamilton, D., Glynn, S., Pickup, S., Liu, W., Gee, J., 2009. A high-resolution computational atlas of the human

hippocampus from postmortem magnetic resonance imaging at 9.4 T. NeuroImage 44, 385–398. https://doi.org/10.1016/j.neuroimage.2008.08.042

Yushkevich, P.A., Amaral, R.S.C., Augustinack, J.C., Bender, A.R., Bernstein, J.D., Boccardi, M., Bocchetta, M., Burggren, A.C., Carr, V.A., Chakravarty, M.M., Chételat, G., Daugherty, A.M., Davachi, L., Ding, S.-L., Ekstrom, A., Geerlings, M.I., Hassan, A., Huang, Y., Iglesias, J.E., La Joie, R., Kerchner, G.A., LaRocque, K.F., Libby, L.A., Malykhin, N., Mueller, S.G., Olsen, R.K., Palombo, D.J., Parekh, M.B., Pluta, J.B., Preston, A.R., Pruessner, J.C., Ranganath, C., Raz, N., Schlichting, M.L., Schoemaker, D., Singh, S., Stark, C.E.L., Suthana, N., Tompary, A., Turowski, M.M., Van Leemput, K., Wagner, A.D., Wang, L., Winterburn, J.L., Wisse, L.E.M., Yassa, M.A., Zeineh, M.M., 2015. Quantitative comparison of 21 protocols for labeling hippocampal subfields and parahippocampal subregions in in vivo MRI: Towards a harmonized segmentation protocol. NeuroImage 111, 526–541. https://doi.org/10.1016/j.neuroimage.2015.01.004

Yushkevich, P.A., Muñoz López, M., Iñiguez De Onzoño Martin, M.M., Ittyerah, R., Lim, S., Ravikumar, S., Bedard, M.L., Pickup, S., Liu, W., Wang, J., Hung, L.Y., Lasserve, J., Vergnet, N., Xie, L., Dong, M., Cui, S., McCollum, L., Robinson, J.L., Schuck, T., De Flores, R., Grossman, M., Tisdall, M.D., Prabhakaran, K., Mizsei, G., Das, S.R., Artacho-Pérula, E., Arroyo Jiménez, M.D.M., Marcos Raba, M.P., Molina Romero, F.J., Cebada Sánchez, S., Delgado González, J.C., De La Rosa-Prieto, C., Córcoles Parada, M., Lee, E.B., Trojanowski, J.Q., Ohm, D.T., Wisse, L.E.M., Wolk, D.A., Irwin, D.J., Insausti, R., 2021a. Three-dimensional mapping of neurofibrillary tangle burden in the human medial temporal lobe. Brain 144, 2784–2797. https://doi.org/10.1093/brain/awab262

Yushkevich, P.A., Muñoz López, M., Iñiguez De Onzoño Martin, M.M., Ittyerah, R., Lim, S., Ravikumar, S., Bedard, M.L., Pickup, S., Liu, W., Wang, J., Hung, L.Y., Lasserve, J., Vergnet, N., Xie, L., Dong, M., Cui, S., McCollum, L., Robinson, J.L., Schuck, T., De Flores, R., Grossman, M., Tisdall, M.D., Prabhakaran, K., Mizsei, G., Das, S.R., Artacho-Pérula, E., Arroyo Jiménez, M.D.M., Marcos Rabal, M.P., Molina Romero, F.J., Cebada Sánchez, S., Delgado González, J.C., De La Rosa-Prieto, C., Córcoles Parada, M., Lee, E.B., Trojanowski, J.Q., Ohm, D.T., Wisse, L.E.M., Wolk, D.A., Irwin, D.J., Insausti, R., 2021b. 3D Mapping of Neurofibrillary Tangle Burden in the Human Medial Temporal Lobe. https://doi.org/10.1101/2021.01.15.421909

Yushkevich, P.A., Wang, H., Pluta, J., Das, S.R., Craige, C., Avants, B.B., Weiner, M.W., Mueller, S., 2010. Nearly automatic segmentation of hippocampal subfields in in vivo focal T2-weighted MRI. NeuroImage 53, 1208–1224. https://doi.org/10.1016/j.neuroimage.2010.06.040

Zeineh, M.M., Chen, Y., Kitzler, H.H., Hammond, R., Vogel, H., Rutt, B.K., 2015. Activated iron-containing microglia in the human hippocampus identified by magnetic resonance imaging in Alzheimer disease. Neurobiol. Aging 36, 2483–2500. https://doi.org/10.1016/j.neurobiolaging.2015.05.022

Zhang, J., Xie, L., Cheng, C., Liu, Y., Zhang, X., Wang, H., Hu, J., Yu, H., Xu, J., 2023. Hippocampal subfield volumes in mild cognitive impairment and alzheimer's disease: a systematic review and meta-analysis. Brain Imaging Behav. 17, 778–793. https://doi.org/10.1007/s11682-023-00804-3

Zhao, Z., Cao, Z., Zhu, Q., Xu, H., Li, S., Zhu, L., Xu, G., Zhu, K., Zhang, J., Wu, D., 2025. Layer-Dependent Effect of Aβ-Pathology on Cortical Microstructure With Ex Vivo Human Brain Diffusion MRI at 7 Tesla. Hum. Brain Mapp. 46, e70222. https://doi.org/10.1002/hbm.70222

Zhao, Z., Zhang, L., Luo, W., Cao, Z., Zhu, Q., Kong, X., Zhu, K., Zhang, J., Wu, D., 2023. Layer-specific microstructural patterns of anterior hippocampus in Alzheimer's disease with ex vivo diffusion MRI at 14.1 T. Hum. Brain Mapp. 44, 458–471. https://doi.org/10.1002/hbm.26062

Zhao, Z., Zhang, L., Wen, Q., Luo, W., Zheng, W., Liu, T., Zhang, Y., Zhu, K., Wu, D., 2021. The effect of beta-amyloid and tau protein aggregations on magnetic susceptibility of anterior hippocampal laminae in Alzheimer's diseases. NeuroImage 244, 118584. https://doi.org/10.1016/j.neuroimage.2021.118584

Zhu, Q., Li, S., Cao, Z., Shen, Y., Xu, H., Xu, G., Li, H., Cui, Z., Zhu, K., Zhao, Z., Zhang, J., Wu, D., 2025. 7 Tesla multimodal MRI dataset of ex-vivo human brain. Sci. Data 12, 845. https://doi.org/10.1038/s41597-025-04932-x